Università degli Studi di Padova

Sede Amministrativa: Università degli Studi di Padova

Dipartimento di Geoscienze (VIA G. GRADENIGO 6, 35131 PADOVA)

CORSO DI DOTTORATO DI RICERCA IN GEOSCIENZE

CICLO XXXIV

# ACTIVE FAULTING AND DEEP-SEATED GRAVITATIONAL SLOPE DEFORMATION IN CARBONATE ROCKS (CENTRAL APENNINES, ITALY):

La tesi è stata redatta con il contributo finanziario dell'European Research Council Consolidator Grant Project (NOFEAR) No 614705 e di progetti finanziati dall'INGV, intitolati "Caratterizzazione microstrutturale di piani di faglia attivi ed esumati e di piani di scivolamento di deformazioni gravitative profonde di versante (DGPV)" e "Investigation of bedrock shear planes microstructures". Principal investigators: Giulio Di Toro and Marco Moro

**Coordinatore:** Ch.ma Prof.ssa Claudia Agnini
**Supervisore**: Ch.mo Prof. Giulio Di Toro
**Co-Supervisori**: Dr. Marco Moro & Dr. Michele Fondriest

**Dottorand**o: Luca Del Rio

## Abstract

Active Normal Faulting (NF) affects the carbonate rocks of the Italian central Apennines since Late Pliocene causing destructive earthquakes and, together with regional uplift, controlling the development of Deep-Seated Gravitational Slope Deformations (DGSDs). The latter are often located in the footwall of active normal faults.

The principal slip surfaces and associated slip zones of DGSD and NF exhume from different depths (100-500 m for DGSDs, 1-3 km for NFs), and are formed and active over a different range of temperatures (< 30°C for DGSDs vs. 0-100°C for NFs), pressures (< 15 MPa for DGSDs, 0-80 MPa for NFs) and slip rates (usually < $10^{-3}$ m/s for DGSDs, up to ~ 1 m/s for NFs). Such large differences in loading conditions should result in the formation of distinctive secondary fault/fracture networks in the damage zones that host the DGSDs, possibly recognizable at the outcrop scale, or in the slip zones microstructures. The individuation of the deformation mechanisms and the discrimination between DGSDs and NFs structures could bring outstanding improvements in geological hazard studies.

To achieve these goals, I investigated four DGSDs located in the footwall of active seismogenic NFs and three normal faults bordering large and small depressions in the central Apennines. I investigated the fracture distribution around DGSDs' and NFs scarps and the microstructures of the associated slip zones. Then, I performed Crystallographic Texture Analyses (CTA) on natural and experimental slip zones in carbonate rocks to identify the Crystallographic Preferred Orientations (CPOs) of microcrystalline aggregates and interpret the deformation mechanisms active during slip.

Based on these studies, I conclude that most DGSDs in the central Apennines re-use pre-existing minor faults or shear fractures located in the footwall of large normal seismogenic faults and that no microstructural indicators can allow to uniquely distinguish between DGSDs and normal faults. Indeed, slip zones associated with both NFs and DGSDs in carbonate rocks are produced by similar deformation mechanisms.

## Sommario

Eventi di fagliazione attiva interessano le rocce carbonatiche degli Appennini centrali italiani a partire dal tardo Pliocene, provocando terremoti e, grazie anche al contributo del sollevamento regionale, controllando lo sviluppo di Deformazioni Gravitative Profonde di Versante (DGPV). Quest'ultime si trovano spesso al footwall di faglie normali attive.

Le *Principal slip surfaces* e *slip zones* relative sia alle DGPV che a faglie normali emergono da diverse profondità (100-500 m e 1-3 km, rispettivamente), e si sviluppano a

diverse di condizioni di temperatura (< 30°C *vs.* 0-100°C), pressioni (< 15 MPa *vs.* 0-80 MPa) e velocità di scivolamento (< 10-3 m/s, fino a ~ 1 m/s). Tali differenze nelle condizioni di carico dovrebbero portare alla formazione di distinti sistemi di fratture e faglie secondarie nelle *damage zones* associate alle DGPV, che possono essere osservate alla scala dell'affioramento, o nelle microstrutture delle *slip zones*. L'individuazione dei meccanismi di deformazione e la discriminazione tra strutture associate a DGSDs o faglie normali potrebbe fornire notevoli miglioramenti negli studi di rischio geologico.

Per raggiungere questi obiettivi, ho studiato quattro DGPV situate al footwall di faglie normali attive sismogeniche e tre faglie normali che bordano bacini intramontani in Appennino centrale. Per prima cosa ho studiato la distribuzione delle fratture associate alle scarpate delle DGPV e le microstrutture delle *slip zones* associate. In seguito, ho eseguito delle Crystallographic Texture Analyses (CTA) su *slip zones* levigate in rocce carbonatiche sia naturali che sperimentali per identificare gli le Orientazioni Cristallografiche Preferenziali degli aggregati microcristallini e interpretare i meccanismi di deformazione attivi durante lo scivolamento.

In base agli studi condotti, concludo che la maggior parte delle DGPV in Appennino centrale riutilizza faglie minori o fratture preesistenti situate al footwall di grandi faglie normali sismogenetiche e che nessun indicatore microstrutturale è in grado di distinguere in modo univoco tra DGPV e faglie normali. Infatti, le *slip zones* associate sia a NF che a DGPV in rocce carbonatiche sono prodotte dagli stessi meccanismi deformativi.

## Table of contents

# 1. Introduction

In this thesis I discuss the structure and the deformation mechanisms of Deep-Seated Gravitation Slope Deformations affecting the footwall of large normal faults in carbonate-built rocks.

## 1.1 Faults and Deep-Seated Gravitation Slope Deformations

Active faulting and Deep-seated Gravitational Slope Deformations (DGSDs) constitute common geological hazards in mountain belts worldwide. The Italian central Apennines are one of the most seismically active regions in Europe, with an average recurrence of one moderate to large in magnitude ($M_w \geq 5.5$) earthquakes per decade (Galli, 2020; Rovida et al., 2020). However, numerous relief slopes of central Apennines are further affected by large deep gravitational landslides (Galadini, 2006; Esposito et al., 2007; Moro et al., 2007, 2009, 2012; Aringoli et al., 2010; Bianchi Fasani et al., 2014; Gori et al., 2014; Della Seta et al., 2017; Mariani and Zerboni, 2020).

DGSDs are large and extremely slow rock-mass movements on high-relief slopes (i.e., present day displacement rates of the order of mm/yr), involving hundreds of meter thick rock volumes from the valley floor to the ridge crest, with relatively small displacements compared with the slope dimensions (Jahn, 1964; Zischinsky, 1966, 1969; Radbruch-Hall et al., 1977; Varnes, 1978; Hutchinson, 1988; Dramis and Sorriso-Valvo, 1994; Agliardi et al., 2001, 2012; Goudie, 2004; Jaboyedoff et al., 2013; Hungr et al., 2014; Panek and Klimeš, 2016; Discenza and Esposito, 2021). The main DGSD body commonly lack of clearly defined lateral boundaries, that often coincide with tectonic lineaments (Agliardi et al., 2001; Jaboyedoff et al., 2013; Esposito et al., 2021) or slope incisions (Agliardi et al., 2012). Instead, the major and secondary slip shear zones and slip surfaces are clearly recognized at the surface, where brittle processes affect the rock-mass, but become much thicker and less continuous in the inner portion of the slope, dominated by ductile and viscous-plastic deformation (Varnes, 1978; Nemčok, 1982; Dramis and Sorriso-Valvo, 1994; Cruden and Varnes, 1996; Martino et al., 2017; Della Seta et al., 2017). Here, the basal shear zone is few meters to tens of meters thick and present a cataclastic fabric with abundant fine matrix (Crosta and Zanchi, 2000; Madritsch and Millen, 2007; Crosta et al., 2013; Di Luzio et al., 2021). The largest DGSDs may further include secondary landslides or rock slope failures in the lower sector of the slope (i.e., toe of the DGSD; Varnes et al., 1990; Ambrosi and Crosta, 2006; Agliardi et al., 2001, 2012; Pánek and Klimeš, 2016; Jarman and Harrison, 2019; Crippa et al., 2020).

Peculiar morphologies associated with DGSDs can be recognized along the entire relief slope-valley floor system (although some are similar or may coincide with purely tectonic structures; Agliardi et al., 2012; Jaboyedoff et al., 2013; Fig. 1.1). Double-crested ridges, ridge-top grabens, trenches, tension cracks, downhill and uphill-facing scarps (or counterslope scarps) are mainly recognized in the upper sector of the slope (Mahr, 1977; Bovis, 1982; Savage and Varnes, 1987; Chigira, 1992; Dramis and Sorriso-Valvo, 1994; Agliardi et al., 2001; Hürlimann et al., 2006; Agliardi et al., 2009, 2012; Jaboyedoff et al., 2013; Fig. 1.1). The middle sector of the slope is characterized by tensile structures that allow the connection between the upper and lower portion, such as uphill-facing scarps, ridge-parallel trenches, grabens and tension cracks (Zischinsky, 1969; Savage and Varnes, 1987; Chigira, 1992; Agliardi et al., 2001, 2012; Jaboyedoff et al., 2013), that may locally lead to the development of toppling structures (Bovis and Evans, 1996; Reitner and Linner, 2009). In the lower part of the slope, the involved rock mass is partially shortened, due to the gradual decrease of deformation toward the DGSD toe, that lead to the formation of folds and inverse structures (Zischinsky, 1969; Mahr and Nemčok, 1977; Záruba and Mencl, 1982; Chigira, 1992; Hermann et al., 2000; Hippolyte et al., 2006; Mahr, 1977; Savage and Varnes, 1987; Fig. 1.1).

DGSDs may develop in different geological-structural and geomechanical settings that directly influence their deformation style (Hutchinson, 1988; Hermann et al., 2000; Agliardi et al., 2001, 2012; Di luzio et al., 2004b; Esposito et al., 2014; Pánek and Klimeš, 2016; Mariani and Zerboni, 2020). As a matter of fact, DGSDs are commonly divided in two large typologies: Sackung and Lateral Spreading (Figs. 1.1, 1.2). Sackung DGSDs (also called Sagging, rock flow or mass rock creep) are extremely slow rock-mass movements that affect homogeneous and coherent lithotypes on high and steep slopes from the ridge crest to the valley floor (Zischinsky, 1969; Savage and Varnes, 1987; Hutchinson, 1988; Hermann et al., 2000; Agliardi et al., 2012; Figs. 1.1a, 1.2). The involved rock-mass, commonly fractured (Agliardi et al., 2012), moves along a discrete and discountinuous sliding surface, rarely exposed in the basal sector of the slope (Cruden and Varnes, 1996), where bulging and secondary landslides locally develop (Zischinsky, 1969; Savage and Varnes, 1987; Agliardi et al., 2001, 2012; Discenza et al., 2011; Crippa et al., 2020). Instead, Lateral Spreading DGSDs (also called rock spreading, rock mass spreading or rock block slide) are characterized by horizontal movements of a coherent and gently dipping sedimentary succession overlying a less competent or more fractured unit (Jahn, 1964; Zischinsky, 1969; Nemčok et al.,1972; Pašek, 1974; Varnes, 1978; Hutchinson, 1988; Agliardi et al., 2012;

Bozzano et al., 2013; Di Maggio et al., 2014; Figs. 1.1b, 1.2). The rock-mass is commonly affected by tectonic residual stress, with unloading processes that allow the spreading through the formation of sub-vertical deformation bands (Martino et al., 2004; Discenza et al., 2011).

Other natural and human factors, and their interaction, control the mechanical behavior of DGSDs, such as the state of the stress and inherited discontinuities (Molnar, 2004; Ambrosi and Crosta, 2006, 2011; Martel, 2006; Martino et al., 2017; Esposito et al., 2021), lithostratigraphic setting and schistosity (Ambrosi and Crosta, 2011; Della Seta et al., 2017), weather and climate (Evans and Clague, 1994; Agliardi et al., 2001), karstic subsidence (Discenza et al., 2011), post-glacial stress release (Crosta et al., 2013) mining operations (Benko and Stead, 1998), seismicity (McCalpin, 1999; Jibson et al., 2004; Moro et al., 2012) and others. Furthermore, most of these factors may also trigger secondary landslides, slope collapses or rock-avalanches, that interrupt the regular slow movements of the rock-mass and may further evolve in potential Rock Slope Failures (RSFs; Di Luzio et al., 2004a; Evans et al., 2006; Hermanns and Longva, 2012; Jarman and Harrison, 2019). The latter represent one of the most important risk factors associated with DGSDs in terms of risk to life and buildings, as they involve large volumes of rock-mass (i.e., tens or hundreds of millions of cubic meters) moving at relatively fast slip rates (Hungr and Evans, 2004; Evans et al., 2006; Chigira et al., 2010; Delchiaro et al., 2019). Therefore, since the end of the last century, DGSDs were largely monitored through remotely sensed analyses (e.g., GPS, Lidar, InSar) or drone mapping, to study their kynematic and deformation rates (Ambrosi and Crosta, 2006; Moro et al., 2007; Agliardi et al., 2012; Panek and Klimeš, 2016; Amato et al., 2018; Frattini et al., 2018; Crippa et al., 2020), and further investigated through numerical modelings (Ambrosi and Crosta, 2011; Bianchi Fasani et al., 2011; Discenza et al., 2011; Albano et al., 2015; Della Seta et al., 2017; Agliardi et al., 2019).

Numerous DGSDs were documented worldwide since 1990s (see Figure 1 in Panek and Klimeš, 2016; Savage and Varnes, 1987; Varnes et al., 1989; Bovis, 1990; Chigira, 1992; Gutiérrez-Santolalla et al., 2005; Cossart et al., 2008; Audemard et al., 2010; Zangerl et al., 2010; Pánek et al., 2011a; Discenza and Esposito, 2021; Fig. 1.1) and even on other planets (Discenza et al., 2021; Fig. 1.1d). In Italy, significant natural hazards are associated with DGSDs, both in the Alps and in the Apennines. Alpine DGSDs were largely studied and monitored in the last 30 years (Agliardi et al., 2001, 2012; Ambrosi and Crosta, 2006, 2011; Crosta et al., 2013; Frattini et al., 2018; Crippa et al., 2021). In this case, the post-glacial unloading stress release represent the main predisposing factor of most Sackung DGSDs,

also controlled by the rock composition, metamorphic foliations, regional and local tectonic stress field (Agliardi et al., 2009, 2019; Ambrosi and Crosta, 2011; Crosta et al., 2013; Mariotto and Tibaldi, 2015).

Instead, the main controlling factor of the formation of DGSDs in central Apennines is the energy relief (i.e., the difference in altitude between the highest and lowest portion) of the hillslope, caused by normal faulting activity (Galadini, 2006; Moro et al., 2007), coupled with strong Quaternary regional uplift (more than 1000 m; D'Agostino et al., 2001) and with interglacial-glacial climate changes (Giraudi, 2001; Giraudi and Giaccio, 2017). The ground shaking caused by fault re-activation may furher trigger small rock-avalanches and collapses interrupting the slow movements of the closest DGSDs, that may evolve in potential catastrophic failures, also favored by karst processes, that facilitate the formation of large fissures and grabens at the ridge top (Moro et al., 2009; 2012; Chigira et al., 2010; Gori et al., 2014).

Active normal faulting has affected the Apennine carbonate rocks since the Late Pliocene (e.g., Elter et al., 1975; Barchi et al., 2000; Galadini et al., 2000; Boncio et al., 2004; Valensise and Pantosti, 2001; Galli et al., 2008; Villani et al., 2018) to accommodate the NE-SW oriented extension of the chain (~ 3 mm/yr of extension rate; D'Agostino et al., 2011), caused by the retreat of the subduction hinge toward E-NE (Malinverno and Ryan, 1986; Carminati and Doglioni, 2012). Most of Quaternary normal faults cut or locally exploit the inherited Miocene-Early Pleistocene thrusts and the earlier Mesozoic normal faults (Elter et al., 1975; Vezzani et al., 2010), are NW-SE oriented, SW dipping (i.e., "Apennine trend") and commonly organized in fault systems with associated intermontane basins (Bosi et al., 1993; Cavinato et al., 2002). During the last 30 years, paleo-seismological trench investigations (Galli, 2020), geomorphological analyses (e.g., Giraudi and Giaccio, 2017), structural geological mapping (e.g., Fondriest et al., 2020) and geophysical investigations (e.g., Chiaraluce et al., 2017), allowed researchers to estimate better the seismic hazard associated with numerous faults cropping out in the central Apennines (Barchi et al., 2000; Calamita et al., 2000; Galli et al., 2008; Falcucci et al., 2016; Galli, 2020).

Recent paleo-seismological, geological, and geomorphological observations pointed out that some sharp scarps outcropping in the central Apennines, commonly interpreted as surface expression of seismic faulting, can also accommodate DGSDs (Moro et al., 2009, 2012; Gori et al., 2014). Indeed, these scarps affect the upper portion of the hillslope, are less than 1 km long along-strike with an arcuate shape at the tips and are not geometrically linked with other structures, thus indicating a lateral confinement of the DGSD body (Moro

et al., 2009). Moreover, photogeological and field analyses allowed for the identification of several geomorphological features associated with DGSDs (e.g., double-crested lines, scarps and counterslope scarps, slope-parallel trenches and open fractures). Such morphological features are the expression of near-surface deformation at the hillslope scale (e.g., their spacing is of the order of tens of meters) and are not expected to be produced by listric normal faults. Furthermore, numerous studies have demonstrated how the onset and development of DGSDs in tectonically active regions is strongly controlled by pre-existing structures, that represent weakness zones exploited by the DGSD (Agliardi et al., 2001, 2012; Di Luzio et al., 2004b; Agliardi et al., 2001, 2009, 2012, 2019; Esposito et al., 2014). Clearly, the interpretation of certain sharp scarps as surface expression of seismic faulting rather than DGSDs may strongly influence the seismic hazard assessment of the area as well as other areas worldwide characterized by moderate to strong seismicity.

In order to address this relevant point, in the first part of the PhD I analyzed the distribution of minor faults and fractures in the footwall of four DGSD scarps located in the Abruzzi Region (central Apennines): The Alto di Cacchia, Mt. Serrone, Sant'Erasmo and Colle Cerese DGSDs (Fig. 1.3). For comparison, I also analyzed the fault zone in the footwall of a relatively small (i.e., < 2 km long) and laterally confined normal fault bordering a narrow basin: the Valle Force fault (see "geological setting" section in chapter 3 for the description of study cases). Abruzzi is one of the regions of central Italy that was strongly affected by seismic faulting in the past. The most recent earthquake that hit the region was the $M_w$ 6.1 L'Aquila April 6, 2009 earthquake, whereas the largest one instrumentally recorded was the $M_w$ 7.0 Avezzano January 13, 1915 earthquake (EWG, 2010; Rovida et al., 2020). Then, from samples collected from the major and secondary outcropping scarps, I further analyzed the micro- to nano-structures of the associated slip zones, that were further compared with those associated with two large seismogenic faults hosting the analyzed DGSDs in their footwall: The Venere (re-activated during the Avezzano earthquake; Rovida et al., 2020; Fig. 1.3a) and Roccapreturo (Fig. 1.3c) normal faults.

The main goals here are the identification of (1) the deformation mechanisms that control the emplacement of DGSDs in carbonates and (2) the meso- and micro-structures, if any, characteristic only of normal faults or DGSDs. These microstructures would represent an independent marker of the style of deformation of these mountain slopes, that could be relevant for geological hazard studies. Indeed, in the central Apennines, the slip surfaces associated with DGSDs and faults, respectively, should be exhumed from different depths (0 to a few hundreds of meters for DGSDs, 0-3 km for active faults; Agosta and Kirschner,

2003), and active over a different range of (a) temperatures (< 15°C for DGSDs, 0-60°C for faults assuming a geothermal gradient of ~ 20°C/km, typical for the central Apennines; Mancinelli et al., 2019), (b) lithostatic pressure (< 15 MPa for DGSDs, 0-80 MPa for faults), and (c) slip rates (usually mm/yr for DGSDs, up to ~ 1 m/s for seismic faults). Such large differences in loading conditions should result in the formation of distinctive secondary fault/fracture networks, possibly recognizable at the outcrop scale, and microstructures of the slip zones.

Meso-scale morpho-structural analyses of DGSDs have been already proposed in Alpine settings (Agliardi et al., 2009, 2019) and fluvial-dominated environments with moderate to high seismicity (e.g., Japan, Taiwan; Chigira, 1992, 2009). These works show how pre-existing fractures may trigger and influence the onset of DGSDs and of the associated morphologies. To my knowledge, this is the first work in which both meso- and micro-structural analyses of slip surfaces are used to study DGSDs in central Apennines (i.e., they affect relief slopes on carbonate-build rocks strongly affected by recent and past seismicity), which are commonly investigated through geomorphological, geological and geophysical (i.e., remote sensing; Tolomei et al., 2013; Albano et al., 2015) analyses.

Instead, analyses at meso- to nano-scale (i.e., < 100 nm in size grains) of exhumed damage zones are largely used to interpret the mechanical behavior of large seismogenic faults (up to 15-20 km long) accommodating hundreds to thousands of meters of displacement (Chester and Chester, 1998; Wibberley and Shimamoto, 2003; Faulkner et al., 2011; Bullock et al., 2014; Viola et al., 2016; Masoch et al., 2021). Structural investigations of fault zones in central Apennines carbonate rocks documented the presence of hundreds of meter-thick damage zones bounding meter-thick fault cores accommodating most of the cumulative displacement (Agosta and Aydin, 2006; Demurtas et al., 2016; Ferraro et al., 2019; Fondriest et al., 2020; Fig. 1.4) and containing multiple cm- to mm-thick principal slip zones (PSZs; Smith et al., 2011; Fig. 1.4) cut by sharp (where karstified) or polished to “mirror-like” (where fresh) slip surfaces (Fondriest et al., 2013, 2015, 2017; Siman-Tov et al., 2013; Fig. 1.5). The latter represent one of the several microstructural indicators, but highly debated, of seismic slip proposed in the literature from experimental and natural observations of fault slip zones (Rowe and Griffith, 2015; Delle Piane et al., 2017; Pozzi et al., 2019; Fig. 1.5).

The regularly spaced set of joints and shear fractures measured in the footwall of DGSD scarps indicate similar formation depth with near-surface normal faults, followed by a recent gravitational activity, as suggested by the numerous (e.g., Alto di Cacchia DGSD)

to few high-angle fissures affecting the host rocks. The slip zones of large normal faults and DGSDs have variable to comparable microstructures (i.e., from ultra-cataclasites to proto-cataclasites, mainly cataclasites; Sibson, 2003), with textures of fine matrix suggesting the activation of low temperature pressure-solution processes during either seismic or aseismic slip. Large normal faults have well-developed and thicker slip zones associated and experienced more pressure-solution because of the larger amount of displacement cumulated with respect to DGSDs.

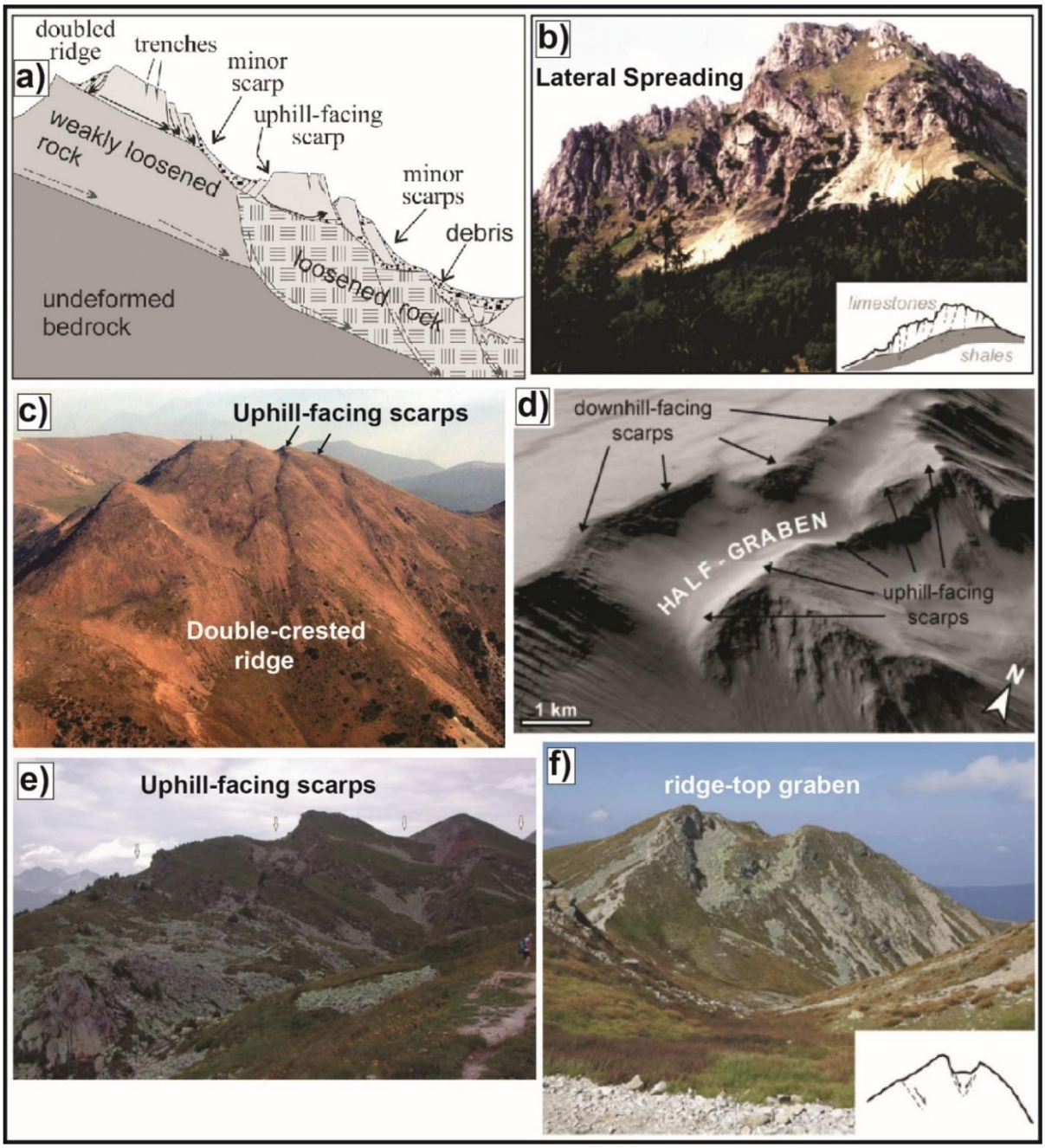


Figure 1.1: a) Main morphological features of a typical Deep-seated Gravitational Slope Deformation (DGSD). b) Mountain-scale lateral spreading of Triassic limestones thrusted over ductile Early Cretaceous marls and shales (Slovakia). c) Double-crested ridge morphology and uphill-facing scarps (British Columbia, Canada). d) Half-graben defined by downhill- and uphill-facing scarps (Mars). e) Multiple scarps and multi-crested ridge in micaschist and paragneiss (Valtellina, Austroalpine domain). f) Ridge-top graben affecting granodiorites (Slovakia). Images from Forno et al., 2013 (a); Pánek and Klimeš, 2016 (b, f); Hungr et al., 2014 (c); Discenza et al., 2021 (d); Crosta et al., 2013 (e).

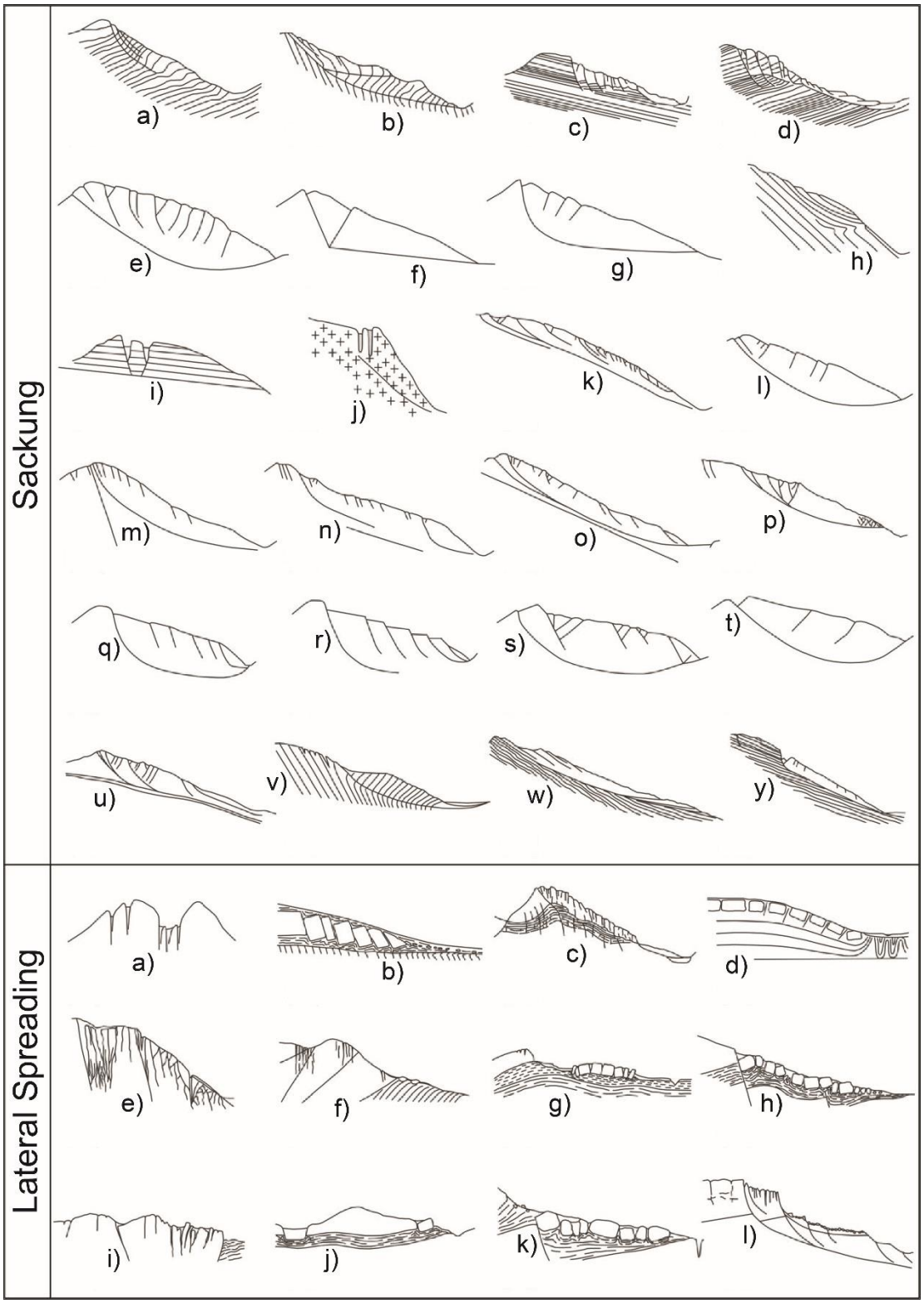


Figure 1.2: Examples of DSGSDs proposed in the literature, divided in Sackung and Lateral Spreading and ordered on the basis of the year of publications (Modified from Discenza and Esposito, 2021). **Sackung:** Zischinsky, 1966 (a, b); Nemčok, 1972 (c, d); Mahr, 1977 (e); Hutchinson, 1988 (f, g); Chigira, 1992 (h, i, j); Agliardi et al., 2001 (k); Ambrosi and Crosta, 2006 (l, m, n, o); Apuani et al., 2007 (p); Bois et al., 2008 (q, r, s, t); Agliardi et al., 2009 (u); Martino et al., 2020 (v); Vick et al., 2020 (w, y); **Lateral Spreading:** Jahn, 1964 (a); Záruba and Mencl, 1969 (b); Nemčok, 1982 (c); Hutchinson, 1988 (d); Martino et al., 2004 (e); Esposito et al., 2007 (f); Di Maggio et al., 2014 (g, h, i, j, k); Pánek and Klimeš, 2016 (l).

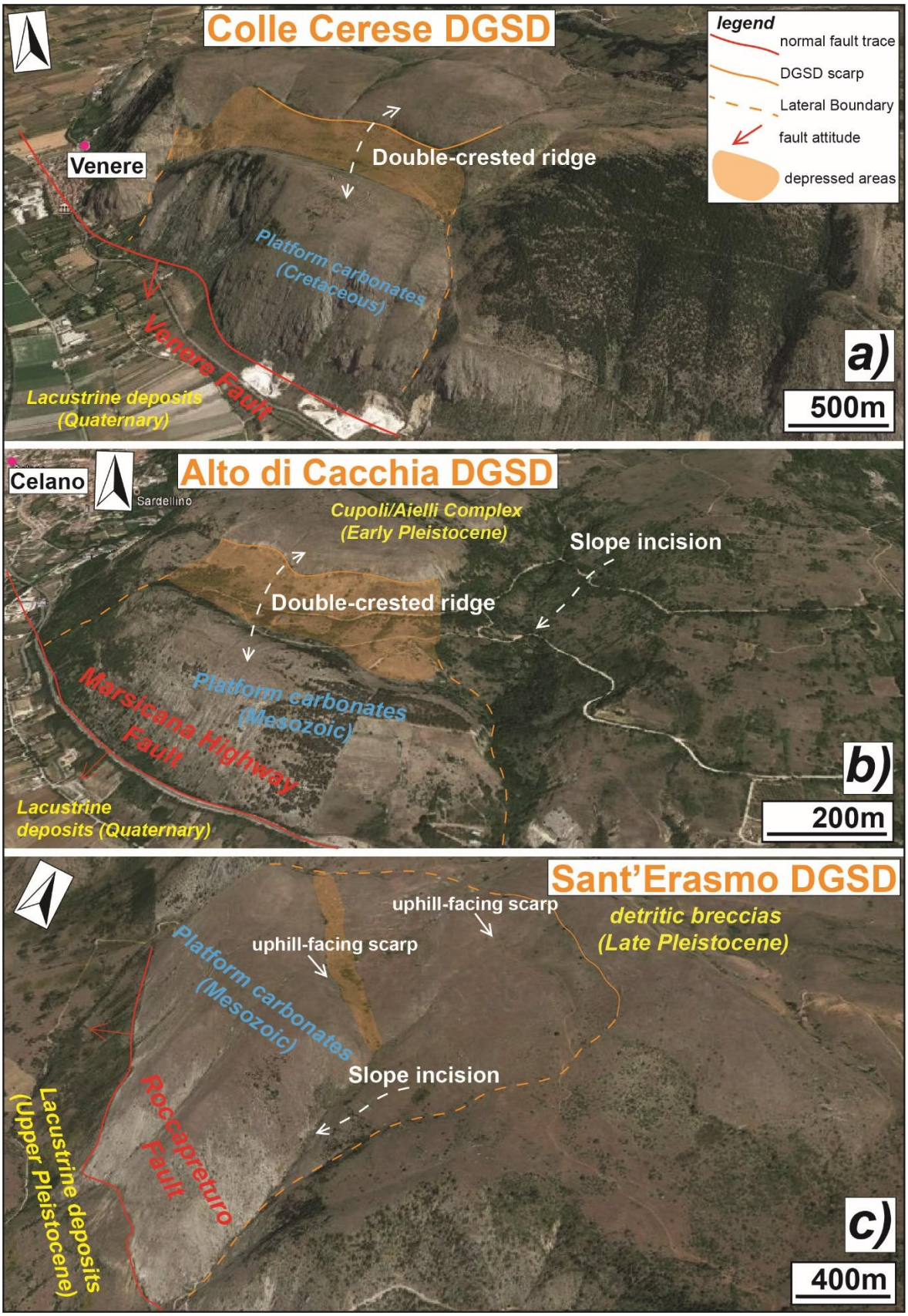


Figure 1.3: Colle Cerese (a), Alto di Cacchia (b) and Sant'Erasmo (c) DGSDs on Cretaceous limestones, located in the footwall of three active seismogenic normal faults. Note the peculiar morphologies associated with the DGSDs, such as double-crested lines and uphill-facing scarps. The DGSDs boundaries are poorly defined and coincide with slope incisions. Images from Google Earth.

The results obtained from analyses of damage and slip zones of DGSDs prompted us to investigate with similar approaches two widely studied normal faults of the Abruzzi Region, located just south to the L'Aquila town: The Campo Felice and Cama normal faults (CFf and Cf, respectively; chapter 4). The latter were inferred to represent the middle and northern segments of a ~ 27 km long in map fault system because of the quite good correlation among the ages of paleo-earthquakes recognized along the fault segments (Pantosti et al., 1996; Salvi et al., 2003). The fault system would represent the ground surface expression of a single deeper seismogenic structure (30-35 km long) capable of producing up to $M_w = 6.8$ earthquakes in case of the entire system rupture (Galli et al., 2008). Nevertheless, several geomorphological features indicative of a Deep-seated Gravitational Slope Deformation (DGSD) were identified across the Mt. D'Ocre range, such as trenches, uphill and downhill facing scarps and counterscarps (Salvi and Nardi, 1995).

The Campo Felice fault displaces of ~ 1000 m Cretaceous shallow-water limestones with a normal pure dip-slip kinematics (Wilkinson et al., 2015) and borders to SW the homonym intermontane basin (~ 20 $km^2$ wide). The Cama fault is one of the three sub-parallel bedrock fault scarps of the Mt. D' Ocre range. The fault cuts the same rocks of the Campo Felice fault with ~ 100 m of normal displacement, bordering to SW three small and narrow valleys. The Campo Felice and Cama faults represent a great opportunity to compare two geometrically linked structures affecting the same host rocks with similar kinematics but with different slip rates and displacement cumulated in time (Salvi et al., 2003; Galadini and Galli, 2000). Furthermore, the DGSDs analyzed in the previous work are all located in the footwall of large seismogenic normal faults, whose activity largely influenced the formation and distribution of fractures in rocks affected by gravitational processes. On the contrary, the fault zones associated with the CFf and Cf are mainly produced by the long-term activity of the two faults. The interpretation of the deformation processes at meso- to micro-metric scale associated with the Campo Felice and Cama fault scarps may contribute to shed more light on the formation, current mechanical behavior and relation between the two faults.

I realized two geological maps of the area affected by the Campo Felice and Mt. D'Ocre faults and two cross-sections oriented perpendicular to the faults to estimate their geological throw. Then, I mapped and compared the distribution of fractures affecting the host-rocks in the footwall of Campo Felice and Cama faults and compared the microstructures of the slip zones associated with the major and secondary fault scarps to identify the main deformation mechanisms produced during slip. Structural features of Campo Felice and Cama fault

zones suggest that the two faults are not kinematically related. The two faults have different slip zones associated (i.e., cataclasite *vs.* crush fault breccia), but produced by similar deformation mechanisms (i.e., cataclasis and pressure-solution).

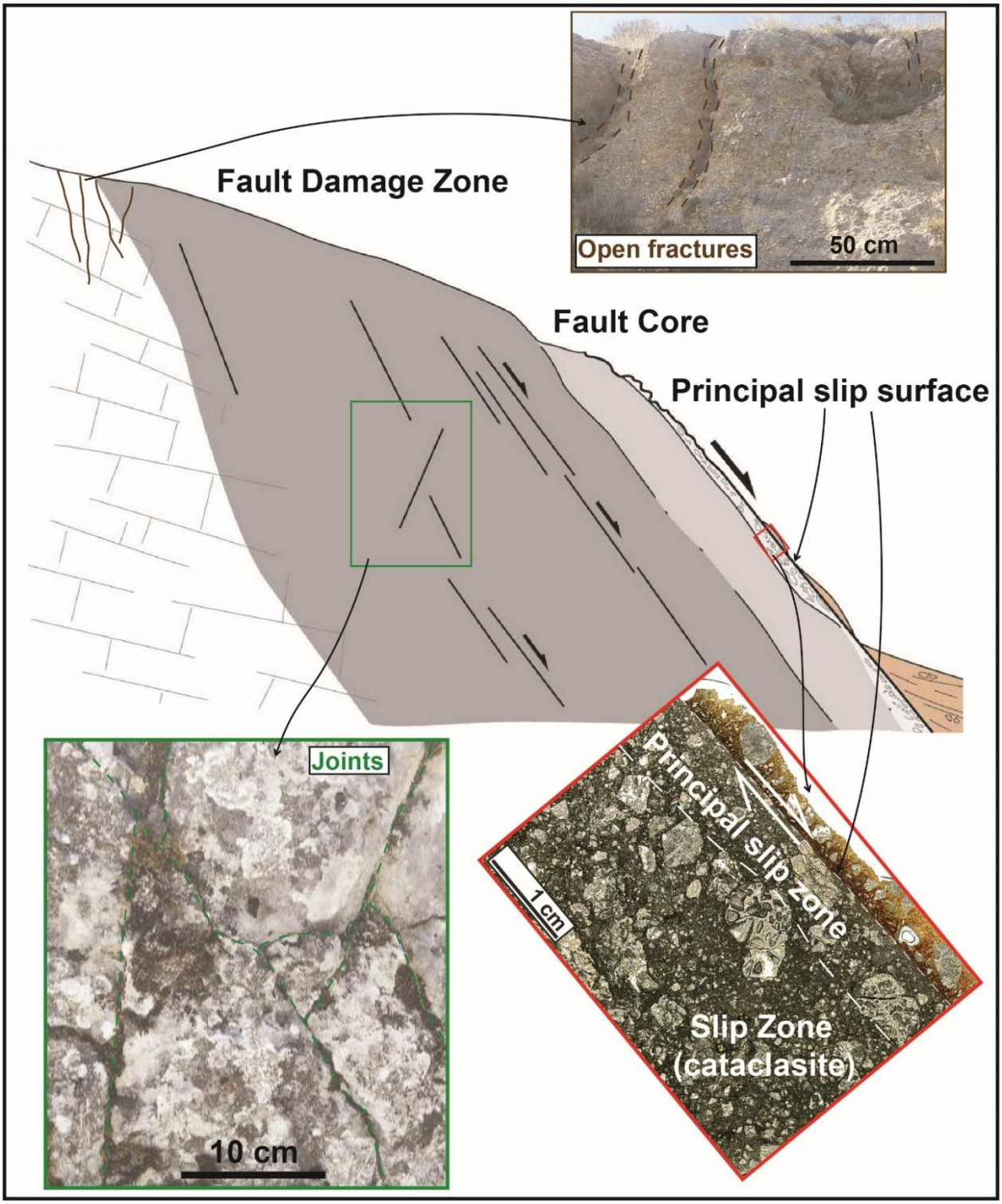


Figure 1.4: Main structural features of a fault zone (modified from Smith et al., 2011): *Open fractures* commonly form in tensional regime and affect the host rocks or rocks slightly deformed by fault activity; *Joints* commonly affect the fault *damage zone*; *fault core* accommodates most of the fault displacement and includes a

cataclastic slip zone close to the principal slip surface that, in turn, can include a < 1 cm thick *Principal Slip Zone* just beneath the fault surface.

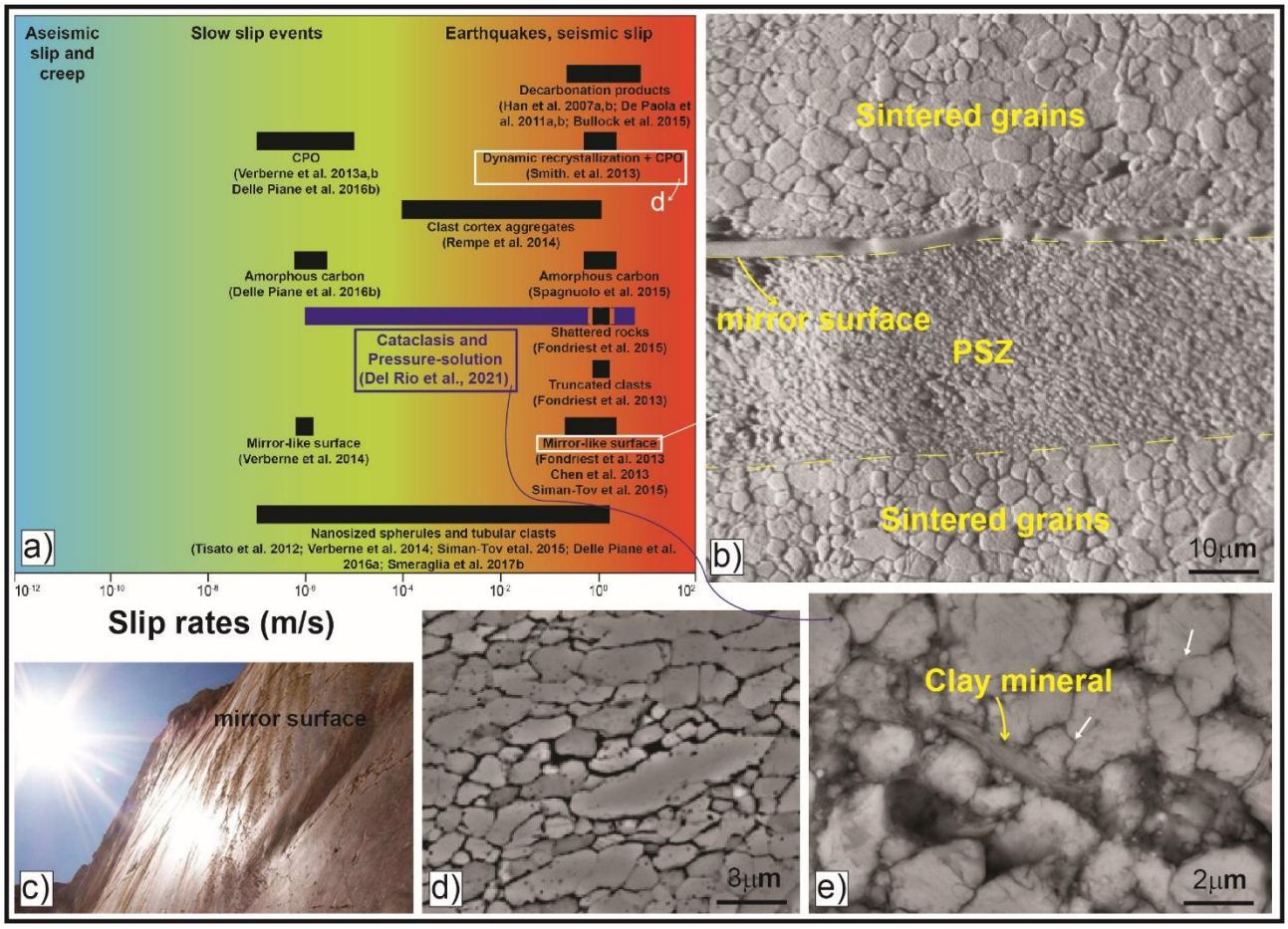


Figure 1.5. a) Potential microstructural seismic markers proposed in the literature and their range of slip rate occurrence (modified from Delle Piane et al.., 2017). b) Sintered micro-grains produced by Grain Boundary Sliding delimited from the PSZ by a mirror-like surface (from Pozzi et al., 2019). c) Example of a mirror-like fault surface in brecciated limestone (Israel; from Siman-Tov et al., 2013). d) Backscattered SEM image of dynamically recrystallized calcite aggregates with strong shape-preferred orientation (from Smith et al., 2013). e) SEM image of the fine matrix close to the slip surface of Sant'Erasmo DGSD, composed of packed calcite micro-grains, locally indented (white arrows) with straight to irregular boundaries and clay minerals partially filling the pore spaces (Del Rio et al., 2021).

## 1.2 Deformation mechanisms in carbonate-built rocks

As briefly mentioned before, most of slip displacement along brittle faults is accommodated within tens of centimetres to meters thick fault cores including few hundreds of micrometers thick PSZs, as a result of extreme deformation (Sibson, 1977, 2003; Caine et al., 1996; Wibberley and Shimamoto, 2003). In carbonate-hosted faults, PSZs are produced by numerous deformation mechanisms (e.g., cataclasis, pressure-solution, decarbonation, dislocation creep, diffusion creep, thermal pressurization etc.) active at

different boundary conditions (e.g., Temperature, Pressure, slip rates etc.) that allow and enhance fault displacement by reducing the fault strength (Sibson, 1977; Rice, 2006; Han et al., 2007b; Gratier et al., 2011; Spaguolo et al., 2015; Smeraglia et al., 2017b; Pozzi et al., 2019). Microstructural analyses of slip zones indicate similar textures of fine matrix between DGSDs and normal faults (chapter 3). The matrix is mainly composed of highly packed calcite micro- to nano-grains with straight to irregular boundaries, indentation structures, incipient triple junctions, and few to numerous pores and cavities, locally filled with secondary calcite or clay minerals and oxides (Fig. 1.5e). Such textures are interpreted to be produced by both brittle cataclastic and congruent pressure-solution creep processes. The latter are expected to be active at very low slip rates (aseismic slip < 1 mm/yr) and surficial boundary conditions (i.e., $P_{litho}$ < 20 MPa and T < 20 °C) and would produce weak Crystallographic Preferred Orientations (CPOs) on the involved rocks (De Bresser and Spiers, 1997; Pozzi et al., 2019).

Instead, PSZs of large carbonate-hosted normal faults are bounded by polished to mirror-like sliding surfaces and commonly composed of nanoparticles *(D* < 100 nm), amorphous materials and sintered nanograins (Smith et al., 2011; Fondriest et al., 2012; 2013; Siman-Tov et al., 2013, 2015; Demurtas et al., 2016; Smeraglia et al., 2017b; Ohl et al., 2020). According to the numerous both low- and high-velocity friction experiments on carbonate rocks conducted in the last 15 years, these textures are mainly produced by a combination of cataclasis and viscous deformation mechanisms (e.g., Grain Boundary Sliding aided by both dislocation and diffusion creep; Verberne et al., 2014; Green et al., 2015; Spagnuolo et al, 2015; De Paola et al., 2015; Pozzi et al., 2019, 2021; Demurtas et al., 2019; Fig. 1.5). The latter are dominant at seismic velocities (i.e., v = ~ 1 m/s), when temperatures along fault slip zone rise up to > 600°C due to frictional heating (Rice, 2006), and drastically reduce the frictional strength of fault from $\mu$ = 0.6-0.85 (Byerlee, 1978) to $\mu$ < 0.2 (Han et al., 2007; Di Toro et al., 2011; Pozzi et al., 2019). Such viscous deformation mechanisms (e.g., dislocation creep) would possibly induce a relatively strong preferred orientation (Poirier, 1985; De Bresser and Spiers, 1997; Kim et al., 2018).

Analysis of CPOs within localized PSZs is a powerful technique to determine the sense of shear, amount of strain, temperature and main deformation mechanisms active during slip (Law et al., 1986; Rutter et al., 1994; Zang and Karato, 1995; Heilbronner and Tullis, 2002; Passchier and Trouw, 2005; Mainprice and Nicolas, 1989; Prior et al., 1999; Pozzi et al., 2019). Electron Backscatterd diffraction (EBSD) analysis applied to Scanning (SEM) and Transmission Elenctron Microscope (TEM) is the most commonly used technique to identify

CPOs. However, the low spatial resolution of SEM images doesn't allow EBSD to properly resolve grains less than 500 nm in size (Pozzi et al., 2019) and the small area (i.e., few tens of square micrometers) of TEM analysis doesn't provide a collection of statistically significant data sets. Furthermore, both the techniques cannot capture the three-dimensional nature of the material.

Instead, Crystallographic Texture Analysis (CTA) is an X-ray (or neutron) diffraction-based technique that measures the intensity of the diffraction signal of each individual crystallite that diffract coherently with the Bragg law to infer the orientation of a specific volume fraction of crystallites in the probed volume (Wenk, 1985; Matthies et al., 1988; Artioli et al., 2007; Chateigner et al., 2019; Suwas and Ray, 2014). The latter can be up to hundreds of million cube microns allowing a strong statistic consistency of the collected data. This technique was mainly applied to industrial metals (Coulomb, 1982; Bunge, 2000). Recently, thanks to the improvement of methods of analysis (Matthies et al., 1997), CTA was also applied to polymineralic rocks for paleontological (Chateigner et al., 2000), archeological (Artioli, 2007), geophysical (Morales et al., 2003) and geological (Wenk, 1985, 2002; Wenk et al., 1996) analyses.

In order to unravel the possible deformation mechanisms operating during fault slip, I applied the CTA technique for the first time on natural fault samples in carbonates. I used samples from the wall rocks of Valle Force fault, the relatively small carbonate-hosted normal fault studied in chapter 3 (Fig. 1.6a-b). For comparison and calibrating the technique, I also analyzed experimentally produced polished slip surfaces from dolomitic marbles deformed at seismic slip velocities (Fig. 1.6c).

Overall, our results indicate similar ambient conditions at which DGSDs and near-surface tectonic faulting occur and deformation mechanisms associated. However, the analysis of meso- to microstructural data set allow (a) to understand better the DGSD formation in central Apennines, (b) to identify the deformation mechanisms associated with the evolution of DGSDs in space and time, (c) to provide further parameters to improve the characterization of seismogenic sources in central Apennines (Falcucci et al., 2016). CTA technique has proven to be a powerful tool to investigate fault slip zones in carbonate rocks.

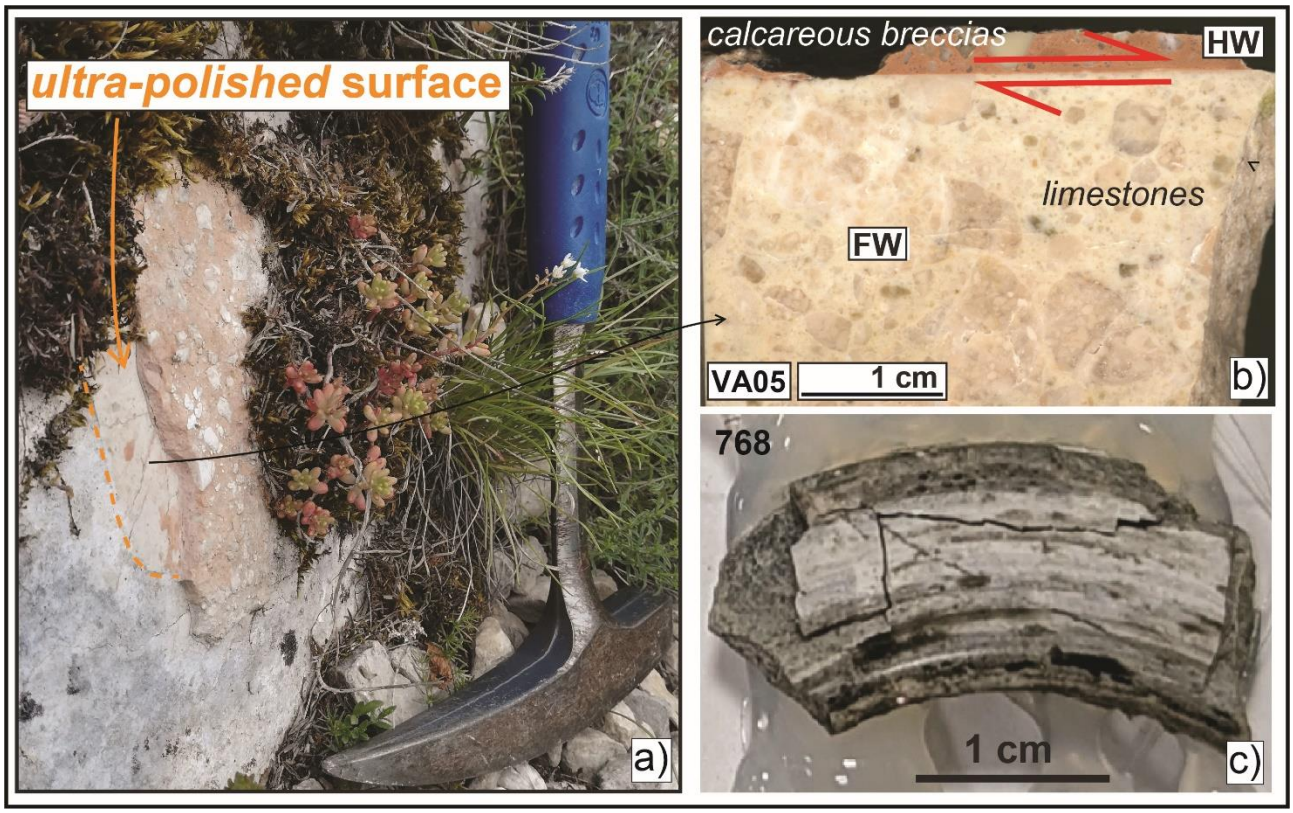


Figure 1.6. a) Valle Force fault scarp with a patch of hangingwall calcareous breccias leant on it that appears ultra-polished where breccias are removed. b) Scan of Sample VA05, showing a very sharp surface separating the wall rocks. c) Sample 768, produced by shearing a cylinder of dolomitic marble at ~ 1 m/sec for ~ 5 m. The slip surface looks ultra-polished and includes striae indicating the sense of shearing.

## 2. Materials and Methods

***Field geology survey techniques:*** In the study area mainly outcrops Jurassic-Cretaceous shallow-water to basin limestones and dolostones plus Plio-Pleistocene cemented conglomerates and Quaternary fluvio-lacustrine deposits (see "geological setting" sections of chapters 3 and 4 for more details). The Alto di Cacchia, Sant'Erasmo, Mt. Serrone and Colle Cerese DGSDs were identified through remote sensing, photogeological and geomorphological analyses, that allowed to recognize several peculiar morphological features associated with deep gravitational processes, such as double-crested lines, scarps and counterslope scarps, slope-parallel trenches and open fractures. The seven cases investigated on field (i.e., the four DGSDs, the Valle Force, Cama and Campo Felice normal faults) are described in the "geological setting" sections of chapters 3 and 4.

I realized two geological maps of the area affected by the Campo Felice and Mt. D'Ocre faults that I used as base to trace two cross-sections oriented perpendicular to the fault strike to estimate their geological throw (see "methods" section of chapter 4 for more details). High-resolution georeferenced orthomosaics of Alto di Cacchia, Sant'Erasmo and Colle Cerese DGSDs and Valle Force, Campo Felice and Cama fault zones were produced by stitching hundreds of nadir-directed photographs taken with a MAVIC 2 Pro drone and processed with Agisoft Metashape Pro software.

Normal faults and DGSDs were, then, investigated in the field by collecting structural data ($n$ = 3870) and samples (see appendix 1) along the outcropping scarps and across the footwall damage zones, that were plotted into stereonets (lower hemisphere, Schmidt equal area). The traces of major and secondary scarps were reported in topographic maps at 1:1000 scale and digitalized using the orthomosaics as base, to realize detailed structural maps of the damage zones (see "methods" section of chapters 3 and 4 for more details and "results" section of chapter 3 for a better description of the terminologies used to describe the fractures).

***Micro- to nano-structural analysis techniques:*** With regards to rock samples, from $n$ = 52 samples collected from the major and secondary faults, we selected 26 samples to produce syton-polished thin sections of the slip zones (see appendix 1) by cutting perpendicular to the slip surface and parallel to the kinematic indicators (where recognizable, otherwise along the dip direction). The thin sections where photo-scanned at high resolution (4000 dots per inch) both in plane and cross polarized Nicols and edited using specific tools of Adobe Photoshop (Ps) to highlight the clast morphology, minor

fractures and veins and the texture of the fine matrix. They were, then, observed under transmitted-light Optical Microscope (OM) and investigated for microstructural analysis with the Scanning Electron Microscope (SEM) CamScan MX3000 installed at the Dipartimento di Geoscienze (Padua Univ.) and with the Field Emission SEM (FESEM) Merlin Zeiss installed at CERTEMA laboratory (Grosseto, Italy; see “methods” sections of chapters 3 and 4 for more details).

***Crystallographic Texture Analyses technique:*** I analyzezed both samples from the Valle Force fault wall (VA05) and experimental samples of dolomitic marble sheared at sub-seismic to seismic velocities (i.e., 0,1 m/s to ~ 1 m/s). Samples were first analysed with XRD to study their composition and then mounted on a four-circle goniometer equipped with a Eulerian cradle and probed with a circular beam ($\lambda$CuK$\alpha$ = 1.5406 A$^o$) ~ 500 $\mu$m in diameter.

All the X-ray data treatment was performed using MAUD program. The obtained direct pole figures were normalized and used to resolve the *Orientation Distribution Function* through the entropy-modified WIMV method (Lutterotti et al., 2004), and finally recalculated and re-constructed starting from the computed ODF. This technique is described in detail in “materials and methods” section of chapter 5.

# 3. Active Faulting and Deep-Seated Gravitational Slope Deformation in Carbonate Rocks (Central Apennines, Italy): A New "Close-Up" View

*This chapter was published as the following paper: Del Rio, L., Moro, M., Fondriest, M., Saroli, M., Gori, S., Falcucci, E., et al. (2021). Active faulting and deep-seated gravitational slope deformation in carbonate rocks (central Apennines, Italy): A new "close-up" view. Tectonics, 40, e2021TC006698. https://doi.org/10.1029/2021TC006698. This study was performed with the collaboration of Giulio Di Toro, Marco Moro, Michele Fondriest, Michele Saroli, Stefano Gori, Emanuela Falcucci, Andrea Cavallo and Fawzi Doumaz. Marco Moro, Michele Saroli, Stefano Gori, Emanuela Falcucci and Giulio di Toro contributed to the work design; I was assisted by Michele Fondriest, Marco Moro, and Giulio Di Toro during field survey, by Andrea Cavallo during SEM analyses and by Giulio Di Toro and Michele Fondriest during microstructural interpretation; Fawzi Doumaz contributed with drone mapping and construction of orthomosaics; I wrote the original draft and discussed the results with Giulio Di Toro, Marco Moro, Michele Fondriest, Michele Saroli, Stefano Gori and Emanuela Falcucci; all the authors approved the final version of the published paper.*

## Abstract

Active faulting and Deep-seated Gravitational Slope Deformation (DGSD) are common geological hazards in mountain belts worldwide. In the Italian central Apennines, km-thick carbonate sedimentary sequences are cut by major active normal faults that shape the landscape, generating intermontane basins. Geomorphological observations suggest that the DGSDs are commonly located in fault footwalls.

We selected five mountain slopes affected by DGSD and exposing the footwall of active seismogenic normal faults exhumed from 2 to 0.5 km depth. Field structural analysis of the slopes show that DGSDs exploit pre-existing surfaces formed both at depth and near the ground surface by tectonic faulting and, locally, by gravitational collapse. Furthermore, the exposure of sharp scarps along mountain slopes in the central Apennines can be enhanced either by surface seismic rupturing or gravitational movements (e.g., DGSD) or by a combination of the two. At the microscale, DGSDs accommodate deformation mechanisms similar to those associated with tectonic faulting. The widespread compaction of micro-grains (e.g., clast indentation), observed in the matrix of both normal faults and DGSD slip zones, is consistent with clast fragmentation, fluid-infiltration and congruent pressure-solution active at low ambient temperatures (< 60 °C) and lithostatic pressures (< 80 MPa). Although clast comminution is more intense in the slip zones of normal faults because of the larger displacement accommodated, we are not able to find micro-structural markers that allow us to uniquely distinguish faults from DGSDs.

# 3.1 Introduction

Deep-seated Gravitational Slope Deformations (DGSDs) are large and slow rock-mass movements (slip rate of a few mm/yr) commonly affecting the entire relief slope and involving ~ 200-300 m thick rock volumes, with relatively small displacements compared to the slope dimensions (Jahn, 1964; Zischinsky, 1966, 1969; Radbruch-Hall et al., 1977; Varnes, 1978; Hutchinson, 1988; Dramis & Sorriso-Valvo, 1994; Agliardi et al., 2001, 2012; Goudie, 2004; Jaboyedoff et al., 2013; Hungr et al., 2014; Panek & Klimeš, 2016; Discenza & Esposito, 2021).

Unlike other types of landslides, DGSDs commonly lack clearly defined boundaries (Crosta et al., 2013). Sackung-type DGSDs (also called Sagging, rock flow or mass rock creep) are commonly produced by slow rock-mass movements that occur on high and steep slopes from the ridge crest to the valley floor and result in bulging of the lower sector of the

slope (Agliardi et al., 2001; 2012; Hermann et al., 2000; Hutchinson, 1988; Zischinsky, 1969; Savage & Varnes, 1987). On the other hand, lateral spreading DGSDs (also called rock spreading, rock mass spreading or rock block slide) are due to lateral mass movements in areas where a thick-bedded and gently dipping sedimentary succession overlies a less competent unit (Agliardi et al., 2012; Bozzano et al., 2013; Di Maggio et al., 2014; Hutchinson, 1988; Jahn, 1964; Nemčok et al.,1972; Varnes, 1978; Zischinsky, 1969).

Peculiar morphologies associated with DGSDs are double-crested ridges, ridge-top grabens, scarps and counterslope scarps, ridge-parallel trenches, tension cracks and bulging slopes (Agliardi et al., 2001, 2012; Bovis, 1982; Chigira, 1992; Dramis & Sorriso-Valvo, 1994; Hermann et al., 2000; Jaboyedoff et al., 2013 Savage & Varnes, 1987; Zischinsky, 1969). Several natural and human factors, and their interaction, control the mechanical behavior of DGSDs, such as the state of the stress and inherited discontinuities (Molnar, 2004; Ambrosi & Crosta, 2006, 2011; Martel, 2006; Martino et al., 2017; Esposito et al., 2021), lithostratigraphic setting and schistosity (Ambrosi & Crosta, 2011; Della Seta et al., 2017; Discenza et al., 2021), weather and climate (Evans & Clague, 1994; Agliardi et al., 2001), karstic subsidence (Discenza et al., 2011), post-glacial stress release (Crosta et al., 2013) mining operations (Benko & Stead, 1998), seismicity (McCalpin, 1999; Jibson et al., 2004; Moro et al., 2012) and others.

Significant natural hazards are associated with DGSDs (Ambrosi & Crosta, 2006; Dramis & Sorriso-Valvo, 1994), in particular due to a sudden acceleration of the slope movements commonly induced by seismic faulting (Chigira et al., 2010; Moro et al., 2007). A large number of DGSDs were documented worldwide since 1990s, in particular in North America, Europe, Japan and New Zealand (see Fig. 1 from Panek & Klimes, 2016; Audemard et al., 2010; Bovis, 1990; Cossart et al., 2008; Chigira, 1992; Discenza and Esposito, 2021; Gutiérrez-Santolalla et al., 2005; Pánek et al., 2011a; Santolalla et al., 2005; Savage & Varnes, 1987; Varnes et al., 1989; Zangerl et al., 2010)

In the central Apennines, the main controlling factor for the formation and triggering of DGSDs is the energy relief (i.e., the difference in altitude between the highest and lowest portion) of the hillslope produced by the large number of active, often seismogenic, normal faults accommodating regional extension (Galadini, 2006; Moro et al., 2007; Fig. 3.1), coupled with strong Quaternary regional uplift (more than 1000 m; D'Agostino et al., 2001) and with the interglacial-glacial climate changes (Giraudi, 2001). Active normal faulting has affected the Apennines since the Late Pliocene (e.g., Barchi et al., 2000; Boncio et al., 2004; Elter et al., 1975; Galli et al., 2008; Galadini et al., 2000; Valensise & Pantosti, 2001). The

Quaternary activity of normal faults is documented by the displacement of fluvio-lacustrine deposits filling intermontane basins (Galadini, 1999) and by historical earthquakes that affected the area (e.g., 1703 $M_w$ 6.8 L'Aquila earthquake; 1915 $M_w$ 7.1 Avezzano earthquake; 2009 $M_w$ 6.1 L'Aquila earthquake; Rovida et al., 2020). In the last 25 years, paleo-seismological and geophysical analyses focused on the mapping and assessment of the seismic hazard associated with these active faults. These interdisciplinary studies also yielded information about the length, Quaternary throw, slip rate and earthquake recurrence intervals of the faults (e.g., Barchi et al., 2000; Calamita et al., 2000; Falcucci et al., 2016; Galadini et al., 2003; Galadini & Galli, 2000; Morewood & Roberts, 2000; Pizzi et al., 2002; Roberts & Michetti, 2004). Field structural investigations of the major (up to 15-20 km long) exhumed seismogenic fault surfaces cutting carbonate rocks documented, in several cases, the presence of a belt of up to hundreds meter-thick damage zones bounding meter-thick fault cores (Caine & Forster, 1999) accommodating most of the cumulative displacement (Agosta & Aydin, 2006; Ferraro et al., 2019; Fondriest et al., 2020) and containing multiple cm- to mm-thick principal slip zones cut by sharp (where karstified) or polished to "mirror-like" (where fresh) slip surfaces (Fondriest et al., 2013, 2015, 2017; Siman-Tov et al., 2013).

Recent paleo-seismological, geological and geomorphological observations pointed out that some outcropping sharp scarps cutting the central Apennines carbonate rocks, commonly interpreted as surface expression of seismic faulting, can also accommodate DGSDs (Moro et al., 2009, 2012; Gori et al., 2014). Indeed, photogeological and field analyses allowed for the identification of several geomorphological features commonly associated with a DGSD (i.e., double crest lines, scarps and counterslope scarps, slope-parallel trenches and open fractures; Figs. 1.3, 3.2). Such morphological features are the expression of near-surface deformation at the hillslope scale (e.g., their spacing is of the order of tens of meters) and are not expected to be produced by listric normal faults. In fact, some minor and major normal faults in the central Apennines are inferred to bend from dip angles of 45-70° at the surface to sub-horizontal at 2 to 10 km depth (Barchi et al., 2000; Valoroso et al., 2014). As a consequence, the deep-seated deformation accommodated by listric faults is manifested at a larger wavelength (e.g., the spacing between intra-mountain basins is of the order of hundreds of meters to kilometers, D'Agostino et al., 1998) than the meso-structures associated with DGSDs. Furthermore, most of the slip surfaces of the analyzed DGSDs in central Apennines affect the upper portion of the hillslope and are less than 1 km long along-strike. Their trenches and scarps commonly show an arcuate shape at the tips and are not geometrically linked to other structures, thus indicating a possible

lateral confinement of the DGSD body (Moro et al., 2009; Figs. 1.3, 3.2). Instead, seismogenic normal faults in central Apennines are up to 10 km long along-strike (Barchi et al., 2000; Boncio et al., 2004; Falcucci et al., 2015), commonly arranged in *en-échelon* patterns, and do not show evidence of lateral confinement.

In the central Apennines, the slip surfaces associated with DGSDs and faults, respectively, should be exhumed from different depths (0 to a few hundred meters for DGSDs, 0 to 3 km for active faults; Agosta & Kirschner, 2003), and active over a different range of (1) temperatures (< 15°C for DGSDs, 0-60°C for faults assuming a geothermal gradient of ~ 20°C/km, typical for the central Apennines; Mancinelli et al., 2019), (2) lithostatic pressure (< 15 MPa for DGSDs, 0-80 MPa for faults) and (3) slip rates (usually < mm/s for DGSDs, up to ~ 1 m/s for seismic faults). Such large differences in loading conditions should result in the formation of distinctive secondary fault/fracture networks, possibly recognizable at the outcrop scale, and microstructures of the slip zones.

In this paper, we discuss four cases of DGSDs located in the footwall of active seismogenic normal faults and one case of a normal fault bordering a relatively small intermontane basin (Italian central Apennines, Figs. 1.3, 3.1, 3.2). We analyzed the fracture network in the footwall of the major slip surfaces and compared the microstructures of the slip zones of the DGSDs with the ones of the associated seismic normal faults. Based on the evidence reported in our study, meso-scale structural data and micro-structural analyses alone do not allow us to distinguish between structures associated with normal faults or DGSDs. Indeed, the ambient conditions at which DGSDs and near surface tectonic faulting occur are partially overlapping. However, the analysis of meso- to micro-structural dataset may allow us to (1) interpret how DGSD commonly form in central Apennines, and (2) identify the deformation mechanisms associated with the evolution of DGSDs in space and time.

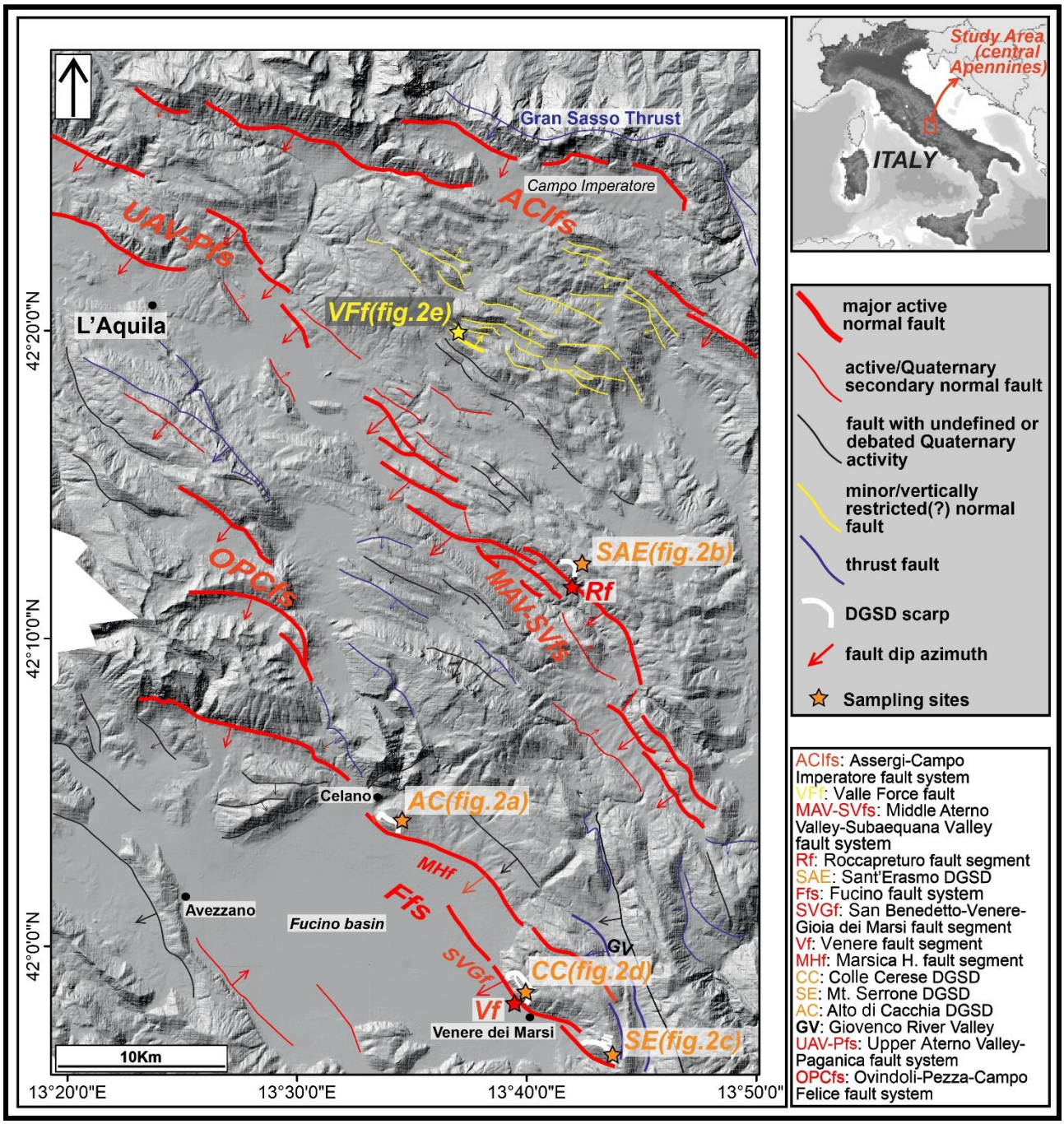


Figure 3.1: Structural scheme of the study area. Major active normal faults (thick red lines): Assergi-Campo Imperatore fault system (Galli et al., 2008); Middle Aterno Valley-Subaequana Valley fault system (Falcucci et al., 2015); Fucino fault system (Galadini & Galli, 1999); Upper Aterno Valley-Paganica fault system (Moro et al., 2013); Ovindoli-Pezza-Campo Felice fault system (Pantosti et al., 1996). Minor vertically restricted normal faults (black in color) are from D'Agostino et al. (1998) and Falcucci et al. (2015). Deep-seated Gravitational Slope Deformations (DGSDs) are widespread in this region, as well as in all the Apennines (see main text for the references). DGSDs analyzed in this work are shown in this figure. Alto di Cacchia, Sant'Erasmo, Colle Cerese and Mt. Serrone DGSDs (White in color) are all located in the footwall of major active normal faults; Valle Force fault (yellow in color) is ~ 2 km long along-strike. Stars indicate the sampling sites of the studied slip zones (next figures).

## 3.2 Geological setting

The structural setting of the central Apennines is the result of the superposition of three main tectonic phases. From the Late Triassic to the Middle Jurassic, an extensional phase affecting the whole Central-Mediterranean area related to the opening of the Liguria-Piedmont Ocean (Western Tethys), led to the fragmentation of the Adriatic plate paleo-margin. The diffuse normal faulting brought to drowning of some sectors of the carbonate platforms and to the formation of basins (e.g., Carminati & Doglioni, 2012; Castellarin et al., 1978; Cosentino et al., 2010). In the Late Miocene, the platform areas were involved in the Apennine orogenesis, caused by the NE-verging convergence between the Adriatic and European plates (Carminati et al., 2012). The study area represents a platform carbonate sector of the Adriatic plate paleo-margin that was involved in the Apennine orogenesis. The slab-rollback of the subducting Adriatic plate caused the back-arc opening of the Tyrrhenian Sea and the migration towards E-NE of the Apennine fold-and-thrust belt (Carminati et al., 2012; Cipollari et al.,1999a; Doglioni, 1995; Malinverno & Ryan, 1986; Vezzani & Ghisetti, 1998). From the Pliocene until present days, extensional tectonics accommodated the migration of the chain towards E-NE. In the central Apennines, this extensional phase started in the Middle Pleistocene. The extension is accommodated by normal faults that cut and locally exploit the inherited Miocene-Early Pleistocene thrusts and the earlier Mesozoic normal faults (Elter et al., 1975; Vezzani et al., 2010). The extensional Plio-Quaternary activity was responsible for the formation of numerous intermontane basins, filled by lacustrine and alluvial deposits and bordered by large normal faults (Bosi et al., 2003; Cavinato et al., 2002; Fig. 3.1).

The main active faults strike NW-SE and dip towards SW, consistent with the NE-SW direction of extension (> 3 mm/yr of extension rate) documented by geodetic data (Serpelloni et al., 2005; D'Agostino et al., 2011), focal mechanisms (Chiaraluce et al., 2003) and borehole breakout data (Mariucci & Muller, 2003). These normal faults cut the pre-Miocene carbonate sequences (> 4 km of stratigraphic thickness in some areas, excluding thickening due to thrust activity, Tozer et al., 2002), and caused destructive earthquakes up to moment magnitude $M_w$ 7.1 (e.g., Avezzano 1915; Fig. 3.1).

### 3.2.1 Stratigraphic and geomorphological characterization of the study cases

The four DGSDs discussed in this work were selected because they include several morphological features commonly associated with deep-seated landslides and their major scarps strike with the same orientation of the large seismogenic faults they are associated

with. Moro et al. (2009, 2012) identified double-crested lines, scarps and counterslope scarps, slope-parallel trenches and open fractures associated with Colle Cerese and Mt. Serrone DGSDs, by means of Remote sensing, photogeological and geomorphological interpretations. The four DGSDs are described below based on their stratigraphic, geomorphic and geological setting; after that, a description of Valle Force normal fault is used for comparison.

**Alto di Cacchia DGSD.** "Alto di Cacchia" is a flat top hill (950 m a.s.l.) located a few km east of Celano town. The hill is about 500 m long along the NW-SE direction and is laterally confined to WNW by the Fucino Basin and to ESE by a fluvial incision. Alto di Cacchia hill is bordered to SW by the NW-SE oriented "Marsicana Highway" fault segment (MHf) (Galadini & Galli, 1999). The MHf, a segment of the Fucino seismogenic fault system, juxtaposes Cretaceous platform carbonates with Quaternary lacustrine deposits filling the Fucino Basin in the hangingwall (Fig. 3.2a). The DGSD affects the uppermost portion of the Cupoli unit (~ 120 m of maximum thickness), consisting of Early Pleistocene gravels intercalated with sands and silt that deposited in lacustrine and fluvial environments (Fig. 3.2a). The Cupoli unit both overlies and is in heteropic contact with the Aielli Conglomerates (~ 400 m thick and made of blocks of carbonate rocks within a silty and clayey matrix: Bosi et al., 2003; Bosi & Messina, 1991). The geomorphological structure of the Alto di Cacchia hillslope was interpreted by us as DGSD based on the following evidences: (1) the continental deposits of the Alto di Cacchia are cut by a curved and discontinuous but sharp scarp that borders a ~ 200 m wide and ~ 500 m long depression interrupting the regular sub-horizontal top of the hill; (2) the presence of scarps and trenches cross-cutting the sub-horizontal continental strata and a characteristic double-crested line topographic morphology typical of DGSDs (Figs. 1.3b, 3.2a); (3) the described landforms only affect the middle sector of the Alto di Cacchia, as no other lineaments or scarps affect the hill towards SE.

**Sant'Erasmo DGSD.** Sant'Erasmo DGSD is located just northwest of the Roccapreturo village, in the Middle Aterno River Valley. The sliding of the rock-mass along the NW-SE oriented major scarp (< 1 km long) produced an about 500 m wide depression on the top of the unstable slope associated with a series of uphill facing scarps (Fig. 3.2b). The lower one (< 400 m long) affects the western flank of the Mt. Acquaro, located in the footwall of the Roccapreturo normal fault segment (Fig. 3.2b), the longest segment of the ~

30 km-long Middle Aterno Valley-Subequana Valley fault system (Falcucci et al., 2011, 2015; Fig 3.1). The fault is about 10 km long along-strike, the estimated Quaternary displacement is about 270 m and the minimum slip rate and earthquake recurrence intervals range from 0.23 to 0.34 mm/yr and 5340 to 1758 yrs, respectively (Falcucci et al., 2015). A small depression (< 100 m wide) filled by Pleistocene-Holocene sub-horizontal breccias with pink-orange matrix, overlying Early Cretaceous platform carbonates ("Calcari a Rudiste e Orbitoline" fm.) dipping at ~ 25° to NE, is associated with this counterslope scarp (Figs. 1.3c, 3.2b). The large depression associated with the major scarp and the counterslope scarp partially arresting the sliding of the rock-mass have been interpreted as a morphological feature that indicates the presence of DGSD.

**Mt. Serrone DGSD.** Mt. Serrone DGSD, located just northeast of Gioia dei Marsi village, is a gravitational rock-mass deformation accommodated by several scarps affecting the western slope of Mt. Serrone (~ 1350 m a.s.l.). The major scarp accommodating the DGSD dips to NE, antithetically with respect to the San Benedetto-Gioia dei Marsi normal fault segment. The latter, which is part of the Fucino seismogenic fault system, borders the south-eastern sector of the Fucino Basin (Fig. 3.1, 3.2c). The depression associated with the DGSD (< 400 m wide) is filled with colluvial and talus deposits resulting from the erosion of the Cretaceous carbonates (average dip angles of ~ 20° to NE) of Mt. Serrone. The carbonate rocks are juxtaposed with the Val Roveto flysch by the thrust bordering the eastern side of Giovenco Valley (Fig. 3.1; Vezzani & Ghisetti, 1998). Here, several morphological features indicative of a DGSD, such as scarps and counterslope scarps, slope-parallel trenches, open fractures and alignments of NW-SE oriented small depressions have been identified through photogeological and field analyses (Moro et al., 2009, 2012).

**Colle Cerese DGSD.** "Colle Cerese" hill (~ 1100 m a.s.l.) is located just northeast of Venere village. An impressive double-crested ridge interrupts the regular morphological slope continuity of the hill towards the Fucino Basin (Fig. 3.2d). San Benedetto-Gioia dei Marsi fault segment (SGf, in this area called Venere sector) crops out at the base of the slope. The normal fault activity resulted in the uplift of the footwall and in its gravitational instability (Moro et al., 2009; Stramondo et al., 2005). The SGf (about 10 km long along-strike) re-activated at the same time of the "Marsicana Highway" fault and other faults belonging to the Fucino fault system during the 1915 $M_w$ = 7.1 Avezzano earthquake (Rovida et al., 2020).

The estimated maximum throw attributed to the SGf ranges between 800 m and 1300 m (Cavinato et al., 2002; Roberts & Michetti, 2004), suggesting a minimum slip rate of 0.24-0.29 mm/yr (Galadini & Galli, 1999). Colle Cerese hill is carved into Cretaceous platform carbonates, juxtaposed by the SGf with the Quaternary lacustrine deposits filling the Fucino Basin (Vezzani & Ghisetti, 1998). The large depression between the two ridge crests (> 1 km long and ~ 400 m wide) is filled with Pleistocene-Holocene fluvio-lacustrine and talus deposits (Moro et al., 2009; Figs. 1.3a, 3.2d). The double-crested ridge morphology is a clear evidence of a DGSD affecting Colle Cerese hill. Other evidences of gravitational deformation, such as counterslope scarps, slope-parallel trenches and open fractures, were described in Moro et al. (2012).

**Valle Force fault (normal fault bordering a small and narrow basin).** Valle Force fault (< 2 km in length along-strike) is one of the several NE dipping normal faults bordering small and narrow intermontane basins located in the area between Campo Imperatore basin, to NE, and Middle Aterno Valley, to SW (D'Agostino et al., 1998; Falcucci et al., 2015; Galadini & Messina, 2004; Fig. 3.1). This "Basin and Range" like area consists on NE dipping (dip angles of 25°-40°) antithetic normal faults bounding southward the tilted blocks, that likely detach onto a splay of the Gran Sasso thrust at relatively shallow depth (~ 2 km). The presence of a shallow-seated detachment fault is supported by the very limited dimensions of the blocks tilted by the fault (D'Agostino et al., 1998; Falcucci et al., 2015). Valle Force fault is located just north-east of Barisciano village (Fig. 3.2e). The fault juxtaposes the Mesozoic platform carbonates ("Calcari a Coralli e Diceratidi" fm.) forming the footwall ridge (~ 1200 m a.s.l.) with Pleistocene-Holocene colluvial deposits and Lower Pleistocene slope-derived calcareous breccias with pink matrix ("Brecce Mortadella" in Demangeot, 1965 or "Brecce di Fonte Vedice" in Bosi & Messina, 1991). The deposition of the "Brecce Mortadella" was coeval to the normal activity of the fault (D'Agostino et al., 1998).

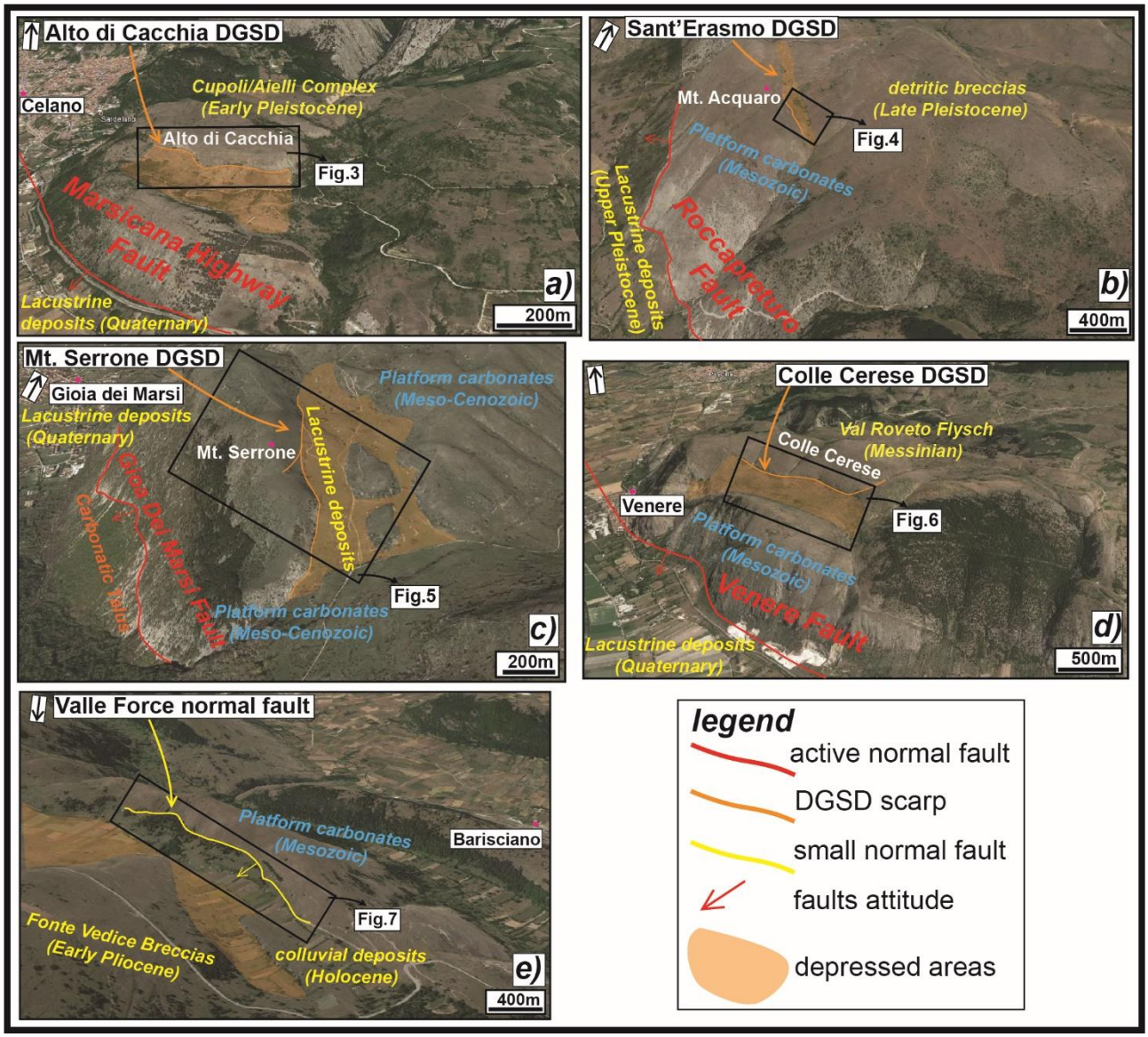


Figure 3.2: Panoramic view of the five case studies: a) Alto di Cacchia DGSD, located in the footwall of the "Marsicana Highway" normal fault segment; b) Sant'Erasmo DGSD, located in the footwall of Roccapreturo normal fault segment; c) Mt. Serrone DGSD, located in the footwall of San Benedetto-Gioia dei Marsi normal fault segment; d) Colle Cerese DGSD, located in the footwall of San Benedetto-Gioia dei Marsi normal fault segment (Venere sector); e) Valle Force normal fault, that borders a small and laterally confined basin. The lateral continuity of the DGSDs is limited compared to the associated faults. Images from Google Earth.

## 3.3 Methods

Photogeological and geomorphological analyses of the study area allowed us to identify peculiar structural features associated with DGSDs. The latter were investigated on the field by measuring the fracture network affecting the host rocks in the footwall of the major slip surfaces. We distinguished joints and shear fractures from open fractures or fissures and measured the attitude and kinematics (i.e., rake) of the major slip surfaces

when possible. The structural data were reported in topographic maps at 1:1000 scale, produced by exploiting the aerial photos (spatial resolution of 10x10 meters) provided by the Abruzzi Geoportal (http://geoportale.regione.abruzzo.it/Cartanet) and plotted as poles into a stereonet (Schmidt equal area, lower hemisphere). We measured the attitude of faults and fractures and their spatial distribution to infer the orientation of the principal stresses at the time of formation. In the case of Alto di Cacchia, Sant'Erasmo and Colle Cerese DGSDs and of the Valle Force fault, we also used high-resolution orthomosaics produced by stitching hundreds of pictures (we used Agisoft Metashape Pro and Pix4D software) taken at 100-150 meters from the ground with a drone (Phantom 4 Advanced and MAVIC 2 Pro).

With regards to rock samples, syton-polished thin sections of the slip zones associated with the major and secondary slip surfaces have been produced by cutting the samples perpendicular to the slip surface and parallel to the slip direction (where recognizable, otherwise along the dip direction). The thin sections were photo-scanned at high resolution (4000 dots per inch) both in plane and in cross polarized nicols and then observed under the Optical Microscope (OM). The scans of the thin sections were edited using specific tools by Adobe Photoshop (Ps) to highlight the shape of the clasts, the presence of minor fractures and veins and the texture of the fine matrix surrounding the clasts.

Most of the thin sections were investigated for microstructural analysis with the Scanning Electron Microscope (SEM) CamScan MX3000 (resolution 300 nm in back-scatter electrons) installed at "Dipartimento di Geoscienze" (Padua Univ.) and with the Field Emission SEM (FESEM) Merlin Zeiss (resolution 200 nm in back-scatter electrons) installed at CERTEMA laboratory (Grosseto, Italy). Pictures were taken in backscattered electron (BSE) mode with an acceleration voltage of 8-10 kV and at a working distance of 4.7-6.1 mm.

## 3.4 Results

### 3.4.1 Structural architecture

In this section, we present structural data (i.e., fault and fractures) collected in the footwall of the five case studies over the entire length of the major scarp. Fractures are distinguished in: 1) **fractures** *sensu strictu* or joints (i.e., extensional fractures that do not exhibit noticeable shear displacement between the fracture surfaces), shear fractures (i.e., small mesoscale fractures accommodating very limited displacement parallel to the fracture surfaces, commonly arranged as conjugate pairs, and with no visible damage zone in the field) and hybrid fractures, a combination of the first two types (Engelder, 1987; Pollard & Aydin, 1988; Fossen, 2010); 2) **slip surfaces** or sharp scarps with associated slip zone and damage zone beneath; 3) **open fractures or fissures** (i.e., joints with > 1 cm of aperture between the two opposite fracture surfaces), locally filled by unconsolidated soil deposits (e.g., Figs. 3.3e, 3.5f, 3.6e). The spatial arrangement of joints, shear fractures, hybrid fractures and fissures allowed us to assess the thickness of the footwall damage zone and to infer the eigenvectors of the stress tensor.

**Alto di Cacchia (DGSD affecting Pleistocene deposits).** Alto di Cacchia DGSD is limited by a ~ 500 m long and discontinuous sharp scarp dipping on average ~ 70° and crosscutting sub-horizontal (dip angles from 4° to 15°) conglomerates mainly dipping towards NNW-NNE (Figs. 3.2a, 3.3a-e). The scarp is karstified and locally smoothen by the rainwater flow. Close to the south-western tip the scarp is about 1 m high, whereas in the north-western tip the scarp has a lateral continuity of ~ 100 m and is up to 3 m high (Fig. 3.3b, d). Here, the slip surface is sharp with some more polished patches, and shows slickenlines plunging 80° East (almost pure normal dip-slip, Fig. 3.3d). Two smaller scarps, less than 1 m high and ~ 50 m long, outcrop discontinuously within the upper depression of the DGSD (Fig. 3.3c, f). Patches of less cemented Holocene deposits filling the upper depression lean on these scarps and locally preserve them from weathering (Fig. 3.3f).

The sub-horizontal cemented conglomerates outcropping in the footwall of the major scarp are cut by fissures (from 1 to 12 cm of aperture) dipping > 70° and, to a less extent, by fractures. The strike of the open fissures is very scattered (stereonets in Fig. 3.3a) and the surfaces of the largest fractures locally mimic the shape of the largest pebbles of the conglomerate (Fig. 3.3e). The smallest open fractures are filled by recent unconsolidated soil deposits.

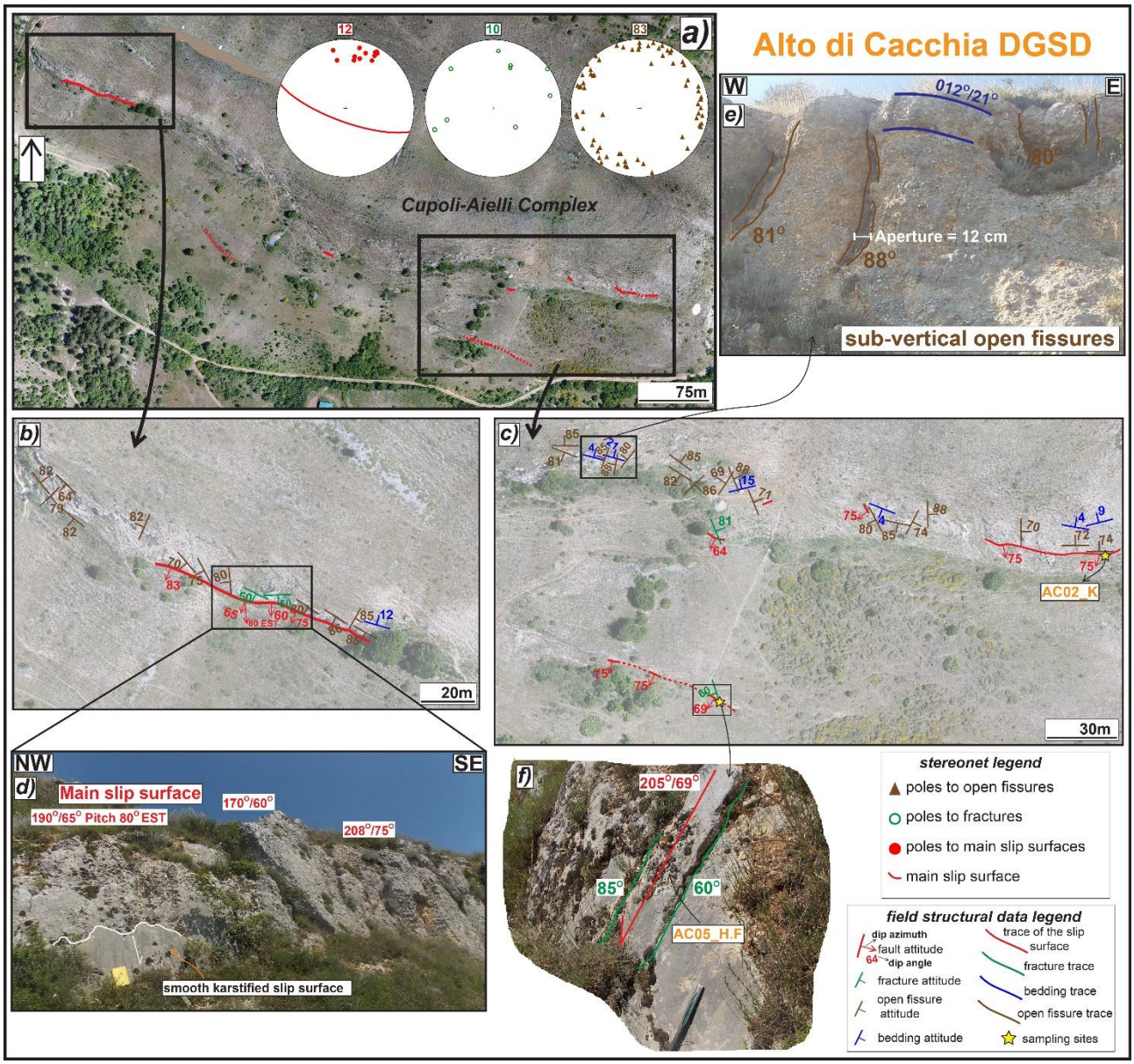


Figure 3.3: structural sketch map of Alto di Cacchia DGSD. a) Orthomosaic of the major and secondary scarps crosscutting the flat top hill carved into Pleistocene conglomerates. b) Zoom on the north-western tip, where the major karstified scarp outcrops for ~ 100 m of length along-strike, locally appearing smooth (d). c) Zoom on the south-eastern sector, where a secondary hangingwall sharp scarp outcrops for ~ 50 m, including patches of Holocene sediments leant on the surface (f) (Sample AC05_H.F). e) Sub-vertical open fissures crosscutting sub-horizontal conglomeratic strata; the surfaces delimiting the fractures partially mimic the morphology of the largest pebbles. The attitude of the structural data is reported as dip azimuth/dip angle or only as dip angle.

**Sant'Erasmo (DGSD in the footwall of a main seismogenic fault)**. Sant'Erasmo DGSD is located in the footwall of Roccapreturo seismogenic normal fault segment and is limited by a ~ 700 m long major scarp striking NW-SE, sub-parallel and synthetic to the Roccapreturo fault (Fig. 3.2b). The field work was conducted on the small counterslope

scarp (< 400 m long along-strike and up to 3 m high) affecting the eastern slope of Mt. Acquaro and bordering a small depression filled by Pleistocene breccias and colluvial deposits (Figs. 3.2b, 3.4a). The counterslope scarp is strongly karstified and displaces Cretaceous platform carbonates with average dip angles of ~ 70°. In the hangingwall of the scarp, small secondary sub-vertical sharp scarps cut the Pleistocene breccias forming small trenches (Fig. 3.4b). In the footwall, the platform carbonates are intensely fractured (in some parts brecciated; Fig. 3.4c) by joints and shear fractures and, to a less extent, by open fractures (tens of centimeters long and up to 5 cm of aperture; stereonets in Fig. 3.4a). The attitude of both fractures and open fissures is scattered with dip angles ranging from 88° to 15° (Fig. 3.4a). However, most of the shear fractures are arranged in two main conjugate sets striking ca. NE (Fig. 3.4a, d).

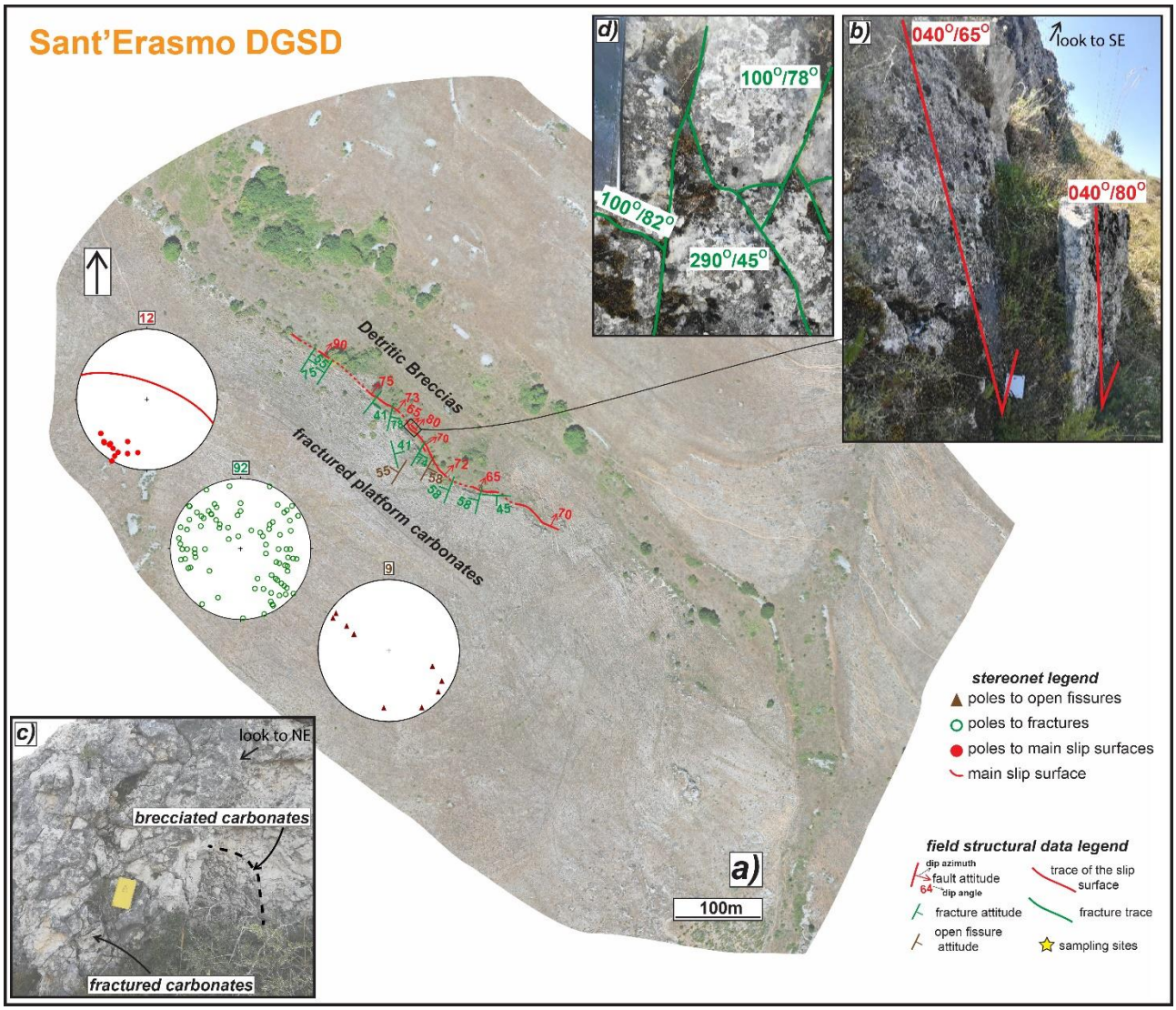


Figure 3.4: structural sketch map of the counterslope scarp delimiting to SW the Sant'Erasmo DGSD. a) Orthomosaic of the scarp juxtaposing Cretaceous fractured limestones with Pleistocene-Holocene detritic

breccias. b) Major sharp scarp with associated a secondary sub-vertical hangingwall scarp cross-cutting the breccias and forming a gravitative trench. c) Fractured footwall carbonates, locally appearing as brecciated. d) Conjugate shear fractures affecting the major slip surface. The attitude of the structural data is reported as dip azimuth/dip angle.

**Mt. Serrone (DGSD in the footwall of a main seismogenic fault)**. This DGSD affects the eastern slope of Mt. Serrone and is limited by a ~ 500 m long sharp scarp displacing sub-horizontal Mesozoic platform carbonates antithetically with respect to San Benedetto-Gioia dei Marsi normal fault (Figs. 3.2c, 3.5a-c). In the middle sector, the scarp is exposed continuously for ~ 200 m along-strike and up to a maximum height of ~ 3 m and dip angles of ~ 50° (Fig. 3.5a, d). Towards south-east, the strike of the scarp rotates from NW-SE to NNW-SSE and steps dextrally to SE. The right-stepped segment is more karstified and dips of ~ 65° to the NE (Fig. 3.5e), similarly to the north-eastern termination of the scarp. Patches of Holocene poorly cemented deposits filling the upper depression of the DGSD are leant on the slip surface of the left stepped segment (Fig. 3.5e). In the relay zone between the N-S and NW-SE oriented scarps, several meter-long sub-vertical fissures (up to 15 cm of aperture) crosscut the carbonate rocks (Fig. 3.5f). As for Sant'Erasmo DGSD case, the shear fractures are arranged into conjugate sets striking at N280°-330° with scattered dip angles (from sub-vertical to sub-horizontal: stereonets in Fig. 3.5a).

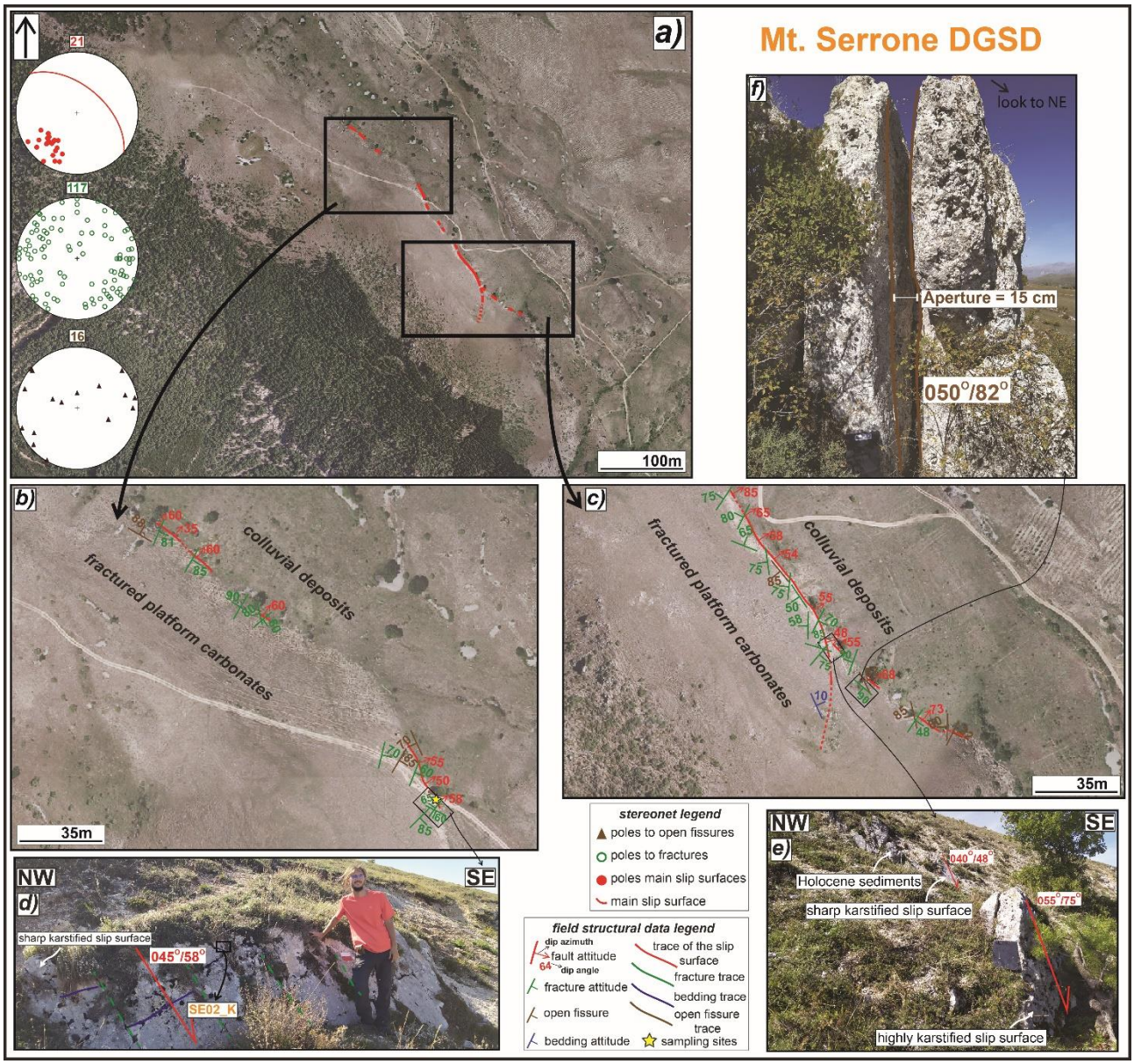


Figure 3.5: structural sketch map of Mt. Serrone DGSD. a) Orthomosaic of the major scarp affecting the north-eastern slope of Mt. Serrone, carved into Mesozoic platform carbonates. b) Zoom on the middle to north-western portion. c) Zoom on the middle to south-eastern portion, where the scarp dextrally steps. d) Detail of the sharp scarp in the middle sector cutting NE dipping carbonates with dip angles of ~ 45° (Sample SE02_K). e) Dextral step between the N-S oriented sharp scarp, locally covered by patches of Holocene cemented sediments, and the much more karstified NW-SE oriented scarp. f) Large sub-vertical fissure affecting the carbonate rocks in the step-over zone. The attitude of the structural data is expressed as dip azimuth/dip angle.

**Colle Cerese (DGSD in the footwall of a main seismogenic fault)**. Colle Cerese DGSD is located in the footwall of San Benedetto-Gioia dei Marsi normal fault segment, in the Venere sector, and is limited by an about 1.5 km long sharp scarp striking NW-SE (Figs. 3.2d, 3.6a). The field work was conducted in the south-eastern sector of the scarp (Fig. 3.6b). Here, the major slip surface juxtaposes Mesozoic platform carbonates with

Pleistocene colluvial deposits and unconsolidated breccias filling the large depression. The scarp dips to SW with dip angles of ~ 45°, locally reaching over 10 m of height (Fig. 3.6c). Patches of more cemented hangingwall breccias are leant on the slip surface and locally preserve it from weathering (Fig. 3.6c, d). A 4-5 cm thick white in color fresh scarp exposure is locally recognized (i.e., "*nastrino*" or ribbon-like scarp; Fig. 3.6d). The sub-horizontal carbonate strata are intensely fractured close to the major scarp, but if analyzed at a distance of tens of meters away, they are cut by few small sub-vertical joints and open fractures (Fig. 3.6e). As in Sant'Erasmo and Mt. Serrone DGSDs, fractures are arranged in conjugate sets striking N290°-340° with scattered dip angles (from sub-vertical to sub-horizontal: see stereonets and Fig. 3.6f).

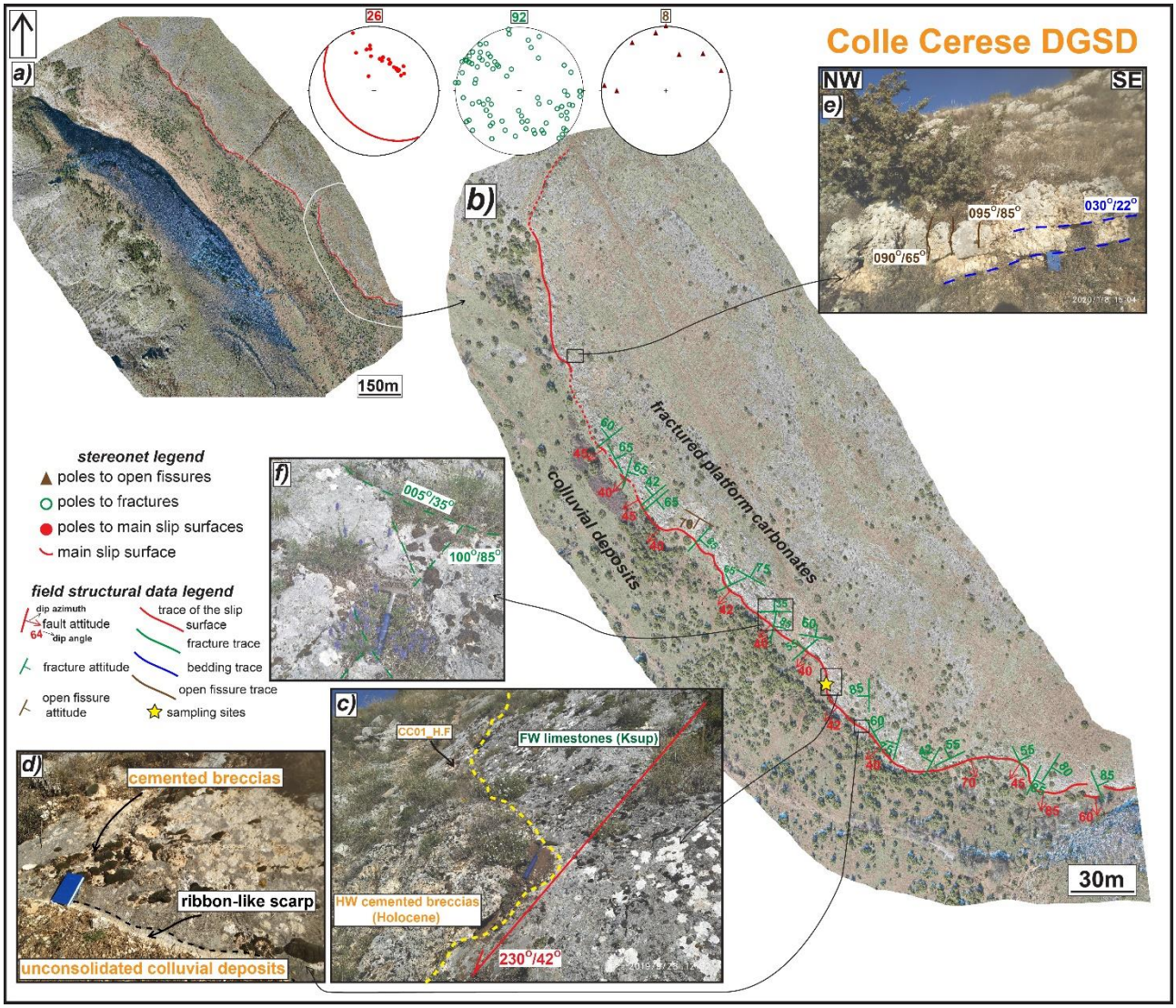


Figure 3.6: structural sketch map of Colle Cerese DGSD. a) Orthomosaic of the major scarp affecting the south-western slope of Cerese Hill. b) Zoom on south-eastern sector, where the sharp scarp juxtaposes Cretaceous platform carbonates with Holocene breccias and colluvial deposits with average dip angles of ~

45° (c) (Sample CC01_H.F). d) Detail of the sharp slip surface, locally preserved by patches of cemented breccias, with ~ 5 cm thick fresh exposure (i.e., ribbon-like scarp). e) Sub-vertical fissures crosscutting the sub-horizontal carbonate-built strata in footwall. f) Conjugate shear fractures affecting the slip surface. The attitude of the structural data is reported as dip azimuth/dip angle.

**Valle Force (minor and vertically confined normal fault).** Valle Force normal fault has a very sharp scarp constantly outcropping for about 1.5 km along-strike, up to 8 m of high in the middle sector, with dip of ~ 50° (Fig. 3.7a-c, e). The fault juxtaposes Cretaceous platform carbonates with colluvial deposits filling the basin (Pleistocene-Holocene in age) and Lower Pleistocene calcareous breccias. Close to the north-western tip, secondary hangingwall scarps dipping to SW with dip angles of 60°-80°, sub-parallel to the major one, displace the Pleistocene breccias, possibly associated with a gravitational instability (Fig. 3.7d). Just south-east along-strike, the fault scarp steps dextrally and deforms the breccias in the relay zone (Fig. 3.7e). In the middle sector of the fault, patches of the hangingwall breccias cover the major scarp, thus preserving the fault core (Fig. 3.7f). Where the breccias are removed, the fault surface is ultra-polished (Fig. 3.7f). As for Sant'Erasmo, Mt. Serrone and Colle Cerese DGSDs, a large number of joints and shear fractures cut the fault surface and the footwall carbonates that sporadically outcrops along the fault strike (stereonets in Fig. 3.7a). Most of the shear fractures are arranged in conjugate sets dipping on average (dip angle/dip azimuth) 60°/N260°-300° and 60°/N130°-180° (Fig. 3.7g). The dip angle of both shear fractures and open fissures is quite scattered, ranging from 80° to 45° (Fig. 3.7a, g).

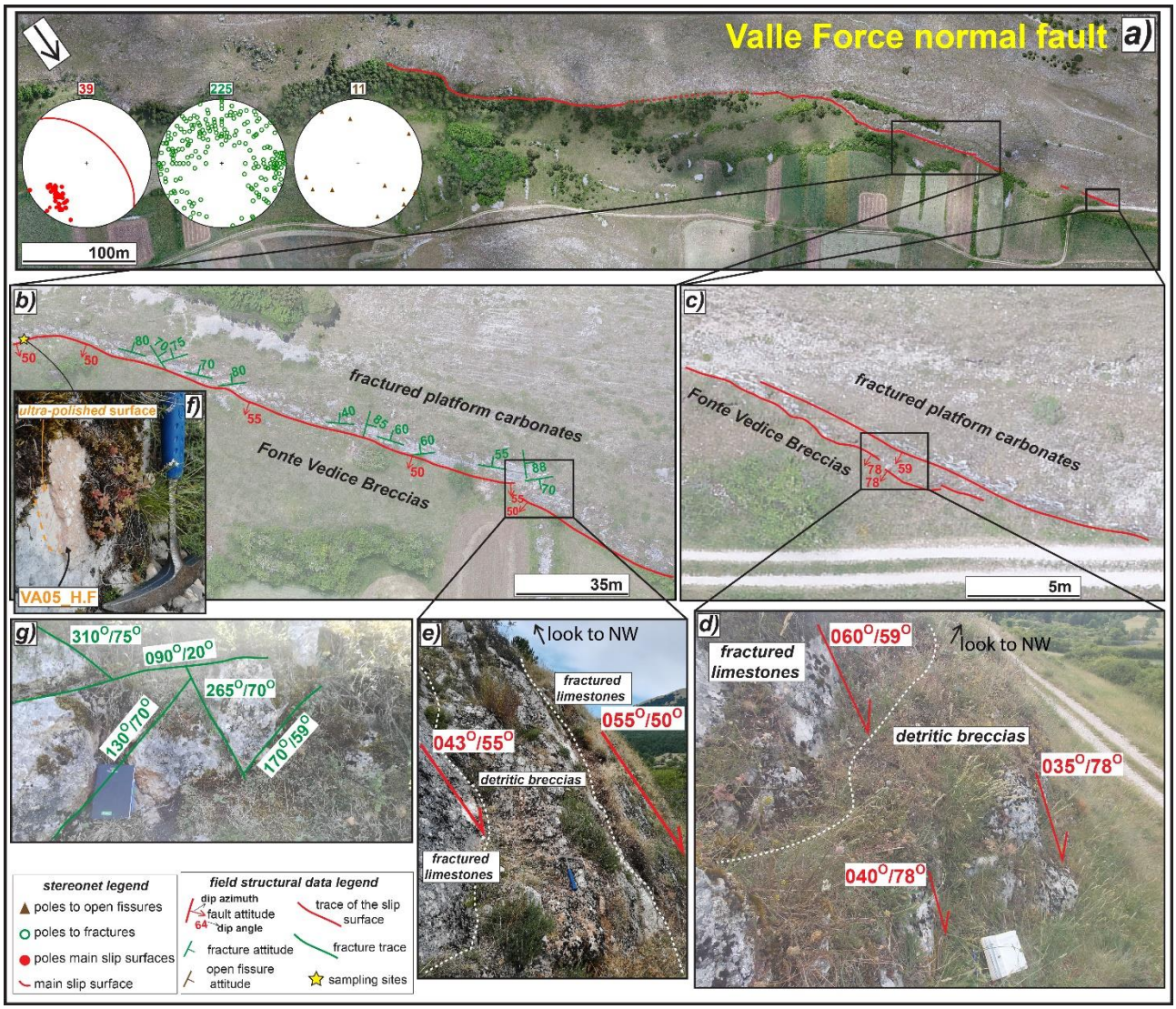


Figure 3.7: structural sketch map of Valle Force normal fault. a) Orthomosaic of the main scarp juxtaposing Cretaceous limestones with Lower Pleistocene breccias and Holocene deposits. b) Zoom on the sharp fault scarp where it steps dextrally involving the hangingwall breccias in the relay zone (e). c) Zoom on the north-western tip, where secondary high angle scarps crosscut the hangingwall breccias (d). f) Patch of hangingwall breccias on the slip surface. The latter appears as ultra-polished where the breccias are removed (sample VA05_H.F). g) Conjugate shear fractures affecting the fault scarp with different attitude. The attitude of the structural data is reported as dip azimuth/dip angle.

## 3.4.2 Microstructures of the slip zones

The microstructures observed in the slip zones associated with the five selected field cases are described below following the fault rocks classification of Sibson (1977; Figs. 3.8-3.11). In addition, the microstructures of the slip zones of two major fault scarps of San Benedetto-Gioia dei Marsi and Roccapreturo large normal faults are used as comparison (Fig. 3.12). We define as **slip surfaces** the exposed karstified scarps and the scarps preserved by the Quaternary hangingwall sediments. The **slip zones** are the deformed

rocks, up to several centimeters thick, located beneath the slip surfaces. Slip zones accommodate shear strain during fault slip; 3) **Principal Slip Zones (PSZs)** are texturally distinct layers, usually < 1 cm thick, located in the slip zone immediately beneath the slip surface. PSZs accommodate most of fault displacement (Sibson, 2003).

**Alto di Cacchia (DGSD affecting Pleistocene deposits).** The slip zone in the footwall of the major scarp of Alto di Cacchia DGSD has a cataclastic fabric made of sub-parallel and several mm thick cataclastic and proto-cataclastic layers (sample AC02_K, Fig. 3.8a). The slip zone is composed of few cm in size sub-rounded clasts and several mm in size angular-to-rounded particles, locally fractured, immersed in a dark fine matrix. Close to the slip surface, a ~ 2 mm thick and discontinuous cataclastic layer made of < 1 mm in size angular to sub-rounded grains was identified (Fig. 3.8a). Under the Scanning Electron Microscope, the fine dark matrix of this layer is mostly composed of up to 5 μm in size calcite grains with straight boundaries forming triple junctions or separated by sub-micrometric in size pores and grains of apatite or clay minerals with euhedral habit (Fig. 3.8b). However, some calcite grain boundaries have irregular and stylolitic-like aspect, suggesting grain indentation (white arrows in Fig. 3.8b).

The slip zone located in the footwall of the secondary hangingwall scarp has a more "mature" cataclastic fabric (sample AC05_H.F). In fact, sub-rounded and fractured mm in size clasts and sub-mm in size angular clasts of the footwall rocks are dispersed in a dark-brownish in color fine matrix, that becomes more abundant (> 60% in volume) towards the slip surface (Fig. 3.8c). The latter is slightly undulated and has a sharp contact with the underlying calcite clasts (Fig. 3.8c, d). The PSZ right beneath the slip surface is about 1 mm thick and made of sub-millimetric in size clasts immersed in a darker fine matrix (Fig. 3.8d). The matrix of the PSZ is composed of packed calcite micro-grains with faint to straight grain boundaries forming triple junctions and by few clay minerals (SEM image, Fig. 3.8e). The hangingwall rocks are separated from the footwall rocks by a 1-2 mm thick and continuous grey in color layer made of sub-millimetric in size calcite grains partially dissolved by karst processes and possibly deriving from the underlying PSZ (Fig. 3.8c). This origin of the calcite grains is also suggested by the convoluted contact of the PSZ with the hangingwall rocks. The latter are formed by dm-to-cm in size rounded carbonate clasts, almost fracture-free, cemented by the precipitation of a porous and ochre in color matrix (Fig. 3.8c, d). This microstructure suggests that the hangingwall rocks were cemented *in-situ* and partially protected the scarp surface from weathering.

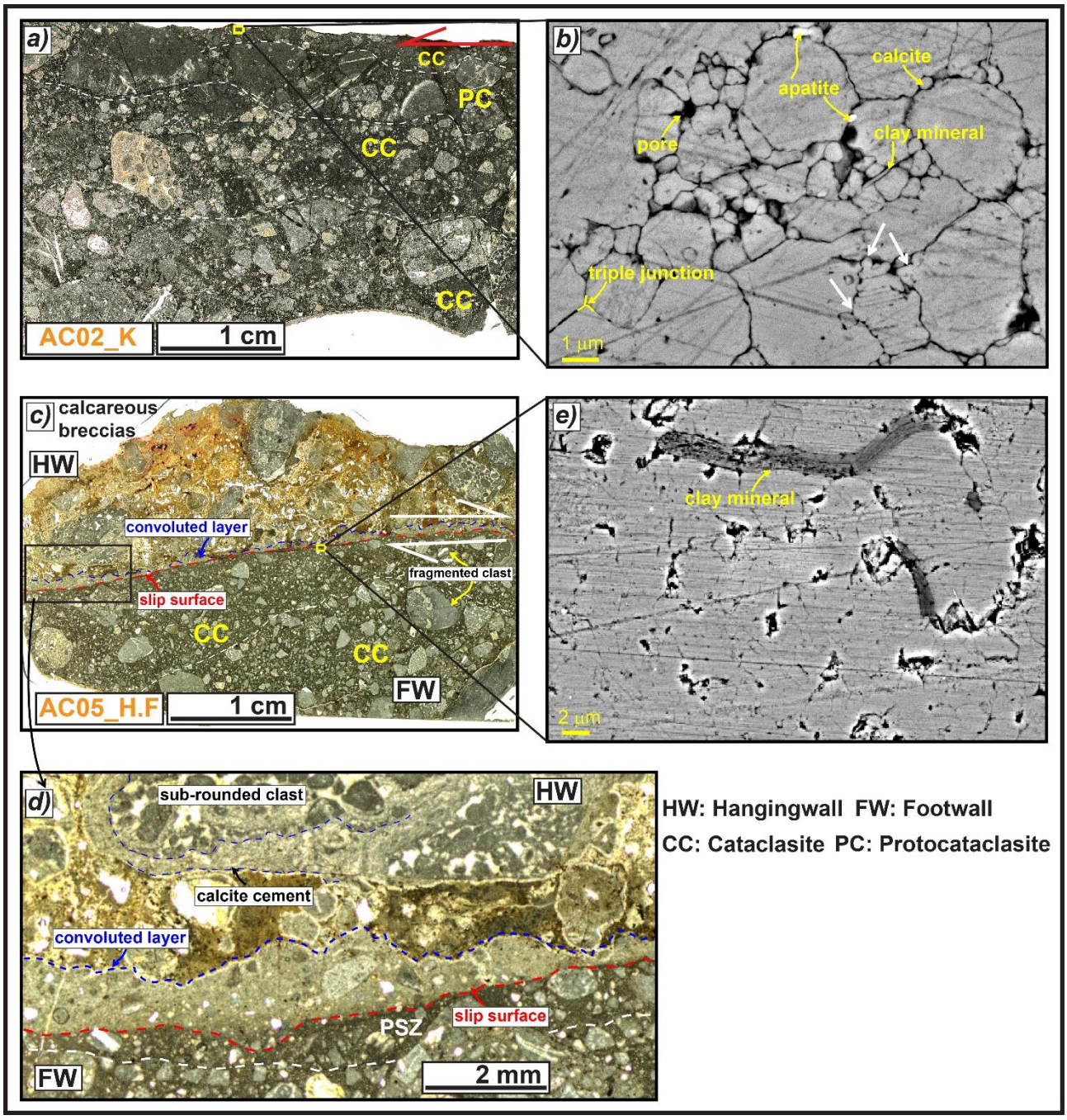


Figure 3.8: microstructures of the slip zones relative to the major and secondary scarps of Alto di Cacchia DGSD. a) Slip zone of the major scarp, made of sub-parallel cataclastic and proto-cataclastic layers, that are difficult to identify in the upper side because of the dark color at optical microscope of both fine matrix and larger clasts (sample AC02_K). b) SEM image of the fine matrix on the top, formed by packed calcite micro-grains separated by sub-micrometric in size pores and grains of apatite or clay minerals. The grain boundaries are straight, locally forming triple junctions, but at some points irregular, suggesting grain indentation (white arrows). c) The wall of the secondary scarp includes a well-developed cataclasite in the footwall and fracture-free, cemented calcareous breccias in the hangingwall (sample AC05_H.F). d) The footwall cataclasite includes a < 1 mm thick PSZ, separated by the hangingwall rocks by a 1-2 mm thick convoluted layer possibly produced by dissolution and precipitation-cementation of the underlying PSZ. e) SEM image of the matrix from

the PSZ, composed of packed calcite micro-grains with faint to straight grain boundaries and including clay minerals.

**Sant'Erasmo (DGSD in the footwall of a main seismogenic fault)**. The slip zone located in the footwall of the counterslope scarp delimiting to SW the Sant'Erasmo DGSD is a crush breccia to proto-cataclasite formed by cm-to-mm in size rounded clasts immersed in a fine and porous matrix. The slip zone is cut by minor fractures sub-parallel and sub-orthogonal to the slip surface (samples SAE02_K and SAE01_K, Fig. 3.9a, c). The fine reddish matrix of the hangingwall breccias fills the fractures located right beneath the slip surface and is part of a discontinuous cataclastic layer (< 5 mm thick) located between the proto-cataclasite and the slip surface (Fig. 3.9c). This discontinuous layer is made of sub-cm and sub-rounded clasts with the long axis oriented sub-parallel to the slip direction, immersed in a brownish ultra-fine matrix (Fig. 3.9c). The matrix is very porous and is mostly composed of sub-micrometric to micrometric in size grains of calcite and clay minerals (Fig. 3.9b). Calcite grains have straight boundaries, locally forming triple junctions, but indentations and sutured contacts are also observed (Fig. 3.9b; left side of Fig. 3.9d). The fine matrix is cut by calcite veins, with pore spaces locally filled by apatite crystals (right side of Fig. 3.9d).

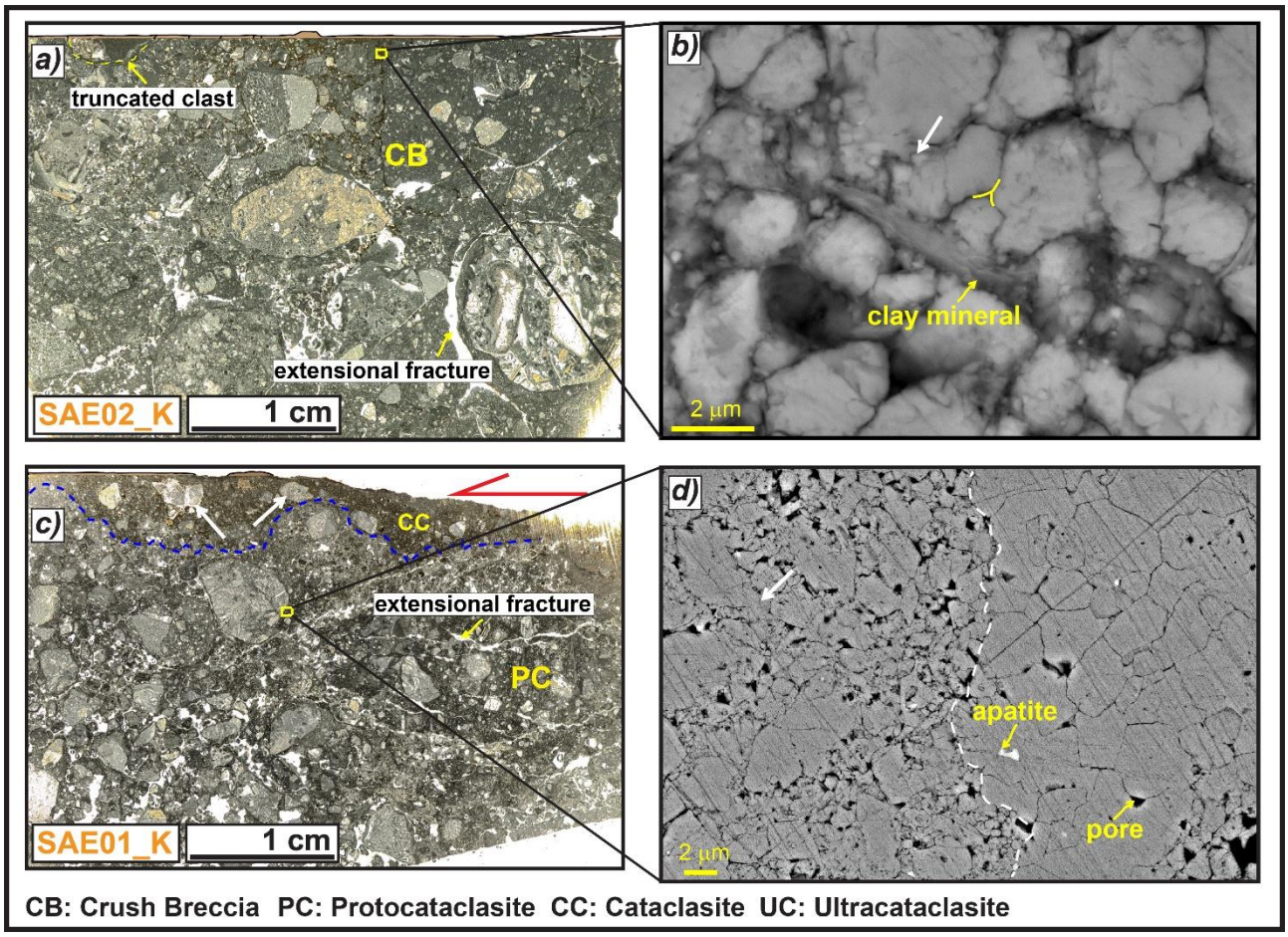


Figure 3.9: microstructures of the slip zone of Sant'Erasmo DGSD. a) Thin section scan of the slip zone, a crush breccia formed by cm-to-mm in size rounded clasts (the slip surface was drawn because it was cut by the scanner) (sample SAE02_K). b) SEM image of the hangingwall matrix filling the fractures right beneath the slip surface, composed of packed calcite micro-grains, with straight to irregular boundaries (white arrow) and clay minerals partially filling the pore spaces. c) Thin section scan of the slip zone where it is found a cataclastic layer close to the slip surface, due to the involvement of the hangingwall matrix during shearing, composed of < 1 cm in size sub-rounded clasts locally oriented with the long axis sub-parallel to the slip surface (white arrows) (sample SAE01_K). d) The porous matrix (left side to the dashed line) is composed of calcite micro-grains with straight contacts, locally indented (white arrow), and is cut by veins of calcite, with pore spaces locally filled by apatite crystals (right side).

**Mt. Serrone (DGSD in the footwall of a main seismogenic fault)**. As for the previous cases, the slip zone of Mt. Serrone DGSD has a cataclastic fabric composed of cm-to-mm in size angular to sub-rounded clasts immersed in a dark ultra-fine matrix (sample SE01_K, Fig. 3.10a). The largest clasts are fractured and have a sharp contact with the slip surface, that appears rough and karstified, suggesting possible dissolution by weathering processes (Fig. 3.10a). The fine matrix is made of sub- to micrometer (> 2 μm) in size calcite grains with straight to stylolitic-like boundaries, locally forming triple junctions; indentation structures are very common (Fig. 3.10b).

**Colle Cerese (DGSD in the footwall of a main seismogenic fault)**. The main slip zone accommodating Colle Cerese DGSD is a proto-cataclasite consisting of cm-to-mm in size fragmented angular clasts immersed in a dark in color ultra-fine and porous matrix (< 40% of the total volume; sample CC01_H.F, Fig. 3.10c). Though in the matrix some sort of grain packing is still recognizable (clast indentation, grain boundaries forming triple junctions, etc.), the slip zone right beneath the slip surface is weathered, as suggested by the occurrence of pores possibly resulting from meteoric exposure and biogenic activities (Fig. 3.10d). The slip surface is rough and covered by a Holocene calcareous breccia. The latter is formed by large in size (> 5 cm) rounded pebbles cemented by a brownish to white in color calcite-rich matrix and by sparite (Fig. 3.10c).

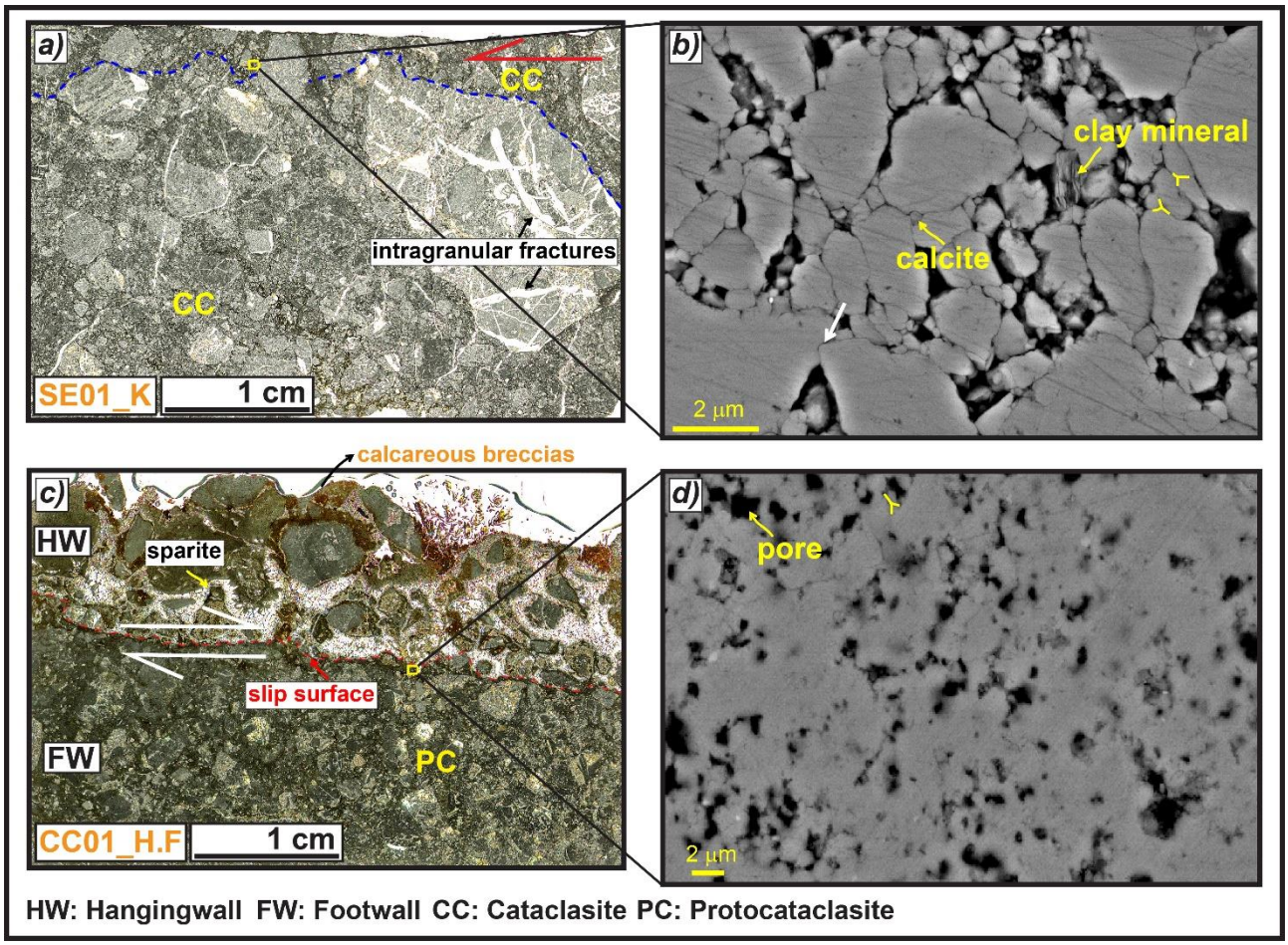


Figure 3.10: microstructures of the slip zones of Mt. Serrone and Colle Cerese DGSDs. a) The slip zone of Mt. Serrone DGSD has a cataclastic fabric composed of cm-to-mm in size angular clasts, internally fractured, surrounded by a dark-grey fine matrix (sample SE01_K). b) SEM image of the matrix close to the slip surface, composed of calcite micro-grains, with straight to stylolitic-like boundaries forming triple junctions and indentation structures (white arrow). The empty spaces among the grain boundaries are locally filled by clay minerals. c) Thin section scan of the scarp wall of Colle Cerese DGSD: a quite rough slip surface delimits a

proto-cataclasite made of calcareous angular to sub-rounded clasts in the footwall with Holocene calcareous breccias cemented by sparite in the hangingwall (sample CC01_H.F). d) The fine calcite matrix right beneath the slip surface is very porous, probably due to weathering and biogenic activity occurred before the sealing of hangingwall deposits, but clast indentation and triple junctions between grains are still recognizable.

**Valle Force (relatively small normal fault).** The slip zone in the footwall of Valle Force normal fault consists of a cataclasite similar to the one found in Alto di Cacchia DGSD (Fig. 3.8c), but the slip surface is smoother and makes a sharp contact with the underlying clasts (sample VA05_H.F, Fig. 3.11a-b). The cataclasite consists of < 1 mm in size sub-rounded clasts and few larger angular clasts (the latter with the long axis sub-parallel to the slip surface) immersed in a fine matrix (Fig. 3.11a). The amount of matrix increases approaching the slip surface. A < 0.5 mm thick convoluted layer composed of both comminuted and packed calcite micro- to nano-grains separates the footwall carbonates from the hangingwall breccias (Fig. 3.11b-c). The convoluted contact with the hangingwall rocks reminds of a dissolution-cementation front similar to the one observed in the scarp wall of Alto di Cacchia DGSD (Fig. 3.8c-d). In general, the slip zone in footwall is formed by < 1 μm to > 5 μm in grain size calcite grains with evidence of clast indentation and rare triple junctions among grains (Fig. 3.11d). The hangingwall breccias are composed of sub-cm in size sub-rounded to angular carbonate clasts cemented by a brownish porous and fine calcite-rich matrix (Fig. 3.11a-c, e). The matrix also includes silica-bearing minerals such as quartz and micas with the long axis oriented sub-parallel to the slip direction (Fig. 3.11e). This preferential alignment and the size reduction of the grains towards the slip surface is indicative of the involvement of the hangingwall rocks in fault slip, but no evidence of mixing structures (e.g., injection or “fluidization” structures; Demurtas et al., 2016) between the hangingwall and footwall rocks was observed (Fig. 3.11b-d).

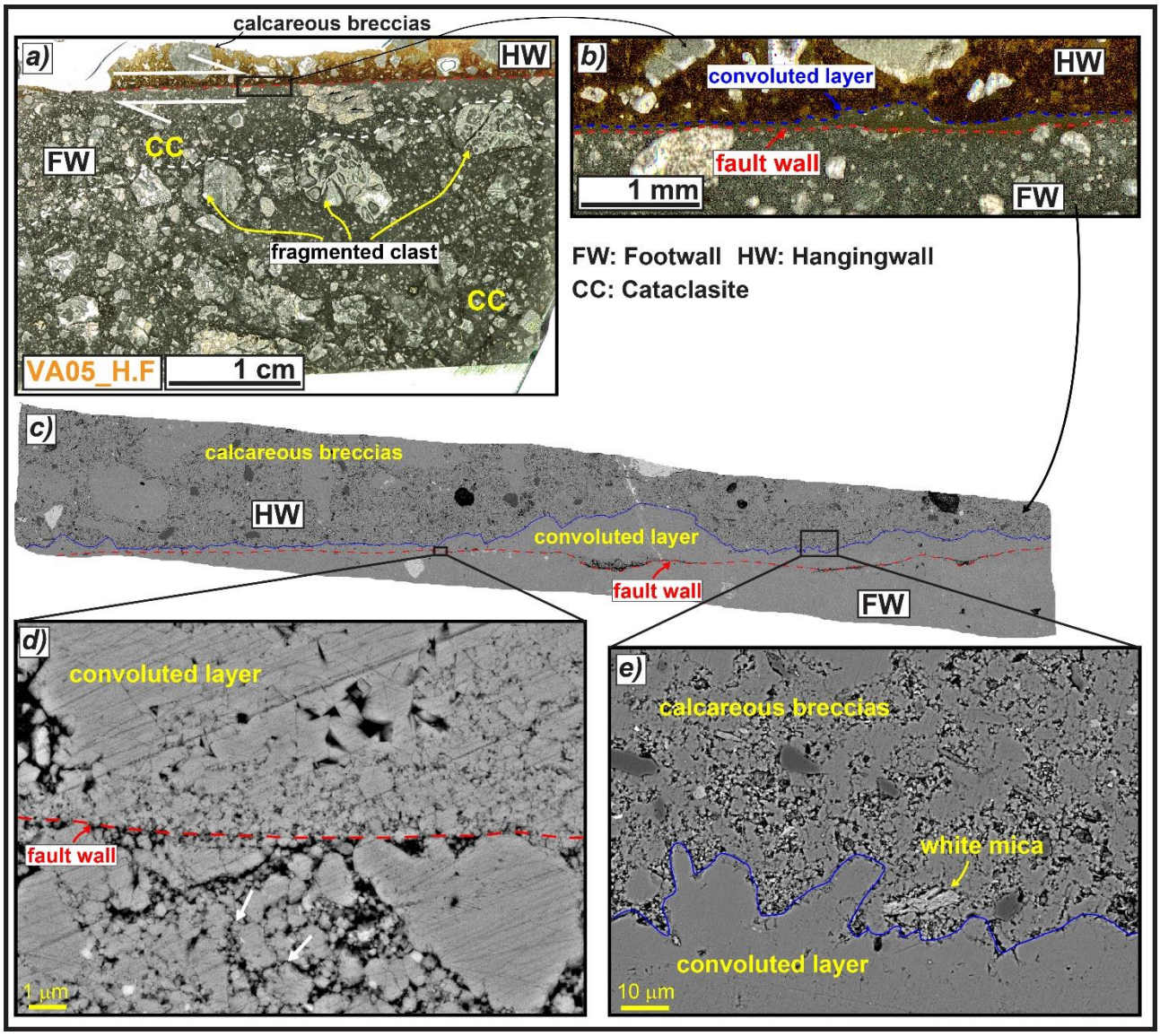


Figure 3.11: microstructures of the Valle Force fault wall (sample VA05_H.F). a) Thin section scan of the fault wall, composed of a well-developed cataclasite in the footwall and calcareous breccias in the hangingwall. b-c) Detail of the fault wall: the hangingwall rocks are separated form the footwall rocks by a < 0.5 mm thick convoluted layer lying above the sharp slip surface, possibly formed by dissolution-precipitation processes involving the footwall cataclasite. d) SEM image of the fault wall highlighting the clast indentation (white arrows) and triple junctions among grains at footwall. e) SEM Image of the convolute contact between the dissolution-precipitation front and the hangingwall breccias. The latter consist of angular clasts made of silica-bearing minerals commonly oriented with the long axis sub-parallel to the slip direction.

**San Benedetto-Gioia dei Marsi and Roccapreturo large seismogenic faults.** In order to compare the slip zones found beneath the main slip surfaces of the DGSDs (Figs. 3.8-3.10) and the Valle Force fault (Fig. 3.11), we describe the main slip zones of two large slip seismogenic faults from the same area. San Benedetto-Gioia dei Marsi (sample Vf01) and Roccapreturo faults (sample Rf01) are both about 10 km long segments of the Fucino and

the Middle Aterno Valley-Subequana Valley fault systems, and are capable of producing up to $M_w$ 7.1 and $M_w$ 6.5 earthquakes, respectively (Barchi et al., 2000; Falcucci et al., 2015) (see also Fig. 3.14). The core measured in the Venere sector of San Benedetto-Gioia dei Marsi fault is up to 1 m thick and includes several matrix- and cemented-supported minor faults (Agosta & Aydin, 2006; Ferraro et al., 2018, 2019). The slip zone of the main fault is made of several cms thick cataclasite consisting of cm-to-mm in size sub-rounded clasts immersed in a sub-millimetric and dark in color ultra-fine matrix (> 50% in volume). The studied slip zones of the two faults lack of their respective slip surfaces. Nevertheless, both slip zones include a well-defined, < 0.5 cm thick, cataclastic/ultra-cataclastic (matrix ca. 80-90% in volume) layer approaching the (inferred) location of the slip surface (Fig. 3.12a, d). The matrix includes few micrometers to tens of nanometers in size calcite grains with straight to stylolitic-like boundaries and local grain indentation (Fig. 3.12b, c). The grain boundaries locally form triple junctions and few isolated pores (Fig. 3.12b-c, e), rarely filled by apatite crystals in the case of the Roccapreturo fault segment (Fig. 3.12f).

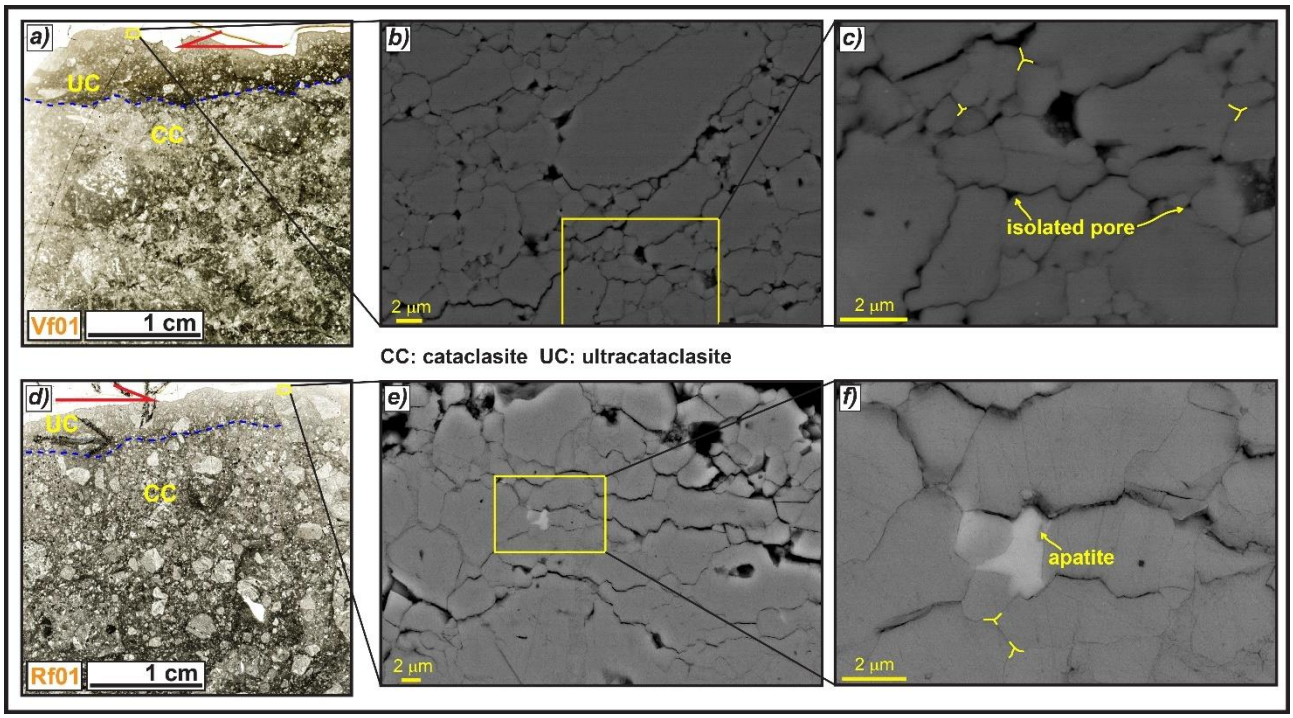


Figure 3.12: microstructures of the slip zones relative to San Benedetto-Gioia dei Marsi (in the Venere sector) and Roccapreturo seismogenic normal fault segments. a) The slip zone of San Benedetto-Gioia dei Marsi normal fault has a well-developed cataclastic fabric and includes a well-defined < 0.5 cm thick cataclastic/ultra-cataclastic layer on the top (sample Vf01). b-c) SEM images of the matrix close to the top, formed by highly packed calcite micro- to nano-grains with straight to stylolitic-like contacts, locally forming triple junctions and few isolated pores. d) The slip zone of Roccapreturo fault has a similar fabric and also includes an ultra-cataclastic level on the top (sample Rf01). e-f) SEM images of the matrix from the ultra-cataclastic level, formed

by highly packed calcite micro-grains with straight to irregular contacts separated by small pores, locally filled by apatite crystals.

## 3.5 Discussion

In this work we have described 1) the fault/fracture network in the footwall of four DGSDs and also of a minor normal fault bordering a small depression (used as comparison) in the central Apennines (section 3.4.1); 2) the micro- to nano-structures of the slip zones of the major and secondary scarps associated with the selected case studies. The slip zones have been compared with those associated with two large seismogenic faults hosting DGSDs in their footwall (section 3.4.2). In the following sections, we discuss 1) the formation and the re-activation of the fractures and slip surfaces associated with the DGSDs (section 3.5.1), 2) the formation of DGSDs in the central Apennines (section 3.5.2) and 3) the deformation mechanisms active in DGSDs hosted in carbonate rocks (section 3.5.3).

### 3.5.1 Formation and re-activation of fault/fracture networks in DGSDs

The fault/fracture networks associated with the DGSD scarps suggest different loading conditions at the time of their formation. Based on the Mohr-Coulomb failure criterion, the numerous sub-vertical open fissures and joints cross-cutting the sub-horizontal conglomerates of Alto di Cacchia DGSD should have been developed in tensional regime or at very low confining pressures, with the maximum principal stress oriented sub-parallel to the slip surface (Figs. 3.13, 3.14). As a matter of fact, open fractures and other tensional structures like gravitational trenches, ridge-top grabens and steep scarps commonly affect the upper and middle portions of DGSDs (Crosta et al., 2013; Esposito et al., 2007; Gori et al., 2014; Hungr at al., 2014). This interpretation is further supported by the observation that Alto di Cacchia DGSD affects the about 400 m thick Pleistocene Cupoli/Aielli Complex, which lies above Cretaceous carbonates. This would imply that the fault/fracture network formed at very shallow depth ($T < 15°C$ and $P_{litho} < 15$ MPa; Fig. 3.14). The scatter of the strike (but not of the dip angle) of the minor faults and fractures might be due to local stress rotations related to (1) the evolution of the syn-sedimentary basin and, (2) exhumation process and hillslope evolution (e.g., with erosion and exhumation, one of the principal stresses may rotate to become normal to the slope surface).

In contrast, in the case of Sant'Erasmo (located in the footwall of the Roccapreturo main fault segment), Mt. Serrone and Colle Cerese (located in the footwall of the San

Benedetto-Gioia dei Marsi main fault segment) DGSDs, the sub-horizontal Cretaceous limestones in the footwall are cut by regularly spaced sets of joints and conjugate shear fractures that have a large scatter of both strike and dip angle (Figs. 3.4-3.6). This spatial arrangement is consistent with the formation of these fractures at larger confining pressures with respect to the Alto di Cacchia and possibly under different stress fields from at least the Pliocene to the Quaternary (Fig. 3.13).

Indeed, the fault/fracture network associated with these DGSDs is similar to the one of Valle Force small normal fault (Figs. 3.7a, 3.13), that should flatten at 2-3 km of depth on a pre-existing low angle fault (D'Agostino et al., 1998; Falcucci et al., 2015; Fig. 3.14), and of the damage zones of large and seismogenic normal faults exhumed from 1-3 km depth (e.g., San Benedetto-Gioia dei Marsi and Vado di Corno fault zones: Agosta & Kirschner, 2003; Agosta & Aydin, 2006; Demurtas et al., 2016; Fondriest et al., 2020; Figs. 3.13, 3.14). However, in the latter cases, most of the minor faults and fractures strike NW-SE, consistently with the NE-SW oriented Middle Pleistocene to Holocene stretching of the central Apennines (D'agostino et al., 2011). In contrast, the few large sub-vertical open fissures cutting the carbonate strata in footwall of Colle Cerese, Mt. Serrone and Sant'Erasmo DGSDs and the absence of veins filling the fractures are consistent with a recent gravitational activity at shallow surficial conditions.

Therefore, most DGSDs in the central Apennines were interpreted by us as the result of gravity induced re-activation of pre-existing minor faults or shear fractures located in the footwall of larger normal seismogenic faults, well-oriented with respect to the actual stress field. Instead, Alto di Cacchia DGSD is the only studied DGSD that exploited fractures formed at very shallow depth, given the above-mentioned structural and stratigraphic constraints. Alto di Cacchia DGSD is accommodated by both newly formed fractures associated with the sliding of Pleistocene conglomerates, and possibly by the re-activation of minor faults and fractures produced by faulting at very shallow depths (200-300 m at maximum) (Fig. 3.14).

The major scarps delimiting Alto di Cacchia, Mt. Serrone and Sant'Erasmo DGSDs (< 500 m long) are ~ 3 m high (Figs. 3.3-3.5), whereas those of Colle Cerese DGSD and Valle Force fault (> 1 km in length) are locally up to 10 m high, respectively (Figs. 3.6-3.7). Such large height values of the scarps are similar to those of most normal fault scarps outcropping in the central Apennines (up to 10 km in length along-strike and accommodating up to 600 m of maximum throw; Ferraro et al., 2018). Moreover, the DGSD scarps appear very sharp although karstified, as well as most of the normal fault scarps cutting the carbonate rocks in

the central Apennines (Agosta & Aydin 2006; Galadini & Galli, 2000; Smeraglia et al., 2017a, b). This would imply that high and sharp scarps can be produced either by gravitational processes or by tectonic, possibly seismic, faulting, or by a combination of the two (Kastelic et al., 2017).

### 3.5.2 Formation of DGSDs in the central Apennines

In the previous section we interpreted the major sharp scarps accommodating the studied DGSDs as pre-existing (i.e., tectonic in origin) fault/fracture surfaces developed in the footwall of large seismogenic faults re-activated by gravitational hillslope deformation. According to this interpretation, the studied DGSDs develop, initially, from both pre-existing and newly formed sub-vertical fractures that spread from the hillslope surface towards the rock mass beneath. At this stage, fractures evolve into large fissures allowing the formation of ridge-top grabens and gravitative trenches at the slope crest (Chigira, 1992; Gori et al., 2014; Mariotto & Tibaldi, 2015). Then, the spreading of the rock mass evolves into a large slide, due to the linkage of the sub-vertical fissures and fractures propagating from the surface with pre-existing minor faults and fractures in the footwall damage zone. The basal surface of the DGSD (i.e., Sackung-type) flattens at few hundreds of meters depth possibly due to re-activation of pre-existing low angle fractures/faults (e.g., P-shear fractures or pre-existing thrust faults) close to the master fault. The rotational sliding of the rock-mass accommodated by the basal surface produces rock topples, trenches and uphill-facing scarps in the middle sector of the slope (Agliardi et al., 2001; Chigira, 1992). In the lower sector of the DGSD, the increase of the compressional forces at the toe causes the bulging of the rock-mass (Chigira, 1992; Hermann et al., 2000; Mariani & Zerboni, 2020).

Unfortunately, and as for most of the Sackung-type DGSDs worldwide, the major slip surface becomes much thicker and less continuous toward the basal sector of the slope and is also buried by the displaced rock-mass that cumulates at the base of the DGSD (Cruden & Varnes, 1996; Della Seta et al., 2017; Di Luzio et al., 2021; Dramis and Sorriso-Valvo, 1994; Martino et al., 2011; Nemčok, 1982; Varnes, 1978). Colle Cerese and Sant'Erasmo are Sackung-type DGSDs affecting carbonate strata dipping in the opposite direction of the slope (i.e., anaclinal slope), allowing the development of scarps, uphill-facing scarps, and a large double-crested ridge morphology (Moro et al., 2009; Figs. 3.2, 3.14). On the other hand, in Mt. Serrone DGSD case, the bedding dips in the same direction of the slope (i.e., cataclinal slope) and the double ridge is less-developed. Here, a series of steep downhill- and uphill-facing scarps delimiting small grabens and gravitative trenches affect the entire

hillslope (Hermann et al., 2000; Mariani & Zerboni, 2020; Figs. 3.2, 3.14). This mechanism of formation of DGSDs is consistent with those proposed for Sackung-type DGSDs worldwide, even though other important factors (e.g., lithology, tectonic setting, glacial retreat, etc.) influence the type, shape and behavior of each DGSD (Panek & Klimes, 2016).

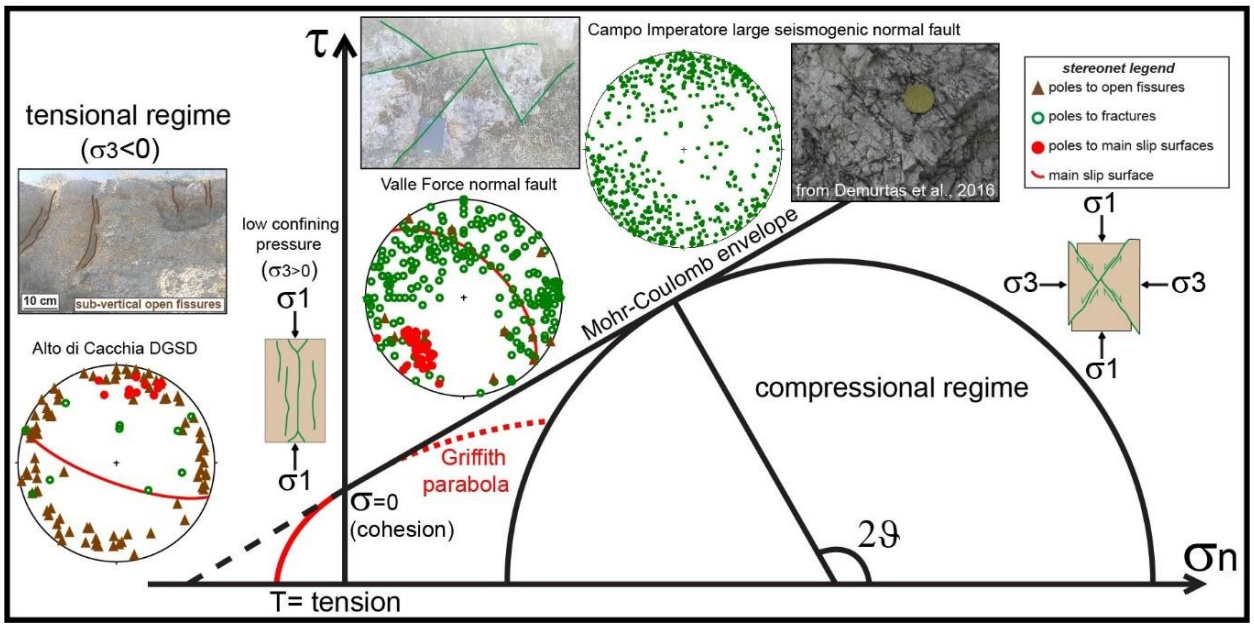


Figure 3.13: stereonets showing the poles of the fractures affecting the footwall conglomerates of Alto di Cacchia DGSD, Valle Force small normal fault and Vado di Corno seismogenic fault (Campo Imperatore fault system) and their relation with the orientation of newly formed fractures according to the Mohr-Coulomb failure criteria in the Mohr space. The large number of fissures and joints dipping at > 70° ("high angle") cutting the footwall rocks of Alto di Cacchia DGSD were reasonably formed under a tensional regime or at very low confining pressures. The conjugate shear fractures affecting the footwall rocks close to the Valle Force fault scarp developed at higher confining pressures and differential stresses. Most of the fractures affecting Vado di Corno fault core strike NW-SE, consistent with the accommodation of larger strains during the last extensional phase and deeper normal dip-slip activity of the structure, exhumed from > 1 km of depth.

### 3.5.3 Deformation mechanisms in carbonate-hosted DGSDs

The slip zones in the footwall of the DGSD and of Valle Force fault scarps show very similar microstructures, especially when observed at micro-metric scale (Figs. 3.8-3.11). At this scale, the textures of the fine matrix are also similar to those found in the slip zones of San Benedetto-Gioia dei Marsi and Roccapreturo seismogenic normal faults (Fig. 3.12), suggesting the activation of similar deformation mechanisms. Here, we will relate the microstructures of the slip zones of both DGSDs and normal faults to the deformation mechanisms active on carbonate rocks at upper crustal conditions.

**Microstructural organization of the slip zones.** In active seismogenic normal faults, the bulk of displacement during co-seismic slip is mainly accommodated by < 1 cm thick principal slip zones (Chester et al., 1993; Chester & Chester, 1998; Power & Tullis, 1989; Sibson, 2003). The major slip surfaces of large San Benedetto-Gioia dei Marsi and Roccapreturo seismogenic faults are associated with a 10-30 cm-thick cataclastic slip zone (Ferraro et al., 2018) that includes a ~ 0.5 cm thick ultra-cataclastic layer (PSZ, Fig. 3.12a, d). In addition, the slip zones of Vado di Corno fault surface (Campo Imperatore fault system) contain mixed clasts and gouges deriving from both the hangingwall Quaternary deposits and the footwall Mesozoic carbonates arranged in "fluidization structures" or injections from the PSZ into the wall rocks (see Fig. 3c and 11c of Demurtas et al., 2016).

In contrast, the slip zones in the footwall of the scarps of Sant'Erasmo, Mt. Serrone and Colle Cerese DGSDs have a proto-cataclastic fabric and lack a well-defined cataclastic/ultra-cataclastic layer (i.e., the PSZ) towards the slip surface (Figs. 3.9a, 3.10a, c). Moreover, the slip zones of Valle Force fault (Fig. 3.11a) and of Alto di Cacchia DGSD (Fig. 3.8c) are similar; indeed, they consist of a well-developed footwall cataclasite delimited from the hangingwall breccias by a sharp slip surface. Nevertheless, the slip surface of Alto di Cacchia DGSD appears rougher than the one of Valle force fault. Furthermore, in both the slip zones of Colle Cerese and of Alto di Cacchia DGSDs "fluidization" or injections structures (which are indicative of mixing between the hangingwall and footwall rocks) were not observed and the hangingwall breccias appear as poorly deformed and cemented (Figs. 3.8c, 3.10c). This would suggest a possible emplacement, and subsequent *in-situ* cementation, of the Quaternary hangingwall rocks right after the exhumation of the scarp. On the contrary, the hangingwall breccias of Valle Force fault were involved in the sliding, as suggested by the grain size reduction towards the slip surface and by the orientation sub-parallel to the slip surface of the long axis of the silicate-built grains (Fig. 3.11a-c, e). However, "fluidization" structures were not found, suggesting lower strains (or strain rates) with respect to the major seismogenic faults (Fig. 3.11b, c).

In conclusion, at the slip zone scale, the major active seismogenic faults differ from DSGDs because of their well-developed cataclastic fabric, that includes extreme localization in ultra-cataclastic layers, thick cataclasites sealed by a dense calcite-vein network and mixing of footwall and hangingwall materials. It seems that these features can be associated with the larger slip accommodated by these faults with respect to the DGSDs or to the small faults. Nevertheless, other than this interpretation, there are no clear evidence regarding the microstructural organization of the slip zones that allowed us to distinguish DGSDs from

tectonic faults. Moreover, since we claim that DGSDs scarps exploit pre-existing minor tectonic faults/fractures (section 5.1), the microstructures observed in the DGSD slip zones could have been mainly produced by tectonic sliding, rather than gravitational sliding. Further studies need to be carried out to obtain better constraints on the exhumation depth of these fault rocks, as for example clumped isotopes analyses of the matrix and cements within and close to the slip zones.

**Matrix of the slip zones**. Cataclastic and ultra-cataclastic layers and their associated slip surfaces are the result of extreme deformation in brittle faults. As a consequence, the associated microstructures, and in particular those relative to the fine matrix, may yield information on the deformation mechanisms active during faulting and DGSD.

The matrix close to the slip surface of Valle Force fault and of the four DGSDs is composed of calcite micro- to nano-grains, with straight to stylolitic-like grain boundaries forming locally triple junctions and isolated pores with widespread clast indentation (Figs. 3.8-3.11). The matrix of the ultra-cataclastic layers of San Benedetto-Gioia dei Marsi and Roccapreturo seismogenic faults is similar, though the grain boundaries among calcite grains are straighter, the triple junctions more widespread and the pore spaces smaller (compare Figs. 3.8b, 3.9b, 3.10b, d and 3.11d with Fig. 3.12b, e). Although similar, this latter fabric differs from the typical foam-like fabric produced in the laboratory by shearing at seismic velocities (i.e., > 0.1 m/s) carbonate-built fault gouges (Demurtas et al., 2019; Fondriest et al., 2013; Pozzi et al., 2019; Smith et al., 2013; Verberne et al., 2013). In these experimental studies, the main deformation mechanism proposed is Grain Boundary Sliding (GBS) aided by diffusion creep, that should be activated at T > 550°C (De Paola et al., 2015; Demurtas et al., 2019; Pozzi et al., 2019). Instead, natural and experimental observations have shown that chemical compaction by pressure-solution driven by fluid-rock interactions is the main process of porosity loss in carbonates, in particular in calcite-rich rocks (Croizè et al., 2013; Ferraro et al., 2019; Gratier et al., 2013, 2015; Meyers & Hill, 1983; Renard et al., 2000; Rutter, 1983; Scholle & Halley, 1985; Tada & Siever, 1989). Pressure-solution occurs in presence of a liquid phase through dissolution at grain contacts, diffusion of the solute matter and precipitation of the latter within the pore spaces. The process is mainly driven by the stress acting at the grain-to-grain contact and does not require high ambient pressures and temperatures to be activated (Croizè et al., 2013; Rutter, 1983).

According to these observations, the textures found in the matrix of the slip zones associated with both normal faults and DGSDs are compatible with the activation of

pressure-solution processes occurring at very low temperatures and confining pressures (i.e., T < 15°, $P_{litho}$ < 15 MPa). Cataclastic flow processes cause clast comminution by frictional sliding, grain crushing and micro-cracks growth. The subsequent ingression and percolation of fluids within the pore spaces (e.g., Lucca et al., 2019) among the calcite grains cause a very efficient pressure-solution process resulting in grain indentation and stylolitic-like grain boundaries, pore space reduction and precipitation of secondary calcite grains and other phases within the fractures closest to the dissolution areas (Agosta et al., 2012; Bathurst, 1971; Carrio-Schaffhauser et al., 1990; Renard & Ortoleva, 1997). The slip zones of San Benedetto-Gioia dei Marsi and Roccapreturo normal faults underwent more pressure-solution than the ones of Valle Force fault and of the DGSDs, probably because of the smaller average size of the grains (Renard et al., 2000; Rutter, 1983; Tada & Siever, 1989). However, other factors that influence the rate of pressure-solution should be considered, such as the relative abundance of clay-rich minerals, which were found in all the slip zones of the DGSDs, and the composition of the percolating fluids (Tada & Siever, 1989, Renard et al., 2001; Croizè et al., 2010).

The major slip surface of Valle Force fault shows ultra-polished patches (where the hangingwall breccias are removed) and has a sharp contact with the underlying clasts of the slip zone (Figs. 3.7f, 3.11a). The ultra-polished surface patches could be the result of the formation of Y-shears due to crack propagation and mechanical abrasion in a lithified fault rock (cataclasite). The mechanical abrasion produces a calcite-rich nano-powder that is spread on the Y-shears. The activation of pressure-solution processes dissolving the finer calcite grains may result in the formation of an ultra-polished surface (e.g., Mercuri et al., 2018; Tesei et al., 2017). Alternatively, ultra-polished slip surfaces produced by extreme co-seismic localization at larger crustal depths (Demurtas et al., 2016; De Paola et al., 2015; Fondriest et al., 2013; Pozzi et al., 2018) might be overprinted by low-temperature pressure-solution compaction during inter-seismic periods and exhumation. This would suggest that, in fluid-saturated systems, ultra-polished slip surfaces are likely associated with textures produced by fluid-driven and low temperature diffusive processes active on smooth surfaces during either seismic or aseismic slip. Recent experiments indicate that seismic slip at low effective stresses (i.e., < 2 MPa and in the presence of pressurized pore fluids) is not able to induce crystal plasticity on carbonate gouges and to produce ultra-polished slip surfaces (Rempe et al., 2020). Instead, carbonate fluid-saturated gouges sheared at very low effective stresses likely deform by granular and, to a less extent, cataclastic flow during earthquakes (Rempe et al., 2020). These experimental results suggest that in the case of

Alto di Cacchia DGSD, that involves deposits that were not affected by significant burial (i.e., < 400 m), the presence of polished slip surfaces might be the result of pressure-solution processes.

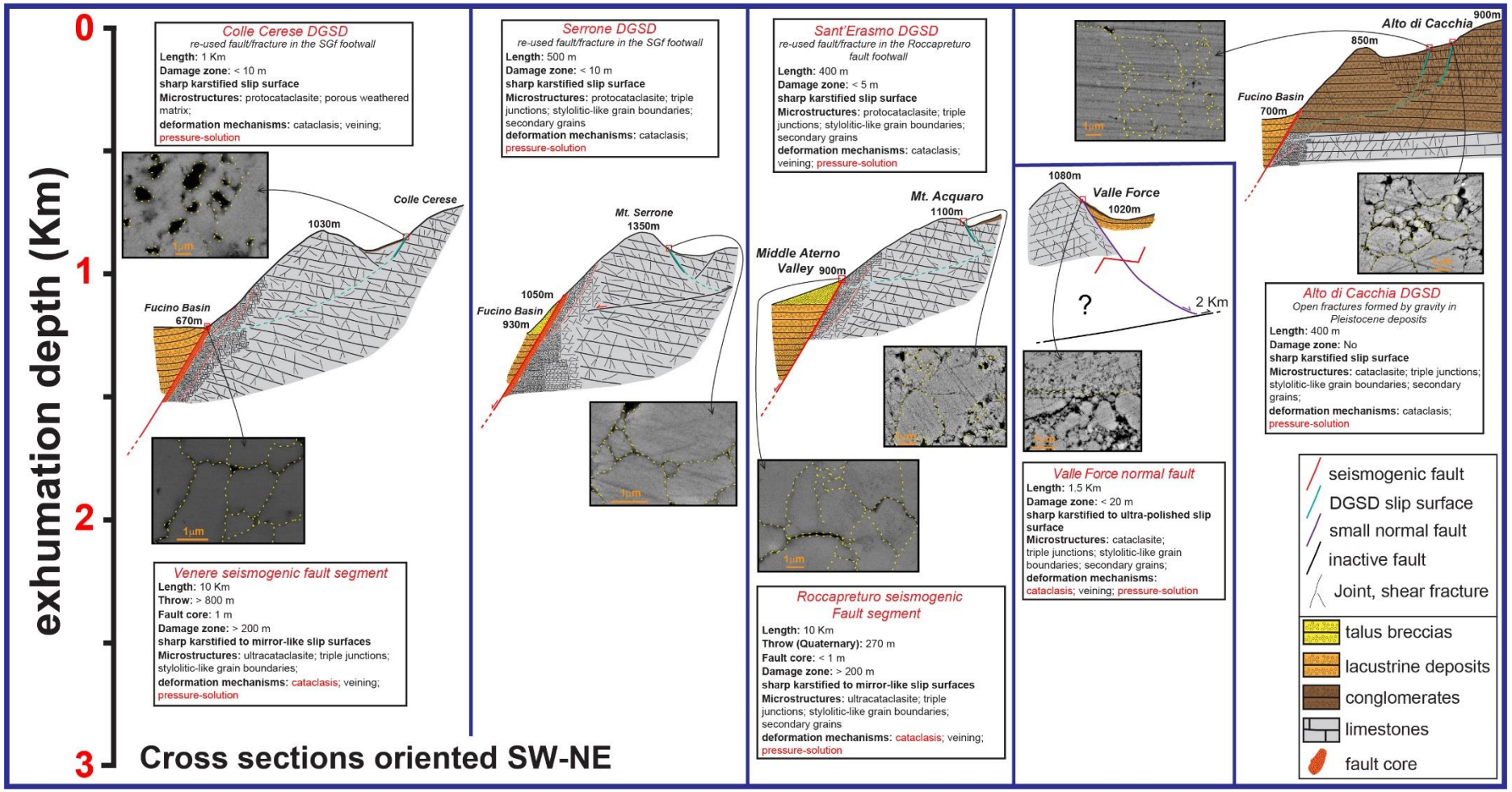
exhumation depth (Km)
0
1
2
3
Colle Cerese DGSD
re-used fault/fracture in the SGf footwall
Length: 1 Km
Damage zone: < 10 m
sharp karstified slip surface
Microstructures: protocataclasite; porous weathered matrix;
deformation mechanisms: cataclasis; veining; pressure-solution
Colle Cerese
1030m
Fucino Basin
670m
1µm
Venere seismogenic fault segment
Length: 10 Km
Throw: > 800 m
Fault core: 1 m
Damage zone: > 200 m
sharp karstified to mirror-like slip surfaces
Microstructures: ultracataclasite; triple junctions; stylolitic-like grain boundaries;
deformation mechanisms: cataclasis; veining; pressure-solution
Serrone DGSD
re-used fault/fracture in the SGf footwall
Length: 500 m
Damage zone: < 10 m
sharp karstified slip surface
Microstructures: protocataclasite; triple junctions; stylolitic-like grain boundaries; secondary grains
deformation mechanisms: cataclasis; pressure-solution
Mt. Serrone
1350m
1050m
Fucino Basin
930m
Sant'Erasmo DGSD
re-used fault/fracture in the Roccapreturo fault footwall
Length: 400 m
Damage zone: < 5 m
sharp karstified slip surface
Microstructures: protocataclasite; triple junctions; stylolitic-like grain boundaries; secondary grains
deformation mechanisms: cataclasis; veining; pressure-solution
Mt. Acquaro
1100m
Middle Aterno Valley
900m
Roccapreturo seismogenic Fault segment
Length: 10 Km
Throw (Quaternary): 270 m
Fault core: < 1 m
Damage zone: > 200 m
sharp karstified to mirror-like slip surfaces
Microstructures: ultracataclasite; triple junctions; stylolitic-like grain boundaries; secondary grains
deformation mechanisms: cataclasis; veining; pressure-solution
1080m
Valle Force
1020m
?
2 Km
Valle Force normal fault
Length: 1.5 Km
Damage zone: < 20 m
sharp karstified to ultra-polished slip surface
Microstructures: cataclasite; triple junctions; stylolitic-like grain boundaries; secondary grains;
deformation mechanisms: cataclasis; veining; pressure-solution
Alto di Cacchia
900m
850m
Fucino Basin
700m
Alto di Cacchia DGSD
Open fractures formed by gravity in Pleistocene deposits
Length: 400 m
Damage zone: No
sharp karstified slip surface
Microstructures: cataclasite; triple junctions; stylolitic-like grain boundaries; secondary grains;
deformation mechanisms: cataclasis; pressure-solution
seismogenic fault
DGSD slip surface
small normal fault
inactive fault
Joint, shear fracture
talus breccias
lacustrine deposits
conglomerates
limestones
fault core
Cross sections oriented SW-NE

Figure 3.14: Geological cross sections showing the main characteristics of the studied cases (displacement of the slip surface, common microstructures associated, inferred deformation mechanisms, exhumation depth of the fault/fracture network, etc.). San Benedetto-Gioia dei Marsi and Roccapreturo fault zones exhumed from > 1 km of depth. Valle Force normal fault exhumed from shallower depths and flattens at about 2 km of depth on a pre-existing thrust. The major slip surfaces of the DGSDs re-use pre-existing faults and fractures developed in the footwall of the associated large normal faults. The microstructures of the slip zones are very similar in both normal faults and DGSDs, suggesting cataclasis and low temperature diffusive processes (i.e., pressure-solution) as the dominant deformation mechanisms active at shallow depth in carbonates.

## 3.6 Conclusions

In the Italian central Apennines, sharp, commonly karstified, scarps displace carbonate rocks and accommodate either seismic ruptures or Deep-seated-Gravitational-Slope-Deformations (DGSDs). We analyzed the cases of Alto di Cacchia, Sant'Erasmo, Colle Cerese and Mt. Serrone DGSDs, located in the footwall of large seismogenic normal faults and the case of Valle Force, a < 2 km long normal fault bordering a karst depression (Figs. 3.1, 3.2). In the footwall of the major scarp accommodating Alto di Cacchia DGSD, the fault/fracture network mainly consists of sub-vertical open fissures: this attitude is consistent with the surficial formation (i.e., < 500 m) of the fractures accommodating the DGSD (Figs. 3.3, 3.13). On the contrary, the fault/fracture networks associated with the other selected DGSDs consist of open fissures, joints and shear fractures, but with a large scatter of the dip and dip angles. This scatter is indicative of a deeper formation depth (i.e., > 1 km of depth) followed by the recent gravitational activity (Figs. 3.4-3.6). In fact, a similar fault/fracture network is measured in Valle Force small normal fault (Figs. 3.7, 3.13). Therefore, we interpret most slip surfaces of the DGSDs in the central Apennines as the result of the exploitation of pre-existing (tectonic-related) faults/fractures located in the footwall of larger normal faults (Figs. 3.13, 3.14).

The maximum height values (up to 10 meters) of the DGSD scarps are comparable to those of the main seismogenic normal faults (up to 10 km of length along-strike) in the central Apennines. Therefore, well-exposed high and sharp slip surfaces, also for large seismogenic faults, can be related to both tectonic faulting and gravity-induced processes. However, structural, geomorphological and geophysical/seismological features and information, such as the along-strike length and lateral continuity of the scarp, the presence of double-crested ridge or up-hill facing scarps or gravitational trenches, the distribution of earthquakes, may allow us to relate the scarps to gravitational rather than to tectonic processes.

The slip zones of the large slip San Benedetto-Gioia dei Marsi and Roccapreturo seismogenic normal faults have a cataclastic fabric and include a ~ 0.5 cm thick continuous ultra-cataclastic layer just beneath the slip surface (Figs. 3.12a, d). On the opposite, the slip zones of Sant'Erasmo, Colle Cerese and Mt. Serrone DGSDs have a proto-cataclastic fabric (Figs. 3.9a, 3.10a, c) and those of Alto di Cacchia DGSD and of Valle Force fault have a cataclastic fabric, but both lack of an ultra-cataclastic layer right beneath the slip surface (Figs 3.8c, 3.11b). The well-developed and thicker slip zones associated with the large normal faults can be explained by the larger amount of slip displacement accommodated by the latter compared to the DGSDs. However, other than these differences in the microstructural organization of the slip zone, there are no microstructural indicators that allow us to distinguish between DGSDs and normal faults.

The microstructures found in the fine matrix of the slip zone may yield information about the deformation mechanisms activated during DGSD. The fine matrix is composed of packed calcite micro- to nano-grains with both straight and indented or even stylolitic-like grain boundaries (Figs. 3.8-3.11). This fabric is interpreted as the result of cataclasis occurring by clast fragmentation and frictional sliding, and low temperature pressure-solution processes (i.e., $T < 15°$, $P < 15$ MPa). The calcite micro-grains forming the matrix of the large slip normal faults are more packed (e.g., well-developed triple junctions, widespread indentation, and a reduced number of pores) with respect to those found in the slip zones of DGSDs possibly because of the smaller average grain size that favors the process of pressure-solution.

Our work stresses the structural convergence (i.e., formation of smooth to ultra-polished slip surfaces) resulting from micro-scale processes (i.e., cataclastic flow and pressure-solution) active on both faults and DGSDs. Therefore, the characterization of the footwall fault/fracture network distribution, together with the interpretation of geomorphological features, are key inputs to relate the presence of sharp scarps to gravity- or tectonic-driven processes.

## Acknowledgments

This research was funded by the European Research Council Consolidator Grant Project NOFEAR No 614705 (L.D.R., M.F. and G.D.T.); by two INGV projects: "Caratterizzazione microstrutturale di piani di faglia attivi ed esumati e di piani di scivolamento di deformazioni gravitative profonde di versante (DGPV)" and "Investigation of bedrock shear planes microstructures". M.F. is supported by MSCA-IF DAMAGE No 839880. We thank Leonardo Tauro for thin section preparation, Nicola Michelon for preparing field materials, Telemaco Tesei for comments on the microstructures and Flavio Giusti for supporting the translation of the work. We thank the Editors, Christie Rowe, Andrea Billi, Federico Agliardi, Nicola De Paola and an anonymous reviewer for their extremely constructive feedbacks.

# 4. Architecture of active faults in carbonates: Campo Felice and Cama Faults, Italian Apennines

*This chapter is in preparation and ready to be submitted. The study was performed with the collaboration of Simone Masoch, Marco Moro, Fawzi Doumaz, Giulio Di Toro, Michele Saroli and Andrea Cavallo. Marco Moro, Michele Saroli, and Giulio di Toro contributed to the work design; I was assisted by Simone Masoch, Marco Moro and Giulio Di Toro during field survey, by Andrea Cavallo during SEM analyses and by Giulio Di Toro during microstructural interpretation; Fawzi Doumaz contributed with drone mapping and construction of orthomosaics; I wrote the original draft and discussed the results with Giulio Di Toro, Marco Moro, Michele Saroli and Simone Masoch.*

## Abstract

The Italian central Apennines are one of the most seismically active regions in Europe. The Ovindoli-Piani di Pezza, Campo Felice and Mt. D'Ocre faults are supposed to form a ~ 27 km long fault system capable of producing up to $M_w$ = 6.8 earthquakes. Nevertheless, several geomorphological features indicative of a Deep-seated Gravitational Slope Deformation (DGSD) were identified across the Mt. D'Ocre range, such as trenches, uphill and downhill facing scarps and counterscarps. We compared the distribution of fractures affecting the carbonate rocks in the footwall of Campo Felice fault and of the southwestern branch of Mt. D'Ocre range (i.e., the Cama fault) and analyzed the microstructures of the slip zones associated. The Campo Felice and Cama faults displace the same rocks with similar attitude, but with different estimated Quaternary slip rates and cumulated geological throws (i.e., ~ 1050 m and ~ 100 m, respectively).

The large differences observed in the fault zones (e.g., core and damage zone thickness, presence of veins, secondary faults) would suggest that the two faults are not linked at depth and that the Cama fault currently accommodates the lateral spreading of Mt. D'Ocre ridge. Microstructural analyses indicate similar deformation mechanisms (i.e., cataclasis and pressure-solution) occurring in both the two faults. However, the slip zones associated have different textures, (i.e., cataclasite *vs.* crush fault breccia) because of the higher slip rates and geological throws of Campo Felice fault. Both macro- and micro-structural analyses provided further parameters to improve the characterization of seismogenic sources in central Apennines.

# 4.1 Introduction

With an average recurrence of one moderate to large in magnitude ($M_w \geq 5.5$) earthquake per decade, the Italian central Apennines are one of the most seismically active regions in Europe (Rovida et al., 2020). During the last 30 years, ~ 80 paleo-earthquakes associated with several normal faults and with estimated magnitudes ranging from $M_w$ 5.6 to 7.0 were identified thanks to paleo-seismological trench investigations (Galli, 2020).

These studies, combined with geomorphological analyses (e.g., Giraudi and Giaccio, 2017), structural geological mapping (e.g., Fondriest et al., 2020) and geophysical investigations (e.g., Chiaraluce et al., 2017), allowed researchers to estimate better the seismic hazard associated with numerous faults cropping out in the central Apennines (Barchi et al., 2000; Calamita et al., 2000; Falcucci et al., 2016; Galli et al., 2008; Galli, 2020).

Most of these active normal faults strike NW-SE and are often disposed in an *en-échelon* array forming large fault systems (Boncio et al., 2004; Fig. 4.1a). Individual fault segments interact one with the other and may rupture either independently or together. For example, during the Amatrice-Norcia 2016-2017 seismic sequence in the northern Apennines, the $M_w$ 6.5 Norcia October 30, 2016 earthquake, that ruptured the whole Mt. Vettore-Mt. Bove fault system (~ 28 km long and composed of three fault segments), was preceded, to the south, by the $M_w$ 6.0 Amatrice August 24, 2016 and, to the north, by the $M_w$ 5.9 October 26, 2016 earthquakes (Chiaraluce et al., 2017; Villani et al., 2018). The occurrence of the three mainshocks and other structural (Iezzi et al., 2019) and geophysical data (Tinti et al., 2016) confirm the internal segmentation of the Mt. Vettore-Mt. Bove fault system (i.e., soft linkage; Peacock and Sanderson, 1991; Kim and Sanderson, 2005; Fossen and Rotevatn, 2015).

Instead, the most recent earthquake that hit the central Apennines was the $M_w$ 6.1 L'Aquila April 6, 2009 earthquake, whereas the largest one instrumentally recorded was the $M_w$ 7.0 Avezzano, 1915 earthquake (EWG, 2010; Fig. 4.1a). In the area comprised between the Ovindoli and L'Aquila towns, three major fault strands, with a right-stepping *en-échelon* arrangement, were inferred to form a ~ 27 km long fault system (i.e., Celano-L'Aquila Fault System in Salvi and Nardi, 1995, or Cerasitto-Campo Felice-Ovindoli-Pezza Fault System in Galli et al., 2008), hereafter called Ovindoli-L'Aquila Fault System (OAFS; Fig. 4.1a). The Ovindoli-Piani di Pezza fault would constitute the southern segment of the OAFS (Fig. 4.1a). The Campo Felice fault (CFf) and the three parallel fault scarps north to Mt. D'Ocre would constitute the middle and northern segments, respectively (Galli et al., 2008; Fig. 4.1a-d).

The Late-Pleistocene-Holocene seismic activity of the fault system was inferred by geomorphological and paleo-seismological analyses (Bosi et al., 1993; Galli et al., 2008). The last faulting event of the CFf, that occurred ~ 2500-3000 yrs ago, was estimated by Giraudi (1995) through geomorphological and chronological analyses of the alluvial fans displaced by the fault. Micro-morphological analyses of the exposed scarp allowed Giaccio et al. (2003) to identify two faulting events between the 860 and the 1300 AD and on ~ 1900 BC. Later, Benedetti et al. (2013) identified four exhumation phases of the CFf scarp (~ 9400 [±500], 4200 [±500], 3400 [±500], 1100 [±300] yrs ago) by means of $Cl^{36}$ dating.

Salvi et al. (2003) dug five trenches across the northernmost sector of Mt. D'Ocre range faults and recognized three faulting events, the first two between 1300 AD and 1690 BC and the third one in the range from 1690-5620 BC. Because of the quite good correlation among the ages of these paleo-earthquakes with the ones recognized along the Ovindoli-Pezza

fault (Pantosti et al., 1996), the Mt. D'Ocre fault branches were interpreted by the authors as the northernmost segments of the OAFS. The latter, in turn, would represent the ground surface expression of a single deeper seismogenic structure (30-35 km long) capable of producing up to $M_w$ = 6.8 earthquakes in case of the entire system rupture. Alternatively, the Mt. D'Ocre faults may rupture independently producing several ~ $M_w$ 6.0 earthquakes (Galli et al., 2008). Nevertheless, the authors do not exclude that the three northernmost scarps of the OAFS may currently accommodate the lateral spreading of the Mt. D'Ocre range, as previously suggested by Salvi and Nardi (1995). Indeed, several geomorphological features indicative of a large Deep-seated Gravitational Slope Deformation (DGSD) were identified, such as trenches, uphill and downhill facing scarps and counterscarps (Salvi and Nardi, 1995; Salvi et al., 2003; Fig. 4.1b).

DGSDs are deep gravitational landslides involving hundreds of meters thick rock-mass volumes moving from the ridge top to the valley floor (Agliardi et al., 2001, 2012; Crosta et al., 2013; Dramis and Sorriso-Valvo, 1994; Varnes, 1978; Zischinsky, 1966, 1969). In the central Apennines, significant natural hazards are associated with DGSDs, where they are mainly localized in the footwall of normal faults (Del Rio et al., 2021). The movement of DGSDs is strongly controlled by normal faults activity, that commonly triggers post-seismic gravitational deformations of the nearest and most unstable relief slopes (Moro et al., 2012; Albano et al., 2015; Del Rio et al., 2021).

In this work we mapped and compared the distribution of fractures affecting the host rocks in the footwall of the CFf and the southwestern branch of the Mt. D'Ocre range (i.e., the Cama fault, Cf; Fig. 4.1b, c) and analyzed the microstructures of the slip zones associated with the major slip surfaces. The interpretation of the deformation processes at meso- to micro-metric scale associated with the Campo Felice and Cama fault scarps may contribute to shed more light on the formation, current mechanical behavior and relation between the two faults.

The interpretation of the deformation processes at meso- to micro-metric scale associated with the Campo Felice and Cama fault scarps may contribute to shed more light on the formation of carbonate-hosted faults in the tectonic context of the central Apennines an on the current mechanical behavior and kinematic relation between the two faults. The possible interpretation of the Mt. D'Ocre faults as principal slip surfaces currently accommodating a large gravitational spreading instead of expression of active normal faults, would mean a reduction of ~ 8-9 km of the seismogenic source associated with the OAFS. This, in turn, would result in a lower maximum expected earthquake magnitude associated

with the entire re-activation of the fault system, since the latter parameter is strongly controlled by the total surface length of the fault (e.g., Wells and Coppersmith, 1994; Leonard, 2010; Wesnousky, 2008; Galli et al., 2008).

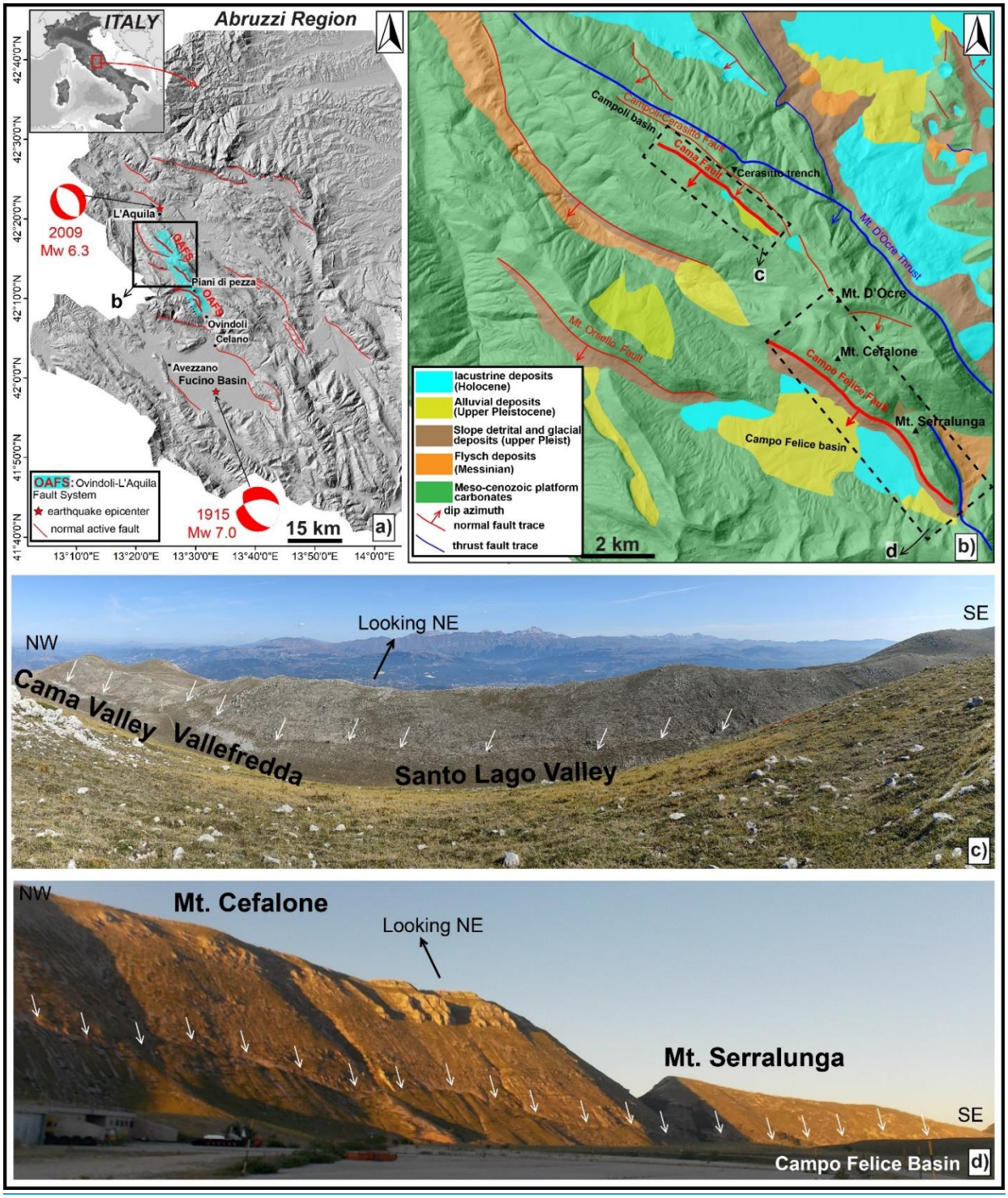


Figure 4.1: Geological setting of the Campo Felice and Cama faults. a) Seismotectonic map of the Abruzzi Region with indicated the main Quaternary active faults (red lines). Thicker red lines indicate the Ovindoli-L'Aquila Fault System (OAFS). Focal mechanisms indicate the mainshocks of the largest (i.e., Avezzano Mw 7.0, 2015) and most recent (i.e., L'Aquila Mw 6.1, 2009) earthquakes striking the region in the past. b) Simplified geological map of the area affected by the Campo Felice and Cama faults (thicker red lines), that

were investigated in this work. c) Panoramic view of the surface expression of the Cama fault, bordering the Cama, Vallefredda and Santo Lago valleys. d) Surface expression of the Campo Felice fault scarp, affecting the SW slopes of Cefalone and Serralunga Mts. and bordering the homonymous intermontane basin.

## 4.2 Geological setting

The Italian Apennine fold-and-thrust belt start to develop since Miocene, due to the NE verging collision between the Adriatic and European Plates (Elter et al., 1975; Carminati et al., 2012; Patacca et al., 1992a). The Apennine orogenesis was characterized by a general eastward migration of the chain thrust front and consequent formation of piggy-back basins associated with the main thrusts (Cosentino et al., 2010). In central Apennines, during this compressional phase, shallow-water and pelagic Meso/Cenozoic limestones were juxtaposed by NE verging thrusts to syn-orogenic foredeep deposits (Cosentino et al., 2010).

Since Upper Messinian to present, a NE-SW oriented crustal extension accommodated the stretching of Apennine chain, caused by the retreat of the subduction hinge toward E-NE (Malinverno and Ryan, 1986; Carminati and Doglioni, 2012). During Quaternary, a strong increase of the regional uplift (i.e., more than 1000 m; D'Agostino et al., 2001) lead to the formation of large intermontane basins filled with continental deposits, bordered by active normal faults (Demangeot, 1965; Dramis, 1992; Galadini and Galli, 2003). The combination of both extensional faulting (Quaternary extension rate of 2-3 mm/yr; Hunstad et al., 2003) and regional uplift is also the main cause of the development of DGSDs in central Apennines (Galadini, 2006).

The current extensional tectonic phase is accommodated by active normal faults that cut and locally exploit the inherited Miocene-Early Pleistocene thrusts and the earlier Mesozoic normal faults (Elter et al., 1975; Vezzani et al., 2010). Most of the active faults in central Apennines are NW-SE oriented and SW dipping (i.e., “Apennine trend”), commonly organized in fault systems with associated intermontane basins (e.g., Campo Felice and Fucino Basins; Bosi et al., 1993; Cavinato et al., 2002), although smaller NE-SW oriented normal faults (i.e., “anti-Apennine trend”) are also spread in the area.

**Campo Felice and Mt. D’Ocre normal faults**. In the area affected by Campo Felice and Mt. D’Ocre faults mainly outcrop Cretaceous and Miocene shallow-water carbonates belonging to the Latio-Abruzzi succession, locally capped by Upper Miocene hemipelagic marls and Messinian flysch deposits (Brandano, 2017; Figs. 4.1b; 4.2a, b).

The Cretaceous Units record the sedimentation in shallow-water platform environments (started during Middle Liassic) along the passive margin of the Adriatic plate and mainly consist of micritic limestones alternated with thin levels of calcarenites or marls (see stratigraphic column in Fig. 4.2a). During the Lower Albian-Early Cenomanian, this carbonate platform underwent three periods of aerial exposure and erosion of the underlying limestones, with consequent formation of karst cavities filled with bauxitic deposits (Mancinelli et al., 2003; Fig. 4.2a). Middle Miocene carbonates (i.e., "Calcari a Briozoi e Litotamni" fm.) consist of thin whitish calcarenites including bryozoans, lithotamnia and corals with high amount of glauconite in the lower portion (Fig. 4.2a). The latter records a shallow-water environment with low rates of sedimentation, also documented by cherty and spongolitic limestones on the top of the pelagic sequences (Civitelli et al., 1988). The Miocene carbonates deposited unconformably or para-conformably above the Cretaceous limestones (i.e., "Paleogene Hiatus"; Damiani et al., 1992). The "Calcari a Briozoi e Litotamni" fm. is part of the "Upper Miocene Latio-Abruzzi Turbiditic Complex", that includes the rocks formed during Apennine orogenesis. Miocene hemipelagic marls record the gradual drowning of the carbonate ramp with consequent increase in clay amount at the expense of lime portion. During Messinian, siliciclastic turbidites filled the foredeep basins according to the eastern migration of the Apennine chain thrust front (Patacca and Scandone, 1989; Figs. 4.1b, 4.2a).

The Campo Felice normal fault strikes for ~ 6 km along the NW-SE direction affecting the south-western slopes of Mt. Serralunga, to SE, and Mt. Cefalone, to NW (Figs. 4.1b, d; 3.2a). The fault juxtaposes Cretaceous shallow-water limestones with talus and slope sediments deposited during and after the Last Glacial Maximum (i.e., ~ 25.000-21.000 BP; Dramis, 1983) with a normal pure dip-slip kinematic (Wilkinson et al., 2015). The CFf borders to SW the homonym intermontane basin (~ 20 $km^2$ wide), filled with Late Pleistocene to Holocene alluvial, lacustrine and glacial deposits (Giraudi et al., 2011; Figs. 4.1b, d, 4.2a). A large thrust fault, called Mt. D'Ocre thrust (MOt; Schirripa Spagnolo et al., 2021), borders the north-eastern side of Serralunga and Cefalone Mts., juxtaposing pre-orogenic calcareous units with syn-orogenic calcareous and siliciclastic deposits (Figs. 4.1b, 4.2a).

The Mt. D' Ocre range is composed of three parallel and discontinuously outcropping bedrock scarps, NW-SE oriented, running to NW from the Mt. D' Ocre to the Campoli Basin and affecting the same rocks of the CFf (Salvi et al., 2003; Figs. 4.1b, 4.2b). The Campoli-Cerasitto fault is ~ 9.5 km long along-strike and borders to SW the Campoli Basin in the

northwestern sector (Salvi et al., 2003; Fig. 4.1b). The Cama fault, ~ 3 km long along-strike, borders to SW three small and narrow valleys (i.e., Cama, Vallefredda and Santo Lago valleys), possibly produced by gravitational spreading of the ridge-top (Salvi et al., 2003; Fig. 1b, c).

## 4.3 Methods

We realized two geological maps of the area affected by the Campo Felice and the Mt. D'Ocre faults (Fig. 4.2a, b) by editing and drawing the geological and stratigraphic information reported in the 1:50.000 scale geological map from ISPRA ("Foglio 359 L'Aquila") over a hillshaded relief from TINITALY (Triangular Irregular Network of Italy) 10-m-resolution digital elevation model (Tarquini et al., 2007).

We traced two cross-sections oriented perpendicular to the strike of Campo Felice and Mt. D'Ocre faults, respectively, to estimate the geological throw (i.e., the vertical component of the fault displacement) and identify possible differences at geological scale associated with the two structures. The geological throw was calculated as the elevation difference between the hangingwall and footwall cutoffs of a selected Cretaceous Unit (Fig. 4.2c, d). We assumed a constant thickness of the geological Units across the two sections. High-resolution georeferenced orthomosaics (spatial resolution of ~ 3 cm/pixel) of Cefalone and Serralunga Mts. and the ridge crest affected by the Cama fault were produced by stitching hundreds of nadir-directed photographs taken with a MAVIC 2 Pro drone and processed with Agisoft Metashape Pro software.

Structural data ($n$ = 3047) were collected along the whole along-strike path of the outcropping master fault scarps and across the footwall damage zones using a handheld GPS (accuracy ± 2 m). We measured the attitude (i.e., dip direction/dip angle) of different structural and stratigraphic elements (i.e., bedding, fractures, major and secondary faults, veins, stylolites). Where possible, the kinematic (i.e., rake) of the secondary faults was measured through kinematic indicators such as S-C fabrics, grooves, slickenlines and/or calcite slickenfibers (Chester and Logan, 1987; Petit,1987).

The trace of master fault scarp and of larger secondary faults (i.e., faults with lateral continuity > 2 m and/or cataclastic core associated) and the thickness of the different structural units were reported in topographic maps at 1:1000 scale (0.2 m/pixel of spatial resolution) provided by the Abruzzi Geoportal (www.geoportale.regione.abruzzo.it). These data were then digitalized with ArcGis 10.7.1 software, using the produced orthomosaics as base, to realize detailed structural maps of the footwall damage zones associated with

Campo Felice and Cama faults. We used different colors to show the structural units identified on field (Figs. 4.3-4.6). Structural units that were not directly observed, but interpreted during the survey, were drawn with higher degree of transparency. Structural measurements were plotted into a stereonet (lower hemisphere, Schmidt equal area) using Stereonet Win software (Allmendinger et al., 2012) Three structural-geological cross-sections across the analyzed fault zones were produced (Figs. 4.4-4.6).

From samples collected from the major and secondary faults ($n$ = 28), we selected 17 samples to produce syton-polished thin sections cut perpendicular to the slip surface and parallel to the kinematic indicators (where recognizable, otherwise along the fault dip direction).

The thin sections were photo-scanned at high resolution (4000 dots per inch) both in plane and cross polarized Nicols and edited using specific tools of Adobe Photoshop to highlight the clast shapes, minor fractures and veins and the texture of fine matrix surrounding the clasts. Transmitted-light optical microscopy (OM) was used to determine microstructural features at thin section scale and to identify areas suitable for microanalytical investigations. Scanning electron microscopy (SEM) was used to acquire high-resolution backscattered electron (BSE) images coupled with semiquantitative energy dispersion spectroscopy (EDS) elemental analysis. SEM investigation were performed with a CamScan MX3000 (resolution 300 nm in back-scatter electrons) installed at the Dipartimento di Geoscienze (Università degli Studi di Padova, Padova, Italy) and with the field-emission SEM (FESEM) Merlin Zeiss (resolution 3 nm in back-scatter electrons, BSE) installed at CERTEMA laboratory (Grosseto, Italy). The images were taken with an acceleration voltage of 15 kV and a working distance of 8.5-5.3 mm.

## 4.4 Results

In this section we describe two geological sections cross-cutting the Campo Felice and Cama normal faults, the structural architecture in the footwall of both the two faults and the microstructures observed in the slip zones associated with the major fault scarps.

### 4.4.1 Geological cross-sections

The cross-section A-A' (~ 8 km long) is oriented SW-NE from Mt. Puzzillo and crosses the Campo Felice basin, the Campo Felice fault, the central sector of Mt. Cefalone and Mt. D'Ocre thrust (Fig. 4.2a, c).

Unfortunately, no geological and geophysical data are currently available to infer the Cretaceous-Miocene stratigraphy and possible secondary structures in the Campo Felice basin. Therefore, assuming a constant dip of ~ 30$^{o}$ of the geological Units, we estimated a maximum geological throw of ~ 1050 m associated with the CFf in this sector (with a possible overestimate of ~ 425 m) from the elevation difference between hangingwall and footwall cutoffs of the Cenomanian Intrabauxitic limestones (IBX fm. Fig. 4.2c). Because of the large displacement, we assumed that the CFf cuts the Mt. D'Ocre thrust at depth. Here, the latter puts in contacts Lower Cretaceous shallow-water carbonates with Upper Miocene syn-orogenic limestones forming a large ramp anticline cut by small faults with tens of meters of displacement (Fig. 4.2c).

The cross-section B-B' (~ 7.25 km long) cross-cut the entire Mt. D'Ocre range, located at the hangingwall of Mt. D'Ocre thrust. In our geological map, we mapped the trace of the Cama fault up to the south-eastern termination of the Santo Lago Valley for two reasons: 1) stratigraphic relations among Cretaceous carbonates infer the presence of a SW dipping normal fault of ~ 100 m of geological throw (Fig. 4.2d) the presence of a sharp fault scarp that outcrops discontinuously along the western slope of Vallefredda and Santo Lago Valleys (Figs. 4.1, 4.5). Because of the relatively low displacement associated, the Cf was interpreted to flatten on the Mt. D'Ocre thrust at depth (Fig. 4.2d). The latter juxtaposes shallow water Cretaceous carbonates with Messinian turbiditic deposits (Fig. 4.2b, d). According to our interpretation, the MOt does not flatten on turbidites, but produces a ramp to accommodate the folding of both Cretaceous and Miocene Units (Marshak et al., 2019). Maximum morphological throw associated with the faults bordering the western side of Il Monte and Rotondo Mts. is ~ 600 m, calculated from the elevation difference between the top of Mt. Rotondo and the lower portion of the basin hosting the Casamaina Village (Fig. 4.2d).

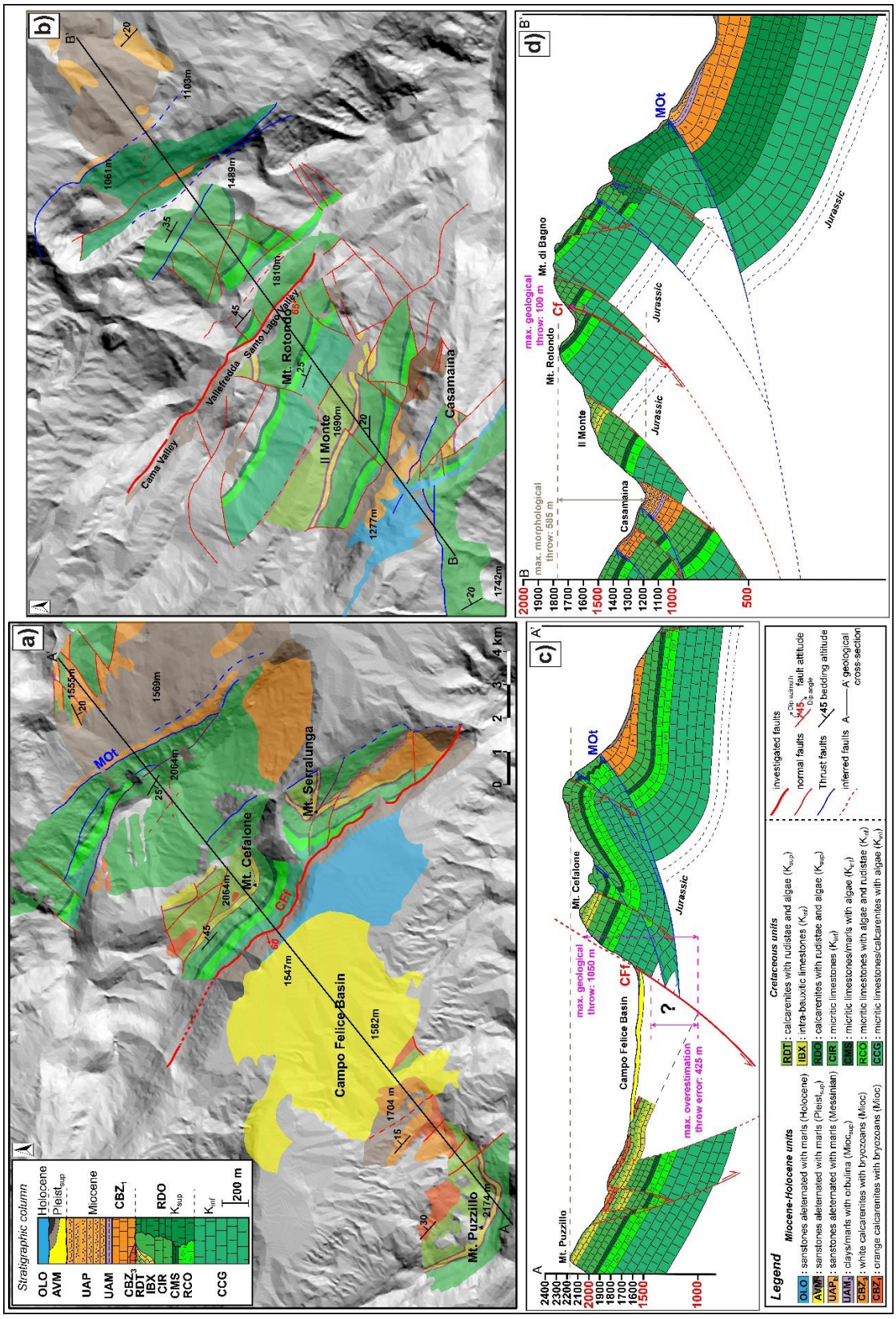


Figure 4.2: Simplified geological maps of the areas affected by the Campo Felice (a) and Cama (b) normal faults including stratigraphic column and trace of cross-sections. c) Cross-section A-A', showing the CFf cutting Cretaceous platform carbonates with ~ 1050 m of geological throw (possible overestimate of 425 m). d) Cross-section B-B', cutting the entire Mt. D'Ocre range, at the hangingwall of Mt. D'Ocre thrust. The Cf displaces Cretaceous carbonates with ~ 100 m of geological throw

### 4.4.2 Fault zones architecture

In this section we describe the spatial distribution and attitude of secondary faults and fractures in the footwall of the Campo Felice and Cama fault zones. Brittle fault zones consist of variable volumes of damaged rocks surrounding the fault core (or multiple fault cores) with different elastic, frictional, and transport properties compared with the surrounding wall rocks (Caine et al., 1996). The *damage zone* includes a volume of fractured rocks where displacement is accommodated by secondary faults and pre-existing stratigraphic and structural features are commonly preserved (Chester and Logan, 1986). The *fault core* is a high-strain rock volume usually composed of low permeability cataclastic rocks where most of fault displacement is accommodated; in this fault volume, pre-existing sedimentary and tectonic structures are fully obliterated (i.e., Sibson,1977). The fault core is mainly produced by repeated slip events along cm-thick slip zones. In general, the intensity of deformation decreases away from the fault core of the master fault towards the damage zone (Chester and Logan, 1986; Caine et al., 1996; Chester et al., 1993; Faulkner et al., 2003; Wibberley et al., 2008; Faulkner et al., 2011; Fondriest et al., 2020).

Though the Campo Felice and Cama faults affect the same host rocks (Figs. 4.1, 4.2), their peculiar structural architecture (i.e., core and damage zone thickness, type and intensity of fractures) may suggest different formation mechanism, evolution and deformation styles.

In our survey, we identified five main structural units based on 1) average spacing among fractures and secondary faults, 2) amount of fine matrix relative to clast abundance in the fault rocks and 3) degree of preservation of primary sedimentary structures (Fig. 4.3) as follows:

***Cataclasite/Breccias (CB)*** (purple in colour in map; Figs. 4.3-4.6) consist of cohesive fault rocks with ultra-cataclastic (i.e., > 90% of fine matrix), cataclastic (i.e., 90-50% of fine matrix; Fig. 4.3a) or proto-cataclastic fabrics (i.e., 50-10% of fine matrix), crush breccias (i.e., < 10% of fine matrix and clast size > 5 mm; *sensu* Sibson, 1977; Fig. 4.3b) or incohesive mosaic breccias (i.e., 60-75% of clasts > 2 mm, *sensu* Woodcock and Mort, 2008; Fig. 4.3c).

The CB rocks represent the core of master and larger secondary faults. Bedding surfaces and other sedimentary structures (e.g., stromatolitic laminations or “burial” stylolites/pressure-solution seams) are not recognized in these units.

***Highly Fractured Rocks (HFR)*** (orange in colour in map; Figs. 4.3-4.6) are cut by numerous high-angle and low-angle fractures spaced horizontally 1-3 cm apart and vertically 1-15 cm apart, with bedding still recognizable (Fig. 4.3e). Where fracture intensity is higher

(i.e., both high and low angle fractures spaced ~ 1 cm apart), the resulting fault rock is a crackle breccia (i.e., incohesive fault breccia with > 75% of clasts > 2 mm, Woodcock and Mort, 2008; Fig. 4.3d).

***Fractured Rocks (FR)*** (yellow in colour in map; Figs. 4.4-4.6), where the fracture spacing ranges between 3-10 cm (Fig. 4.3f).

***Weakly Fractured Rocks (WFR)*** (light-blue in colour in map; Figs. 4.4-4.6), where fractures spacing is > 10 cm and fractures are oriented perpendicular to the bedding and form lozenge-like structures (Fig. 4.3g).

The HFR, FR and WFR represent the footwall damage zone, also affected by numerous secondary faults (particularly in the HFR domain) with both synthetic (i.e., with similar dip azimuth) and antithetic (i.e., with opposite dip azimuth) attitude with respect to the master fault.

***Karst-Gravity Deformed Rocks*** (brown in colour in map; Figs. 4.4-4.6) are intact carbonate strata affected by high-angle fractures and fissures (i.e., tensional fractures with > 1 cm of aperture between the two opposite fracture surfaces; Fossen, 2010), spaced > 20 cm apart, with fracture surfaces very rough due to karst-related processes (Fig. 4.3h).


Figure 4.3: Main structural units identified within the Campo Felice and Cama fault zones. Cataclasites (a) Crush Breccias (b) and mosaic breccias (c) represent the fault core, whereas, crackle breccias (d), Highly Fractured (e), Fractured (f) and Weakly Fractured Rocks (g) represent the fault damage zone. Refer to main text for detailed description of each structural unit.

### 4.4.2.1 Campo Felice Fault Zone

The Campo Felice master fault is exposed along the western slope of Cefalone and Serralunga Mts. with an impressive scarp that outcrops for ~ 5.8 km along-strike (Figs. 4.4, 4.5). The fault scarp has an average height of about 3-4 m (maximum value of ~ 15 m; Fig. 4.7a) and outcrops almost continuously along Cefalone Mt., whereas along Serralunga Mt. the scarp is less continuous and more undulated along-strike (Figs. 4.4, 4.5). The exposed fault surface is very sharp, but also strongly karstified, except in the south-eastern tip, within a small incision on the bauxitic levels, where the fault surface is preserved and appears very polished (Fig. 4.7b). The fault dips 45°- 75° (on average 55°) to SW and sharply truncates the carbonate host rocks whose bedding dips 5°- 50° to NW (stereonets in Figs. 4.4, 4.5). In contrast, along the numerous sinistral step-over and transfer zones, the master fault surface dips to S-SE and the wall rocks in the relay ramp dip towards SE-SW.

The fracture intensity is very high close to the master fault and within the step-over zones, where CB and HFR units outcrop. CB rocks mainly consist of ~ 0-40 cm thick cataclasites with white to reddish in colour matrix close the master fault scarp and increase up to 3 m in thickness in the step-over zones (Figs. 4.3a, 4.4, 4.5, 4.7c). Fault breccias are commonly 50 cm to 2 m thick, up to 5-15 m thick in master fault step-overs and bends (see cross-section A-A' in Fig. 4.4). Highly fractured rocks outcrop either directly close to the master fault or just after the fault core, with a thickness ranging from 15 to 150 m. In these domains, most of the joints dip steeply (60° to 90°) and are arranged roughly in two sets striking NE-SW and NW-SE in the central part and almost N-S moving towards the fault tips (Figs. 4.4, 4.5). Both highly fractured and cataclastic rocks are cut by calcite-bearing veins and are also affected by numerous steeply dipping (60° to 90°) secondary faults, most of them striking NW-SE and dipping both antithetically and synthetically with respect to the master fault (Figs. 4.4, 4.5, 4.7d). In core units, principal slip zones strike N-S and E-W. Here, some fault surfaces are very polished and have kinematic indicators with almost pure dip-slip and rarely strike-slip kinematics (Figs. 4.4, 4.5, 4.7c). the fracture intensity within the damage zone slightly decreases towards the master fault tips (i.e., average fracture spacing > 3 cm), particularly in the north-western sector, where FR domains are more abundant and CB and HFR units are only restricted in volumes affected by numerous secondary faults (Figs. 4.4, 4.5).

Fracture intensity also drastically decreases ~ 60-120 m away from the master fault surface, where the host rocks are cut by sub-vertical joints spaced > 10 cm each other (i.e., WFR unit). FR domains commonly represent the transition between HFR and WRF,

although sharp contacts between highly fractured and weakly fractured rocks were also mapped, most of them due to the presence of a large secondary fault surfaces.

Core (~ 15 m thick) and damage zone units extend for > 400 m across a large incision feeding the fan located in the middle sector of Mt. Cefalone (see cross-section A-A' in Fig. 4.4). In this area, the intensity of fractures affecting the host rocks increases again at about 150 m away from the master fault, probably due to secondary normal faults, which are difficult to identify in this area. In the damage zone, the FR unit outcrops across the incision for ~ 160 m, after which a second WFR is exposed. In the latter, the fractures are spaced 15-30 cm apart, dip towards SW and NE at dip angles of 65°- 90° and cut > 1 m thick carbonate strata.

In both core and damage zones, pressure-solution processes affecting the carbonate host rocks result in the formation of stylolites and pinch-out (black arrows) or S-C like structures at different scales (e.g., Figs. 4.3a, b, f, 4.7e).

#### 4.4.2.2 Cama Fault Zone

The Mt. D'Ocre range is composed by three NW-SE oriented fault branches spread from Mt. D'Ocre, to SE, to Campoli Basin to NW (Fig. 4.1b). The Cama fault represent the south-western branch of the Mt. D'Ocre range. The field work was conducted along this fault because of the very sporadic outcrops of the major scarp and footwall host rocks associated with the Campoli-Cerasitto fault.

The fault is ~ 3.4 km long along-strike and borders the Cama Valley in the north-western sector and Vallefredda and Santo Lago Valleys in the middle and south-eastern sectors, respectively (Figs. 4.1b, 2b, 4.6). The fault scarp outcrops mainly in the middle and southern sectors (maximum height of ~ 2 m), although discontinuously, and strikes 195°-253° (Fig. 4.6). The scarp sharply cuts with 49°- 70° of dip angles (~ 60° on average) the carbonate host rocks N-NE dipping and with dip angles of 15°- 70°; Figs. 4.6, 4.7f).

Fault core and damage zone outcrop for a total thickness < 40 m. Fault core is ~ 1 m thick only close to the south-eastern tip and mainly consist of proto-cataclasites, whereas highly fractured and fractured rocks (up to 15-30 m in thickness) are mainly distributed in the area located between Vallefredda and Santo Lago Valley. Few karstified secondary faults and calcite veins, mostly arranged in conjugate systems, were mapped (Figs. 4.6, 4.7g). Where the intensity of fracture decreases along the master fault, 15-35 m thick weakly fractured domains crop out, with both high-angle (i.e., dip angles of 60°- 90°) joints and

fissures spaced > 10 cm apart. As in the case of CFf, joints in the damage zone are mainly arranged in two sets striking NW-SE and NE-SW.

Just outside the damage zone, the carbonate rocks appear almost unaffected by cataclasis or mechanical fracturing. In fact, they are mainly affected by sub-vertical joints and fissures (1-20 cm of aperture) spaced 20 cm to 1 m apart and very scattered in dip azimuth, with exposed bedding and fracture surfaces very rough due to karst processes (i.e., Karst-Gravity Deformed Rocks; Fig. 4.6). Moving up to the hillcrest top, the host rocks show the same type of deformation, with blocks of carbonate rocks cracked and tilted towards the slope (Figs. 4.3h, 4.7h). Close to the top of the crest, the bedding surfaces are steeper (i.e., 50°- 70° of dip angles).

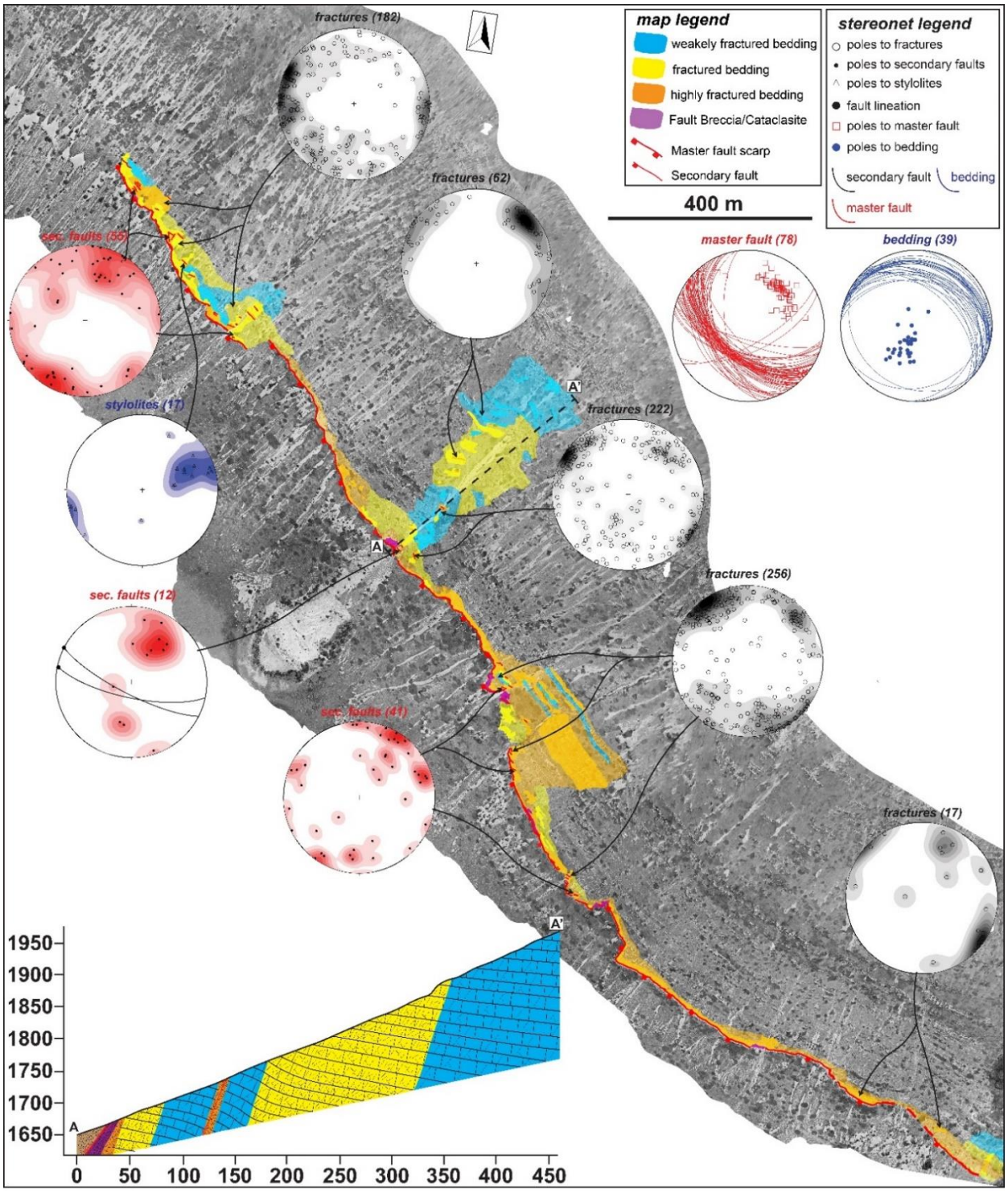


Figure 4.4: Structural Sketch map of the Campo Felice fault zone in the Mt. Cefalone sector including structural data collected within the different structural units, plotted in Equal Area-Lower Hemisphere stereonets with density contours areas (see figure legend for symbols description). Interpreted structural units were drawn with higher degree of transparency.

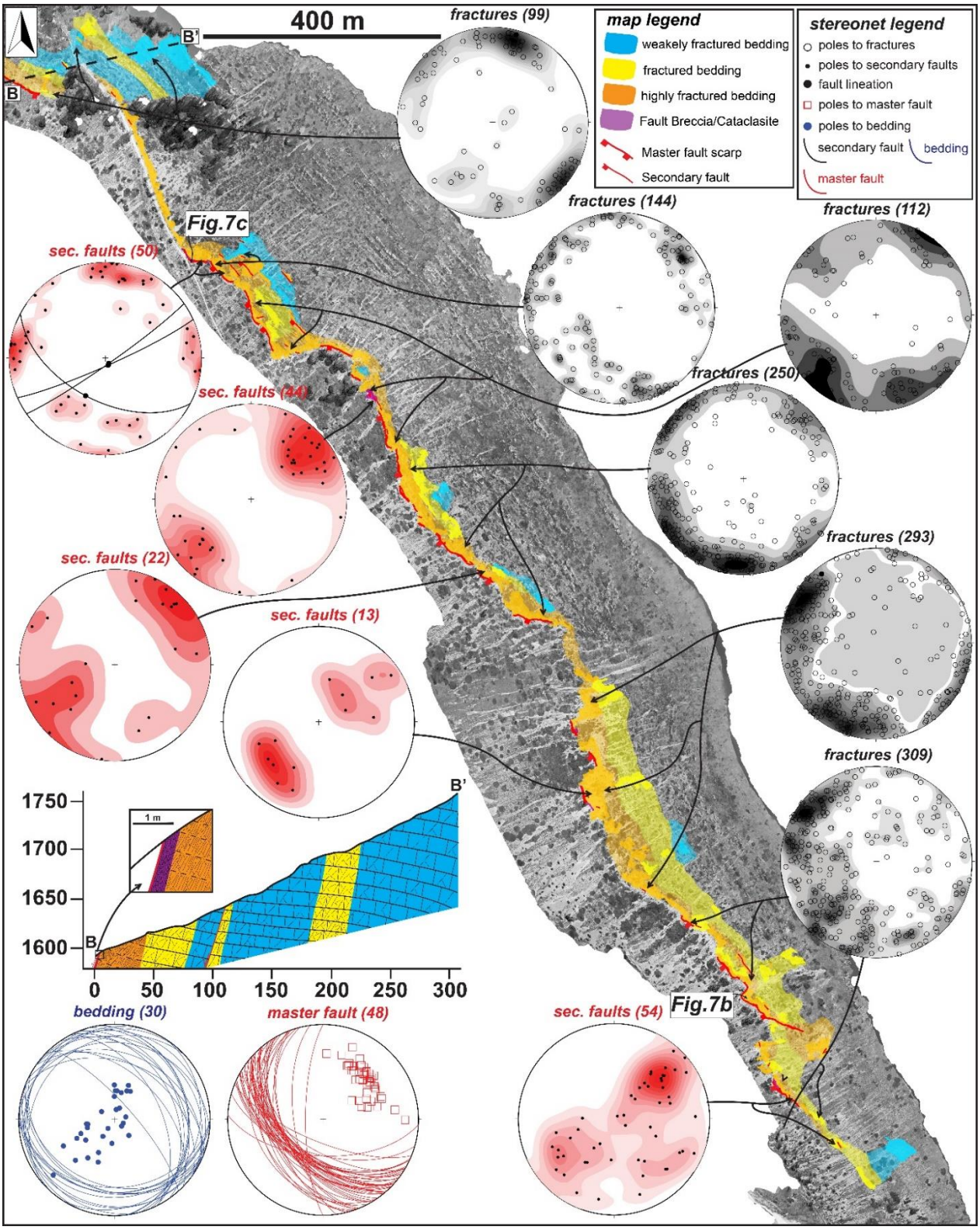


Figure 4.5: Structural Sketch map of the Campo Felice fault zone in the Mt. Serralunga sector including structural data collected within the different structural units, plotted in Equal Area-Lower Hemisphere stereonets with density contours areas (see figure legend for symbols description). Interpreted structural units were drawn with higher degree of transparency.

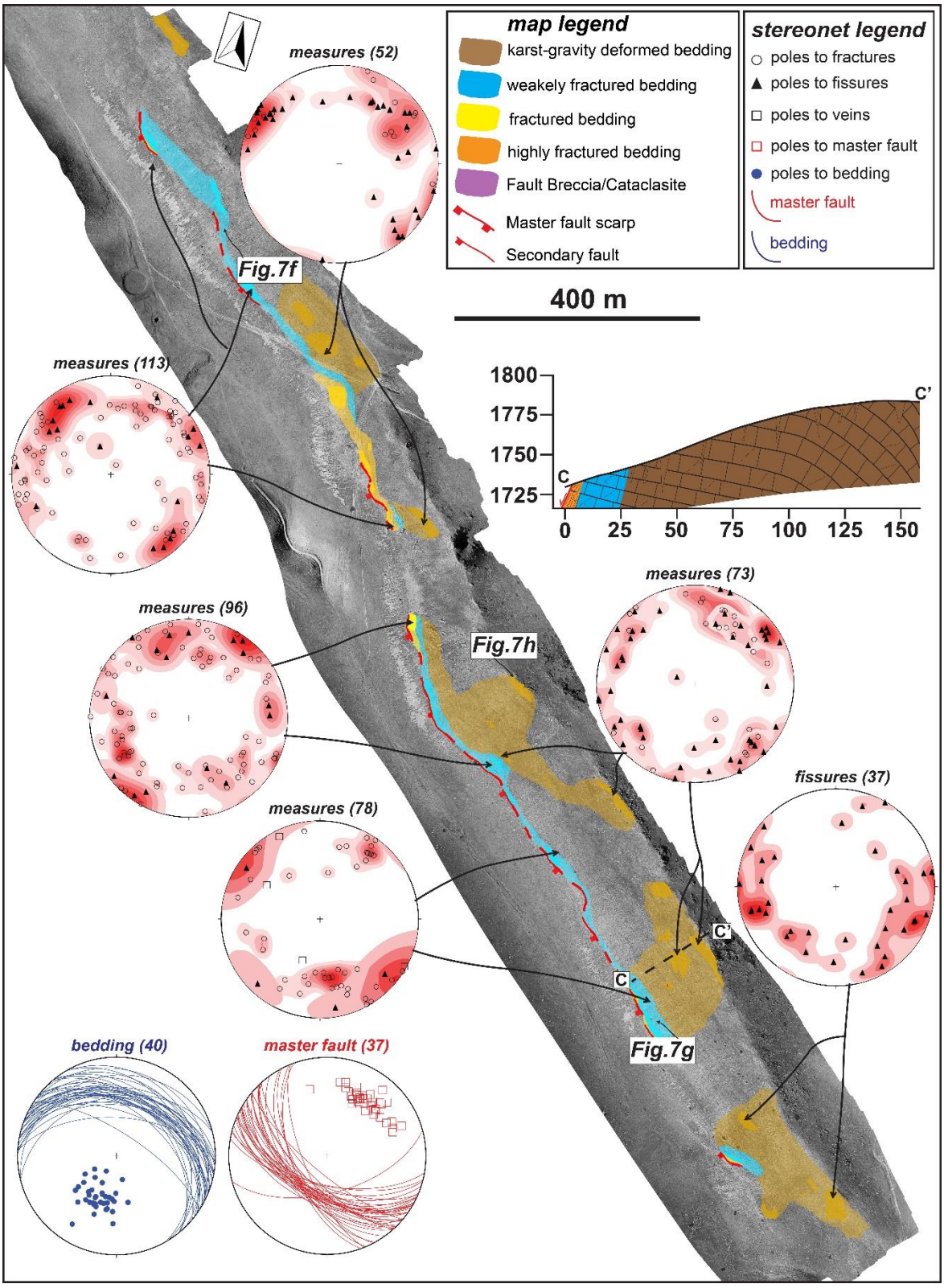


Figure 4.6: Structural Sketch map of the Cama fault zone including structural data collected within the different structural units, plotted in Equal Area-Lower Hemisphere stereonets with density contours areas (see figure legend for symbols description). Interpreted structural units were drawn with higher degree of transparency.

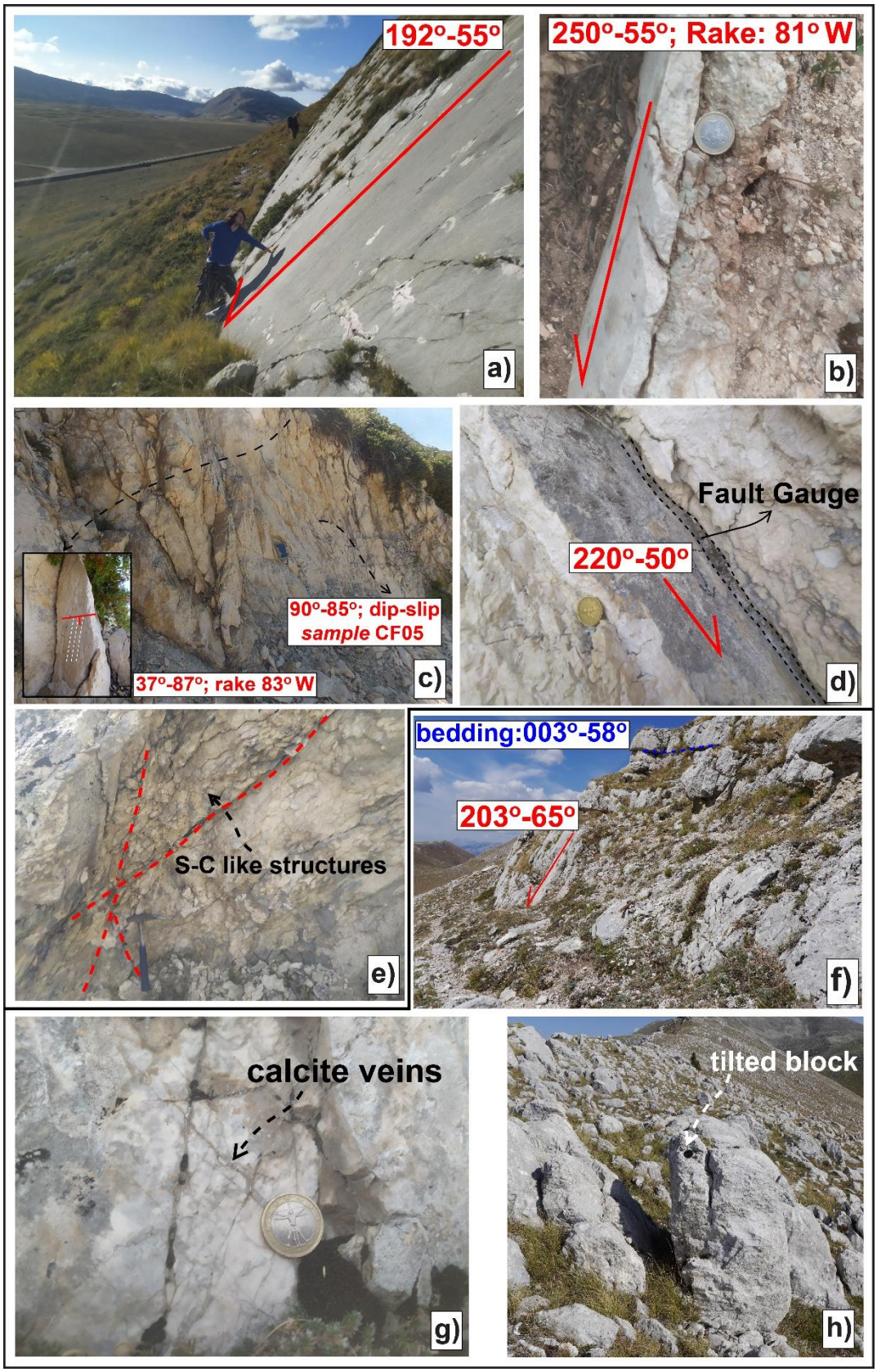


Figure 4.7. a) Campo Felice fault scarp affecting the western slope of Mt. Cefalone with a maximum height of ~ 15 m. b) Polished Campo Felice master fault surface within a small incision in the Cenomanian bauxites. c) Cataclastic fault core outcropping in between a sinistral step-over zone affected by numerous secondary faults with polished slip surfaces showing an almost pure dip-slip kinematic. d) large secondary fault with fault gouge

associated, synthetic with the master fault. e) S-C like structures affecting a highly fractured rocks domain in the Campo Felice Fault zone. f) Cama fault scarp sharply cutting sub-horizontal carbonate host rocks. g) Small and thin calcite veins, conjugated themselves, affecting the karstified Cama fault surface. h) Blocks of carbonate host rocks cracked and tilted down to the slope close to the hillcrest top.

### 4.4.3 Microstructures of the slip zones

In this section we describe the microstructures of the slip zones of Campo Felice and Cama faults following the classification of Sibson (1977, 2003). We define as slip surfaces the exposed fault surfaces, either polished or karstified. With slip zones (up to several centimeters thick) we indicate the deformed rocks located beneath the slip surface that accommodate the shear strain produced during fault slip (Chester and Chester, 1998; Sibson, 2003). Where present, Principal Slip Zones (PSZs) consist of texturally distinct layers, usually few mm thick, located immediately beneath the slip surface. PSZs accommodate most of the fault displacement (Smith et al., 2011).

The slip zone associated with the Campo Felice master fault surface (quite rough, due to karst- erosional processes) has a proto-cataclastic fabric consisting of angular to sub-rounded calcite grains (1-5 mm thick) surrounded by a fine matrix (white or reddish in colour in the field and dark grey or brownish in colour under the OM; Fig. 4.8a). Moving toward the slip surface, the fabric becomes more cataclastic, as the amount of fine matrix increases up to > 50% of the total volume (Fig. 4.8a). The slip zone is cut by numerous shear fractures oriented sub-parallel (i.e., Y-shear fractures) or up to ~ 40$^{o}$ with respect to the slip surface (i.e., P-shear fractures), some of them filled with calcite (see black arrows), oxides or clay minerals (Fig. 4.8a-d). Where clay minerals and oxides are abundant, the texture of fine matrix is composed of calcite micro-grains with irregular to stylolitic-like boundaries, commonly indented and forming incipient triple junctions, with numerous pore spaces locally filled with clay minerals (Fig. 4.8b, c).

Where the fault surface is locally preserved along-strike by sub-aerial exposure, the slip surface is very smooth and has a net contact with the underlying grains (Fig. 4.8e). The slip zone is a well-developed cataclasite composed of millimetres to centimetres in size sub-angular grains cut and partially surrounded by few thin veins filled with sparite and oxides (Fig. 4.8e).

The minor secondary faults affecting the fault core in the step over zones have a very smooth slip surface and a slip zone made of angular to sub-rounded clasts, ~ 2-8 mm thick and internally fractured, immersed in a dark fine matrix (< 50% of the total volume), as the one in Fig. 4.8f. The slip zone includes also a ~ 1-2 mm thick discontinuous ultra-cataclastic

level close to the slip surface, made of > 90% of fine matrix surrounding few rounded grains < 0.5 mm thick (Fig. 4.8f). The matrix is composed of sub-euhedral down to nanometric in size calcite grains with straight boundaries, forming well-developed triple junctions (when pores and clay minerals are present among grains), locally indenting each other (Fig. 4.8g).

The fault rock close to the Cama fault surface is a chaotic to mosaic breccia (Woodcock and Mort, 2008) composed of incipient angular clasts (1-10 mm in size), with stylolitic boundaries (yellow arrows) cut by numerous fractures, locally filled with secondary sparite cement (Fig. 4.9a). Fractures are commonly oriented sub-orthogonal to ~ $50^{o}$ with respect to the slip surface (the latter is very rough due to karst processes) and commonly form conjugated pairs (Fig. 4.9a). In the few and small (i.e., 2-5 m along-strike) areas where the intensity of fracture increases along scarp, the slip zone shows a cataclastic fabric composed of < 1 mm to 5 mm in size sub-angular clasts surrounded by a brownish in colour fine matrix (Fig. 4.9b). The slip zone includes numerous pores and fractures oriented both at high-angle or parallel with the slip surface, rarely filled with calcite, and thin irregular layers close to the top possibly due to dissolution-precipitation processes. Overall, this texture is quite similar to the one observed in the slip zone of Campo Felice fault (Fig. 4.8a-e).

The calcite micro-grains filling fractures are almost euhedral, with straight to indented boundaries (white arrows), locally forming triple junctions (Fig. 4.9c-d).

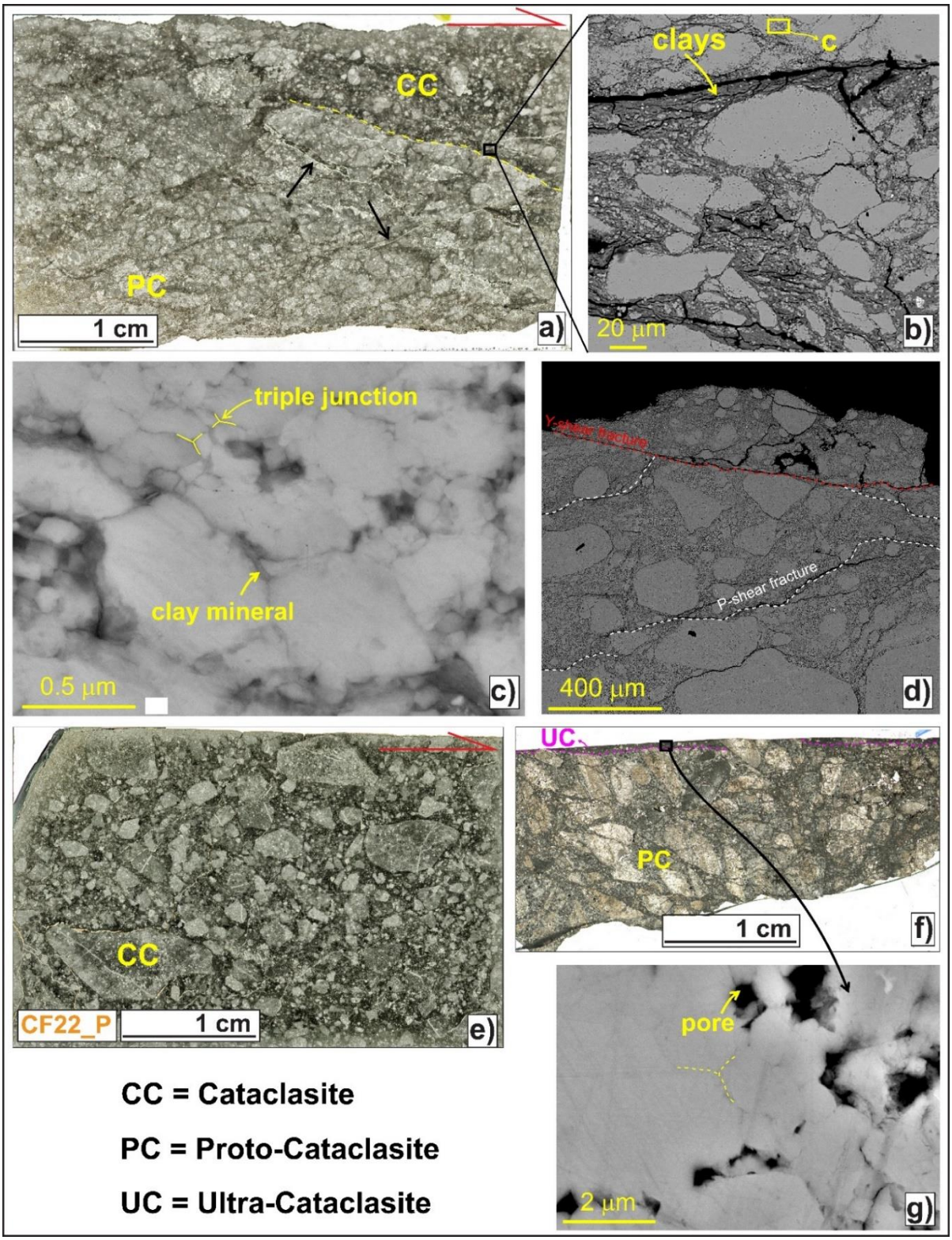


Figure 4.8. a) Slip zone associated with the Campo Felice master fault surface (quite rough, due to karst-erosional processes), showing a proto-cataclastic to cataclastic fabric consisting of angular to sub-rounded calcite grains (1-5 mm thick) surrounded by a fine grey matrix, cut by thin fractures and calcite veins (black arrows). b-c) Clay minerals filling the fracture spaces and surrounding the calcite grains, showing stylolitic-like boundaries, indentation structures and incipient triple junctions. d) Y-shear and P-shear fractures cutting the slip zone close to the slip surface. e) The slip surface is very smooth where preserved by sub-aerial exposure and the associated slip zone is composed of heterogeneous in size sub-angular grains with few thin calcite

veins. f) Slip zone of a minor secondary fault made of ~ 2-8 mm thick clasts immersed in a dark fine matrix and including a discontinuous ultra-cataclastic level (i.e., PSZ) close to the very smooth slip surface. g) The matrix of the PSZ is composed of sub-euhedral calcite grains with straight boundaries, forming well developed triple junctions and locally indented.

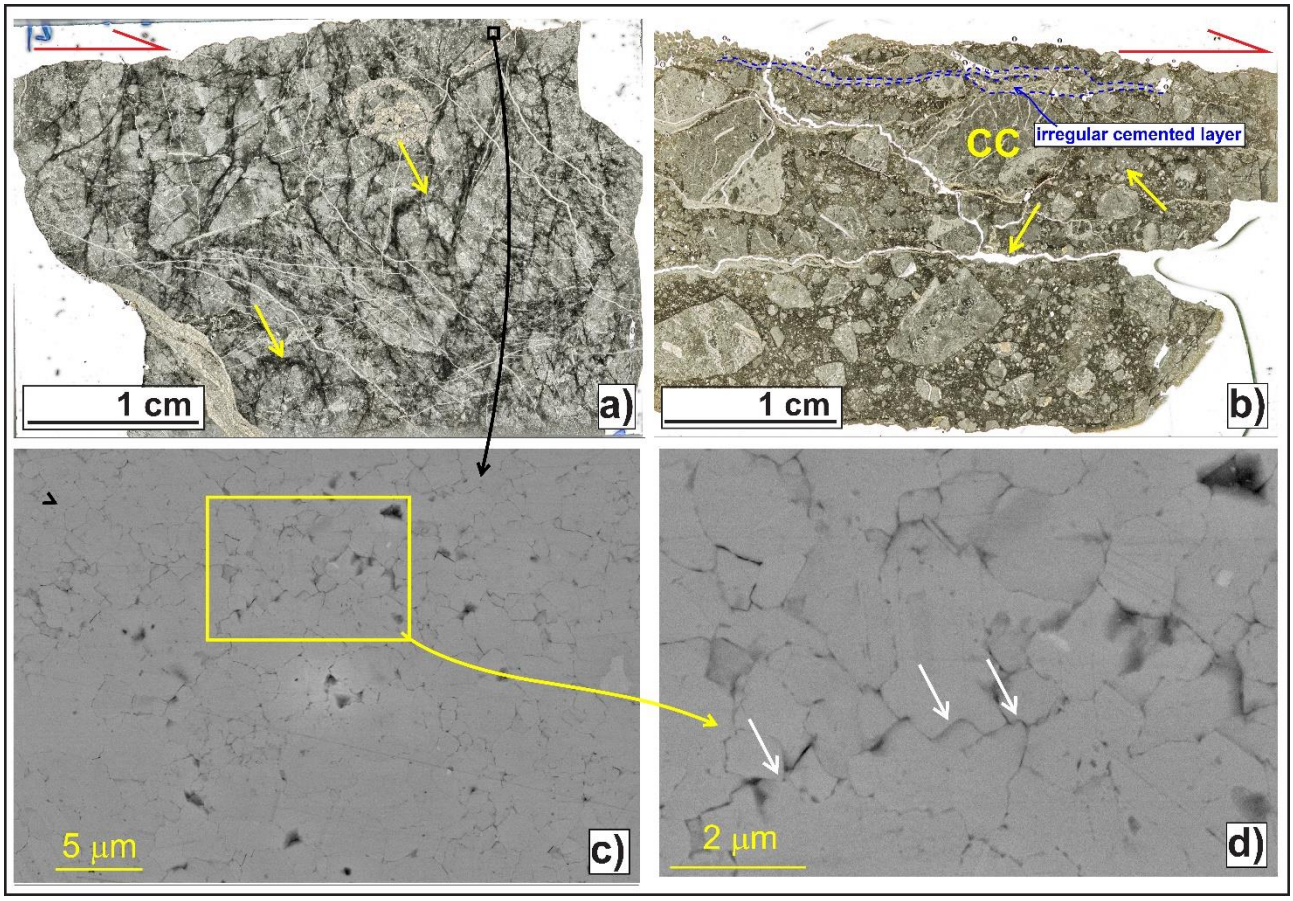


Figure 4.9. a) The slip zone associated with the Cama fault consist of chaotic to mosaic breccias composed of < 1 cm in size angular clasts with stylolitic boundaries (yellow arrows), cut by numerous fractures oriented at high angles with the very rough slip surface, locally filled with sparite. b) Slip zone where intensity of fractures increases, showing a cataclastic fabric composed of sub-angular clasts with different size surrounded by a fine matrix cut large fractures oriented both at high-angle and parallel with the rough slip surface. c-d) Calcite grains filling fractures are almost euhedral, with straight to indented boundaries (white arrows), somewhere forming triple junctions.

## 4.5 Discussion

In this work we compare two normal faults of the central Apennines cutting with similar attitude the same host rocks: The Campo Felice and Cama faults. The two faults are inferred to be geometrically and kinematically linked (Salvi et al., 2003; Fig. 4.1). We describe the geological and structural characteristics at macro- to micro-scale of the two faults, shown in table 1. In the following sections we will discuss the structural differences between the

Campo Felice and Cama fault zones (Section 5.1) and the deformation mechanisms active in these carbonate-hosted faults (Section 5.2).

### 4.5.1 Relation between the Campo Felice and Cama faults

The Campo Felice fault has an almost continuously exposed sharp fault scarp ~ 3-4 m high on average, up to 15 m in some areas (e.g., Fig. 4.7a), locally undulated along-strike (Figs. 4.4-4.5). The fault core decorates the fault scarp for several kilometres and mainly consists of cataclasites (~ 0-40 cm thick) and crush fault breccias (50 cm to 2 m thick). The latter are cut by several high-angle secondary faults and calcite veins, also affecting highly fractured rocks domains (~ 30-150 m thick), where fractures are spaced < 3 cm apart (Figs. 4.4-4.5). The fault is composed of numerous segments arranged in *én-echelon* step-over zones where fault core is wider (i.e., up to 15 m thick) and fracture intensity strongly increases, thus favoring fluid-assisted processes and the development of stylolites and S-C like structures (Figs. 4.3a, 4.7e). Such structural features were also observed in other large displacement normal faults in the central Apennines (e.g., San Benedetto-Gioia dei Marsi fault segment, Agosta and Aydin, 2006; Campo Imperatore fault system, Fondriest et al., 2020; Demurtas et al., 2016) although these faults have wider fault cores (i.e., 1- 40 m thick) and damage zones (up to thousands of meters) associated.

Instead, the fault zone associated with the Cama fault is much less developed compared with the one of Campo Felice fault. The fault scarp is discontinuous and outcrops only in the middle and southern sectors, with maximum height of ~ 2 m. Fault core is absent, except close to the south-eastern tip, where it mainly consists of mosaic fault breccias (Woodcock and Mort, 2008) and damage zone thickness is < 40 m. With few exceptions, fractures in the damage zone are usually spaced > 10 cm apart, and no secondary faults and small and thin calcite veins were observed (Figs. 4.5, 4.7g). These fault features could be typical of immature or small displacement faults and would be consistent with the ~ 100 m of maximum geological throw (cross-section B-B'; Fig. 4.2d) and the estimated low Quaternary throw rates (0.2 mm/yr; Salvi et al., 2003).

Indeed, the Cf borders to SW a narrow (i.e., < 400 m wide; Figs. 4.1, 4.2, 4.6) valley instead of a wide Quaternary basin, that is commonly associated with large active normal faults, although in central Apennines several Quaternary basins could have been inherited and not directly produced by the bounding normal faults (e.g., Mancinelli et al., 2021).

Furthermore, the numerous high-angle fissures affecting both the Cama fault zone and surrounding host-rocks possibly formed in tensional regime (i.e., negative values of

minimum principal stress) or at very low confining pressures with maximum principal stress oriented sub-parallel to the fracture surface (i.e., Mode I fracture; Fossen, 2010). Average fracture aperture increases toward the hill top, also favored by karst processes, causing the formation of several gravitational trenches with blocks of carbonate rocks commonly tilted down to the slope (Figs. 4.3h, 4.7h). As a matter of fact, the Mt. D'Ocre range is characterized by numerous landforms typically associated with gravitational processes such as double-crested lines, scarps and trenches, mainly aligned in the NW-SE direction (Salvi et al., 2003; Albano et al., 2015). Mt. D'Ocre range faults may have been formed during Quaternary to accommodate the NE migrating crustal extension (Hunstad et al., 2003; Cosentino et al., 2010; Carminati and Doglioni, 2012). On the other hand, these normal faults could have been also formed during Apennine orogenesis to accommodate the bending of carbonate strata (the bedding increases from ~ 15°- 35° to ~ 70° uphill towards the crest; Fig. 4.6) close to the anticline fold hinge, with associated geomorphic scarps currently accommodating gravitational processes (Fig. 4.2d; Li et al., 2018; Tavani et al., 2015; Bazalgette et al., 2010).

The observed structural features would suggest that the Cama fault does not represent a segment of the Ovindoli-L'Aquila active fault system (Salvi et al., 2003; Galli et al., 2008). Instead, the major slip surface may currently accommodate the lateral spreading of Mt. D'Ocre Range, mainly moving by creep, together with the Campoli-Cerasitto fault and other faults of the area (Figs. 4.1, 4.2b, d). This interpretation may have important implications in terms of seismic hazard assessment of the study area. Indeed, the seismogenic source associated with the Ovindoli-L'Aquila Fault System would be reduced of ~ 9 km, thus reducing the maximum expected earthquake magnitude of the fault system from ~ 6.8 to ~ 6.5 (Wells and Coppersmith, 1994; Leonard, 2010). However, given the proximity with the CFf, episodic movements along these faults can likely be induced by ground shaking produced by earthquakes, (Salvi and Nardi, 1995; Albano et al., 2015), also consistent with the average fault dip angles of ~ 60° (Fig. 4.5).

### 4.5.2 Deformation mechanisms on carbonate rocks

In active fault zones, the bulk of displacement cumulated during individual earthquakes is mainly accommodated in the fault core, in particular within highly localized cataclastic mm-cm thick principal slip zones (Caine et al., 1996; Chester and Chester, 1998; Chester et al., 1993; Power and Tullis, 1989; Sibson, 2003; Smith et al., 2011, 2015).

The Campo Felice fault surface appears quite rough where the exposed fault scarp is karstified (Fig. 4.8a). The associated slip zone shows a proto-cataclastic to cataclastic fabric, including thin calcite veins and both Y-shear and P-shear fractures, but lack of a well-defined ultra-cataclastic layer close to the slip surface (i.e., the PSZ), possibly obliterated by weathering (Fig. 8a, d). Where preserved by surficial alteration, the fault surface is smoother, with a net contact with the larger clasts of the underlying cataclastic slip zone (Fig. 4.8e). The well-preserved slip surfaces of secondary faults are very smooth to polished, with an associated proto-cataclastic/cataclastic slip zone that includes a ~ 1-2 mm thick ultra-cataclastic PSZ (Fig. 4.8f).

On the contrary, the slip surface of Cama fault is very rough, in part due to weathering of the exposed fault scarp and lacks of a neat principal slip zone. Indeed, the fault rock beneath the slip surface is a chaotic to mosaic fault breccia cut by numerous fractures and calcite veins (0.1-0.2 mm thick) oriented at high-angles (i.e., > 50°) with respect to the slip surface (Fig. 4.9a).

The different textures observed in the slip zones of the Campo Felice and Cama faults can be explained by higher geological throws cumulated in time by the CFf compared with the Cama fault. Indeed, in the rare areas where the intensity of fracture increases along the Cama fault, the slip zone shows a cataclastic fabric quite similar to the one observed in the slip zone of Campo Felice fault (compare Fig. 4.8a-e, with Fig. 4.9b).

The fine matrix surrounding clasts in the Campo Felice fault core is whitish, but locally appears as reddish in color, due to the presence of clays and Fe-oxides and hydroxides, probably deriving from the bauxitic layers of the unit IBX (see Fig. 4.2). In these reddish fault core volumes, the texture of fine matrix is composed of calcite micro-grains with irregular to stylolitic-like boundaries and pores locally filled with oxides and clay minerals, incipient triple junctions and indentation structures, interpreted as due to pressure-solution processes (Rutter, 1983; Gratier et al., 2013; Fig. 4.8b, c). Pressure-solution is a water-assisted process mainly driven by the stress acting at the grain-to-grain contacts that occurs through dissolution at grain boundaries, diffusion of the solute matter, and precipitation of the latter within pore spaces (Rutter, 1983; Tada and Siever, 1989; Lehner, 1995; Gundersen et al., 2002; Croizè et al., 2013). Pressure-solution is one of the most important processes of compaction and healing of carbonate hosted faults and does not require high ambient pressures and temperatures to be activated (Renard et al., 2000; Yasuhara et al., 2005; Fondriest et al., 2020). Numerous factors can influence the rate of compaction due to

pressure-solution, such as temperature, porosity, fracture connectivity, grain size, water composition and the presence of clay minerals. The latter commonly promote pressure-solution processes as they prevent grain boundary healing by maintaining the grain boundaries open (Renard et al., 2001), thus favoring dissolution and formation of stylolites (Ehrenberg, 2006; Aharonov and Katsman, 2009). As a matter of fact, where fine matrix in the CFf fault core appears whitish in the field (Fig. 4.7b, c), it is mainly composed of more packed sub-euhedral calcite grains, with straighter boundaries and more developed triple junctions (Fig. 4.8g). However, this texture can be also favored by the higher degree of grain comminution within the ultra-cataclastic principal slip zones, since grain size also enhance pressure solution rates (Renard et al., 2000; Rutter, 1983; Tada and Siever, 1989).

In case of Cama fault slip zone, the sub-grains of fault breccia have irregular to stylolitic boundaries and are affected by numerous veins filled with secondary sparite (Fig. 4.9a), composed of sub-euhedral calcite micro-grains with straight contacts and indentation structures (Fig. 4.9b). These features suggest fluid circulation and pressure-solution processes active during and after fault slip to seal the fractures.

Microstructural analyses indicate that similar deformation mechanisms (i.e., cataclasis and pressure-solution) occur in both Campo Felice and Cama faults. However, the slip zones associated with the two structures have different textures, (i.e., Cataclasite *vs.* crush fault breccia) mainly because of the higher average long-term slip rates (~ 1 mm/yr for CFf and 0.2 mm/yr for Cf; Galadini and Galli, 2000; Salvi et al., 2003) and cumulated geological throws of Campo Felice fault (Table 1).

Table 1: Comparison of the main geological and structural features of the Campo Felice and Cama faults

| | Campo Felice fault | Cama fault |
|---|---|---|
| *Along-strike length* | ~ 6 km | ~ 3 km |
| *Fault scarp heigth* | ~ 4 m, up to 15 m | max. 2 m |
| *Max. geol throw* | 1050 m (error 425 m) | ~ 100 m |
| *throw rates* | ~ *1 mm/yr* | 0.2 *mm/yr* |
| *Damage zone thickness* | > 400 m | ~ 40 m |
| *Core thickness* | ~ 40 cm, up to 15 m | almost absent, up to 2 m |
| *Secondary faults* | numerous in both core and damage zone | not found |
| *Veins* | numerous in both core and damage zone | only close to the fault scarp and very thin (< 5 mm) |
| *Slip zones microstructures* | Cataclasite to Ultra-cataclasite | Crush breccia to cataclasite |
| *Deformation mechanisms* | Cataclasis and pressure-solution | Cataclasis and pressure-solution |

## 4.6 Conclusions

In this work we have compared the fault zone architecture in the footwall and the microstructures of the slip zones of two carbonate hosted normal faults in the Italian central Apennines: The Campo Felice and Cama faults (Table 1).

The maximum estimated geological throw of Campo Felice fault is ~ 1050 m, with a possible overestimate of ~ 425 m (Fig. 4.2c). The fault scarp (3-15 m high) is continuous along-strike and composed of numerous segments arranged in én-echelon step-over zones. Fault core (40 cm to 15 m thick) and highly fractured rocks domains (50-150 m thick) are cut by several high-angle secondary faults and veins (Figs. 4.4, 4.5). On the contrary, the Cama fault scarp (~ 2 m high) discontinuously outcrops only in the middle and southern sectors. Fault core is almost absent and fractures in the damage zone (< 40 m thick) are usually spaced > 10 cm apart, consistent with the ~ 100 m of maximum geological throw and the estimated low Quaternary throw rates (Figs. 4.2d, 4.6). Furthermore, the numerous high-angle fissures and gravitational trenches affecting the footwall host-rocks suggest a rotational sliding accommodated by the major fault scarp.

Therefore, in spite of their proximity (i.e., ~ 2 km of along-strike spacing) and similar attitude, the large differences observed in the fault zones and summarized in table 1 would

suggest that two faults do not link at depth, as previously hypnotized by Salvi et al., 2003. According to this interpretation, the seismogenic source associated with the Ovindoli-L'Aquila Fault System would be reduced up to 8-9 km, thus reducing the maximum expected earthquake magnitude of the fault system from ~ 6.8 to ~ 6.5 (Wells and Coppersmith, 1994; Leonard, 2010). Nevertheless, recent throw distribution and structural field analyses suggest a possible shallow soft-linkage to NW between the Campo Felice and Mt. Orsello faults (Fig. 4.1; Schirripa Spagnolo et al. 2021).

The slip zone of Campo Felice fault is a proto-cataclasite to cataclasite composed of angular to sub-rounded grains (1-5 mm thick) surrounded by a fine matrix whose amount increases toward the slip surface. The latter appears quite rough due to karst-related process (Fig. 4.8a), but it is very smooth where preserved by surficial alteration (Fig. 4.8e). On the contrary, the slip zone of Cama fault is a mosaic breccia with 1-10 mm thick angular clasts cut by numerous fractures filled with sparite and oriented at high angles with the very rough slip surface (Fig. 4.9a). In some areas, the slip zone locally shows a cataclastic fabric quite similar to the one observed in the slip zone of Campo Felice fault (Fig. 4.9b).

The fine matrix of Campo Felice and Cama fault slip zones show similar textures, composed of calcite micro-grains with irregular to stylolitic-like boundaries and pores locally filled with oxides and clay minerals, with incipient triple junctions and indentation structures, due to pressure-solution processes. These textures are more developed in the Campo Felice slip zone because of the higher cumulated geological throws and amount of clay minerals with respect the Cama fault. Such observations are consistent with the macro-structural features observed in the Campo Felice and Cama faults and show how normal active faults displacing the same host rocks may have variable to comparable slip zones associated, produced by similar deformation mechanisms.

In conclusion, both macro- and micro-structural analyses provide further parameters to improve the characterization of seismogenic sources associated with neighbouring faults affecting similar host-rocks (Falcucci et al., 2016; Galadini et al., 2012) and to understand better the formation and current mechanical behaviour of DGSDs in tectonically active regions.

# 5. Crystallographic Texture Analyses on slip zones in carbonate rocks

*This chapter is in preparation. The study was performed with the collaboration of Evgeny Borovin, Giulio Di Toro, Gilberto Artioli, Luca Luterotti and Marco Moro. Giulio Di Toro and Gilberto Artioli contributed to the work design; I was assisted by Evgeny Borovin during XRD, XRF and texture analyses; I wrote the original draft and discussed the results with Giulio Di Toro, Evgeny Borovin, Gilberto Artioli and Luca Luterotti.*

## Abstract

Most of slip in carbonate-hosted faults is accommodated within < 1 cm thick Principal Slip Zones (PSZs), produced by both high (e.g., dislocation and diffusion creep) and low (e.g., cataclasis, pressure-solution and precipitation) temperature deformation mechanisms. To unravel the possible deformation mechanisms operating during fault slip, we performed Crystallographic Texture Analyses (CTA) on a sample from a normal fault in the central Apennines (VA05). The normal fault is < 2 km long and cuts marine limestones. For calibrating the technique, we also investigated polished slip surfaces from dolomitic marbles sheared in the laboratory at seismic slip velocities.

The PSZ of VA05 is a cataclasite with the fine matrix composed of 1-5 μm in size and packed calcite micro-grains, locally indented, consistent with brittle cataclastic and congruent pressure-solution mechanisms active during and after slip at very low boundary conditions (i.e., $P_{litho}$ < 20 MPa and T < 20°C) and slip rates (i.e., mm/sec to μm/sec). The activation of these processes is also in agreement with CTA results, that indicate a weak preferred orientation of calcite micro-grains in the PSZ. Only the experimental sample sheared at v ~ 1 m/s show evidence of decarbonation during slip, with secondary periclase possibly nucleated at T ~ 600°C and crystalized with the {100} glide planes oriented parallel to the shear direction, representing a possible seismic slip indicator. CTA technique has proven to be a powerful tool to study polished fault slip zones as it allows to investigate hundreds of micrometers thick rock volumes with great accuracy and is less time-consuming than alternative techniques.

# 5.1 Introduction

Most of slip displacement along brittle faults is accommodated within tens of centimeters to meters thick fault cores dominated by cataclastic and pressure-solution processes (e.g., Sibson, 1977; Caine et al., 1996; Gratier et al., 2011). In particular, field observations of active faults (surface ruptures, fault trenches, etc.) and exhumed faults (e.g., presence of pseudotachylytes, Sibson 1975) and microstructural observations of fault rock specimens show that the bulk of co-seismic displacement during individual earthquakes occurs within highly localized slip zones less than few centimeters thick (Chester et al., 1993; Sibson, 2003; Wibberley and Shimamoto, 2003).

Furthermore, faults cutting carbonate rocks commonly show zones of extreme slip localization (i.e., Principal slip zones; PSZs), few hundreds of micrometers thick, bounded by polished to mirror-like slip surfaces, composed of nanoparticles *(D* < 1μm), amorphous

materials and sintered nanograins (De Paola et al., 2008; Smith et al., 2011, 2013; Fondriest et al., 2012; 2013; Siman-Tov et al., 2013; Demurtas et al., 2016; Ohl et al., 2020).

Most of the both low- and high-velocity friction experiments conducted on carbonate rocks show that these textures are mainly produced by a combination of cataclasis and viscous deformation mechanisms (e.g., Grain Boundary Sliding aided by both dislocation and diffusion creep; Verberne et al., 2014; Green et al., 2015; Spagnuolo et al, 2015; De Paola et al., 2015; Pozzi et al., 2019, 2021; Demurtas et al., 2019). The latter are dominant at seismic velocities (i.e., v = ~ 1 m/s), when temperatures along fault slip zone rise up to > 600°C due to frictional heating (Rice, 2006), and drastically reduce the frictional strength of fault from $\mu$ = 0.6-0.85 (Byerlee, 1978) to $\mu$ < 0.2 (Han et al., 2007; Di Toro et al., 2011; Pozzi et al., 2019).

Recent microstructural analyses on both carbonate-hosted normal faults and Deep-Seated Gravitational Slope Deformations (DGSDs; Moro et al., 2012) indicate variable to comparable slip zones microstructures and similar textures of fine matrix close to the slip surface (Del Rio et al., 2021). The latter is mainly composed of highly packed calcite micro- to nano-grains with straight to irregular boundaries, indentation structures, incipient triple junctions, and few to numerous pores and cavities, locally filled with secondary calcite or clay minerals and oxides. Such textures were inferred to be produced by both brittle cataclastic and congruent pressure-solution creep processes active at both high and very low slip rates (i.e., from m-cm/sec to mm/yr) and shallow crustal levels (i.e., $P_{litho}$ < 20 MPa and T < 20°C; Del Rio et al., 2021).

Analysis of Crystallographic Preferred Orientations (CPOs) within localized PSZs is a powerful technique to determine the sense of shear, the amount of strain, the temperature and the deformation mechanisms active during slip (Law et al., 1986; Mainprice and Nicolas, 1989; Rutter et al., 1994; Zang and Karato, 1995; Prior et al., 1999; Heilbronner and Tullis, 2002; Passchier and Trouw, 2005; Pozzi et al., 2019). Electron Backscattered diffraction (EBSD) analysis applied to Scanning (SEM) and Transmission Electron Microscope (TEM) is the most commonly used technique to identify CPOs. However, spatial resolution of SEM images does not allow EBSD to properly resolve grains less than 500 nm in size (Prior et al., 2009; Pozzi et al., 2019). On the contrary, TEM has a maximum spatial resolution < 1 nm, but the area of analysis is too small (i.e., few tens of square micrometers) to allow a collection of statistically significant dataset. Demurtas et al. (2019), applied a Transmission Kikuchi diffraction (TKD) to a nanogranular PSZ and managed to index ~ 1350 grains, most of them ~ 200-300 nm in size on an area of ~ 450 square micrometers. However, the section

analysed is still too small to allow a good statistical significance and do not capture the three-dimensional nature of the material.

Instead, Crystallographic Texture Analysis (CTA) is an X-ray (or neutron) diffraction-based technique that measures the intensity of the diffraction signal of each individual crystallite that diffract coherently with the Bragg law to infer the orientation of a specific volume fraction of crystallites in the probed volume (Wenk, 1985, 2016). The latter can be up to hundreds of million cube microns allowing a strong statistic consistency of the collected data (Artioli, 2007; Chateigner et al., 2019).

In this work we applied the CTA technique for the first time on natural fault samples in carbonates. The selected normal fault is the Valle Force fault (VFf), that crops out in the Italian Central Apennines (Fig. 5.1). The fault is relatively small (i.e., < 2 km long along-strike), less than 3 km deep and borders a narrow and laterally confined basin affected by karst and gravitational processes (D'Agostino et al., 1998; Del Rio et al., 2021). The main goal is to unravel the possible deformation mechanisms operating during fault slip. For instance, brittle cataclastic processes combined with pressure-solution creep are expected to be active at low slip rates (aseismic slip < 1 mm/yr) and would produce weak preferred orientations (De Bresser and Spiers, 1997; Pozzi et al., 2019). Instead, viscous deformation mechanisms, such as dislocation creep, possibly associated with seismic slip (> 1 m/s) would possibly induce a relatively strong preferred orientation (Poirier, 1985; De Bresser and Spiers, 1997; Kim et al., 2018). For comparison and calibrating the technique, we analyzed experimentally produced polished slip surfaces from dolomitic marbles deformed at seismic slip velocities. Unfortunately, the Covid impact during this work strongly limted the possibility to do more experiments on natural samples of DGSDs scarps.

## 5.2 Materials and Methods

Samples from the Valle Force fault wall (VA05) includes Cretaceous carbonates, in the footwall, and Lower Pleistocene calcareous breccias, in the hangingwall (Fig. 5.1a-c). The latter breccias preserve by weathering and karts alteration the fault scarp, so that the scarp appears ultra-polished where the breccias are removed (Fig. 5.1a).

Experimental samples were produced through friction experiments performed at different conditions with the Slow to HIgh Velocity Apparatus (SHIVA; Di Toro et al., 2010; Niemeijer et al., 2011) installed at National Institute of Geophysics and Volcanology (INGV) of Rome on solid cylinders (50/30 mm external/internal diameter – for sample preparation see Nielsen et al., 2010) of dolomitic marble from Apuane Alps.

Samples 762 and 768 (Fig. 5.1d) were first loaded at a normal stress $\sigma$n = 10 MPa and then sheared at slip velocities of v = 10 cm/s for ~ 5 mm and v = 1 m/s for ~ 5 m, respectively. Sample 916, used as comparison, was prepared as the two previous samples and then loaded at $\sigma$n = 10 MPa but not sheared. Sample 034, sheared at 6.5 m/s at $\sigma$n = 10 MPa for 20 m, was used as a reference for mineralogical and chemical elemental analysis.

X-Ray diffraction (XRD) quantitative phase analyses were performed with the X-Ray diffractometer installed at Trento University, using monochromatic wavelength ($\lambda$CuK$\alpha$ = 1.5406 A$^o$) in a Bragg-Brentano $\theta$-2$\theta$ geometry. The samples were fixed on a sample holder (about 1x2 cm wide; Fig. 5.1e) mounted on a four-circle goniometer equipped with a Eulerian cradle (Fig. 5.1f) and probed with a circular beam ~ 500 $\mu$m in diameter. To enlarge the representing volume of analysis and increase the grain statistics, the samples were oscillated during the entire measurement along the longitudinal direction for ~ 1 cm. In case of VA05 sample, the surface of hangingwall breccias was artificially polished before analyses (i.e., VA05_HWB; Fig. 5.1e) and then removed to a depth of 0.1 mm to analyze the footwall rocks beneath (i.e., VA05_FWC) using a polishing and grinding machine.

Direct Pole figures were obtained by measuring at specific points the diffracted intensities relative to each {hkl} crystal plane that diffract coherently with the Bragg law along a specific direction. Diffracted x-rays were collected by the 2D DECTRIS Eiger R 1M solid state detector in reflection mode. Sample investigation depth ranged from ~ 70 microns from the sample's slip surface with an angle of 55$^o$ of the incident beam to the surface and ~ 20 microns with an incident beam angle of 15$^o$.

During the measurement (lasted ~ 18 hours in such configuration), samples were moved at regular increments of 10$^o$ for azimuthal angles ($\phi$ = 0-350$^o$) and 25$^o$ for polar angles ($\chi$ = 0-50$^o$) in a Bragg-Brentano $\theta$-2$\theta$ geometry (i.e., the detector moves of 2$\theta$ and the Eulerian cradle of $\theta$). All the X-ray data treatment was performed using MAUD program (L. Lutterotti, S. Matthies, and H.-R. Wenk. *MAUD: a friendly Java program for material analysis using diffraction*. IUCr: Newsletter of the CPD, 21:14-15, 1999.).

Numerous corrections were applied at pole figures during data treatment, such as defocusing, background (Huijser-Gerits and Rieck, 1974), or absorption (Chateigner et al.,1995) corrections, as completed routinely in MAUD.

Direct pole figures were normalized and used to resolve the probability equation of *Orientation Distribution Function* (f(g)):

$$\frac{dV(g)}{V} = \frac{1}{8\pi^2} f(g) dg$$

This function describes the volume density of crystallites ($dV(g)$) within the probed polycrystalline aggregate ($V$) with a given orientation ($g$) with respect to the sample orientation. The orientation ($g$) of each crystallite within the G space (i.e., the space containing all possible orientations) is described by the three Euler angles, which make coincident the reference frame of crystallite with the one of probed sample. For this study, we chose the Euler angles following the Bunge convention (i.e., $\phi1,\Phi,\phi2$; Bunge, 1969).

We measured the ODF as m.r.d. (multiples of a random distribution) and normalized it so that $f_r(g) = 1$, where $f_r(g)$ refers to a sample with all randomly oriented crystallites.

To resolve this equation from the normalized pole figures, we used the entropy-modified WIMV (E-WIMV) method, that needs a small number of pole figures compared with other methods (Lutterotti et al., 2004; Morales et al., 2002). Finally, pole figures were recalculated and re-constructed starting from the computed ODF.

To complement samples characterization, Syton-polished thin sections of the investigated samples were produced by cutting perpendicular to the slip surface and parallel to striae or along the dip direction. Thin sections of experimental samples were observed with the Field Emission-Scanning Electron Microscope (FE-SEM) installed at INGV. Images were taken in backscattered electron mode (BSE) with an acceleration voltage of 6 kV and a working distance of 7.3 mm. Thin sections of natural sample VA05 were observed with the FE-SEM Merlin Zeiss (resolution 200 nm in back-scatter electrons) installed at CERTEMA laboratory (Grosseto, Italy). Images were taken in backscattered electron mode (BSE) with an acceleration voltage of 15 kV and a working distance of 8.5-5.3 mm.

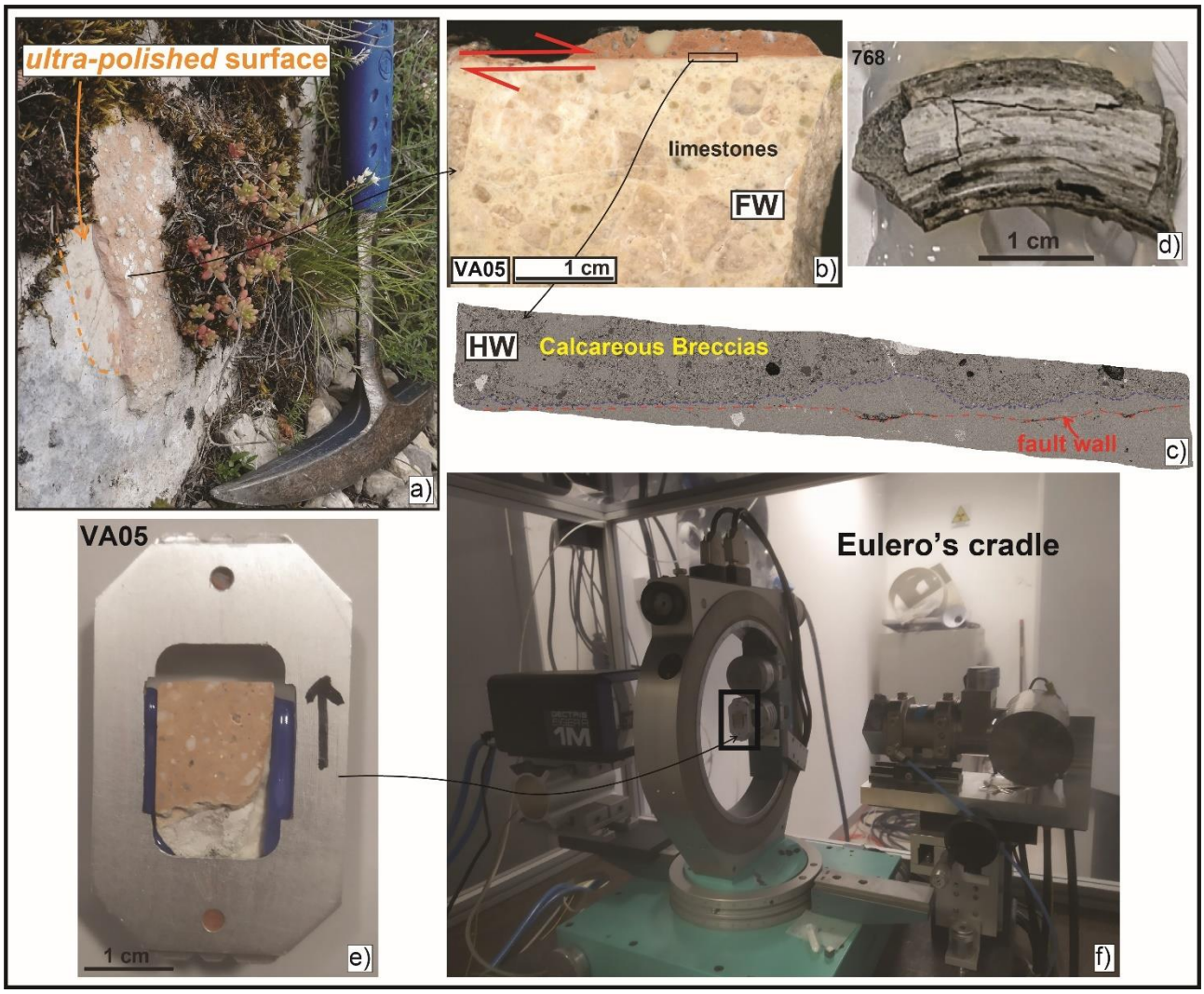


Figure 5.1. a) Valle Force fault scarp with a patch of hangingwall calcareous breccias leant on it that appears ultra-polished where breccias are removed. b) Scan of Sample VA05, showing a very sharp surface separating the wall rocks, further highlighted in the SEM image of Fig. c. d) Sample 768, produced by shearing a cylinder of dolomitic marble at ~ 1 m/sec for ~ 5 m. The slip surface looks ultra-polished and includes striae indicating the sense of shearing. e) sample VA05 with slip surface artificially polished before to be analyzed with the four-circle goniometer (f). The black arrow indicates sample orientation to ($\phi$ = 0°) and ($\chi$ = 0°).

# 5.3 Results

## 5.3.1 Slip zones microstructures and composition

In this section we describe the microstructures of the slip zones of Valle Force fault wall, sample 768 and of sample S034, the latter further investigated with Electron Probe Micro-Analyzer (EPMA). We define as slip surface the exposed fault surface, either polished or karstified, and as slip zones the deformed rocks located beneath the slip surface that accommodate the shear strain produced during slip (Chester and Chester, 1998; Sibson, 2003). Finally, Principal Slip Zones (PSZs) are texturally distinct layers, usually few mm

thick, located immediately beneath the slip surface that accommodate most of the fault displacement (Smith et al., 2011).

The PSZ in the footwall of the Valle Force fault is composed for > 99% of the total volume of 1-5 μm in size calcite grains with evidence of clast indentations and rare triple junctions among grains (Figs. 5.2a, 5.3a). The medium crystallite size of 2.5 μm agrees between bulk XRD analysis and SEM sampling observations.

The matrix of the hangingwall breccias is composed of calcite micro-grains with irregular contacts and also includes silica-bearing minerals such as quartz (~ 5% of the total volume; Fig. 5.3b) and possibly very low amounts of micas with the long axis oriented sub-parallel to the slip direction (Fig. 5.2b). The fault wall rocks are locally separated by a < 0.5 mm thick convoluted layer composed of both comminuted and packed calcite micro- to nano-grains that reminds of a dissolution-cementation front (Figs. 5.1c, 5.2b).

Sample 768 has a polished slip surface decorated with < 1 μm thick patches of gouge produced during slip with striae indicating the slip direction (Figs. 5.1d, 5.2c). The PSZ beneath the slip surface is composed of sintered nano-grains of calcite (~ 62%), periclase (~ 24%) and dolomite (~ 13%) with straight boundaries and few pores and cavities among grains (Figs. 5.2c, 5.3c). XRD patterns relative to samples 762 and 916 indicate no development of secondary calcite and periclase from the initial dolomite during experiments (Fig. 5.3d, e). Instead, the PSZ associated with sample 034 includes four distinct layers (Fig. 5.3d, e). ***Layer 1*** is composed of 50% $CaCO_3$ and 50% MgO and includes few micro-pores and cavities; ***Layer 2*** is Ca-rich with larger pores; ***Layer 3*** is still Ca-rich with respect to the initial dolomite and made of decarbonated dolomite grains immersed in a microporous matrix; ***Layer 4*** is the starting dolomite, with cracks formed during the experiment (probably due to thermal heating, expansion and unloading) sub-parallel to the slip surface.

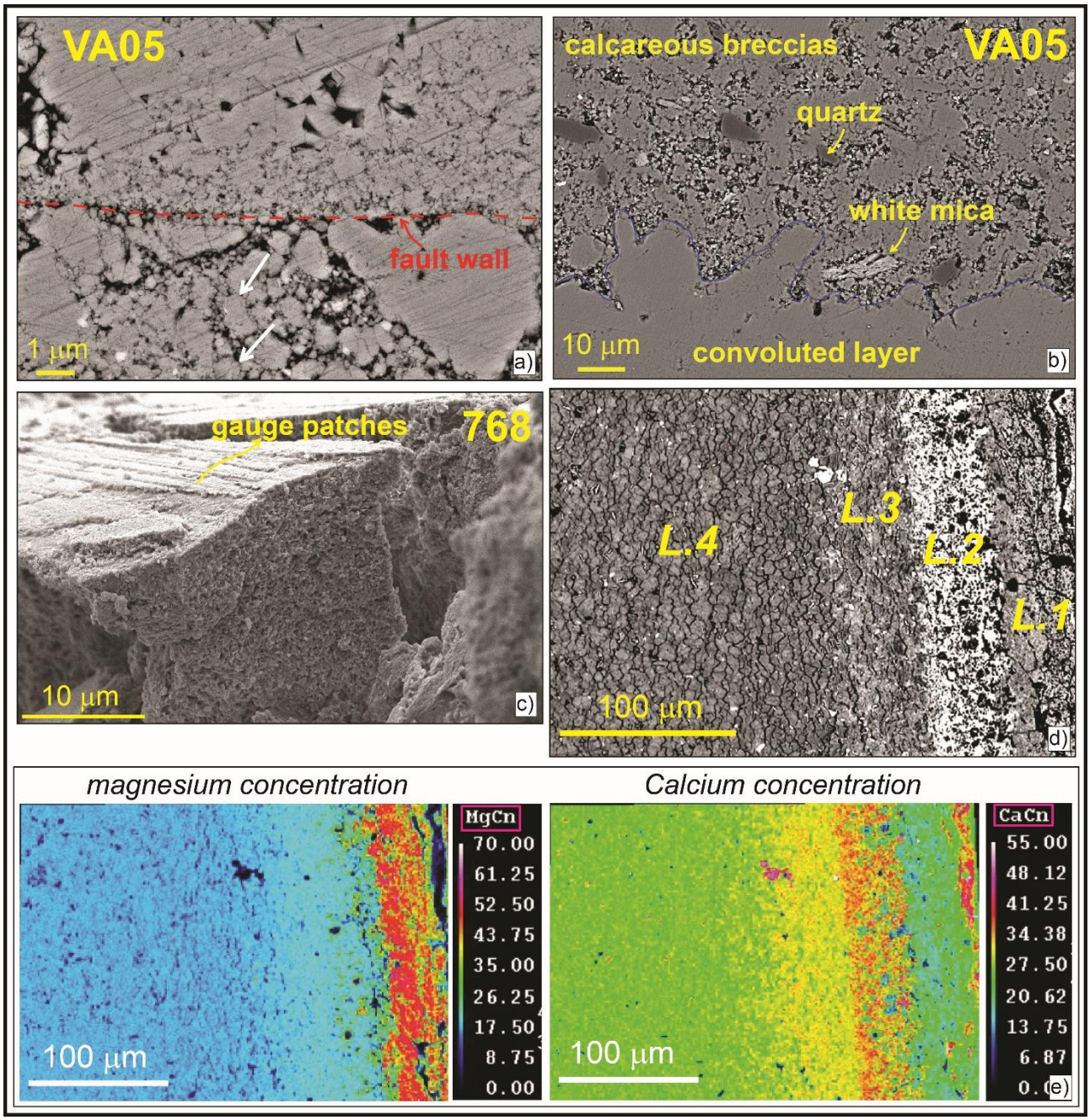


Figure 5.2. Microstructures of slip zones of Valle force fault (VA05) and experimental samples 768 and 034. a) SEM-BSE image of the Valle Force fault wall, composed of packed calcite micro-grains with pores and indentation structures. b) SEM-BSE image of the hangingwall breccias, that include also silicate minerals among calcite micro-grains, partially oriented with the sense of slip. c) SEM-SE image of the PSZ of sample 768, composed of sintered nano-grains with straight boundaries and few micro-pores and cut by a polished slip surface decorated with thin patches of striated gauge. The decarbonated porous layer lies immediately beneath. d) SEM-BSE image of sample 034, which include four distinct layers with different degree of porosity and Mg-Ca concentrations, as shown in the EMPA map in (e). The slip surface is located to the right. (e) EMPA maps of Mg (left) and Ca (right) of sample 034.

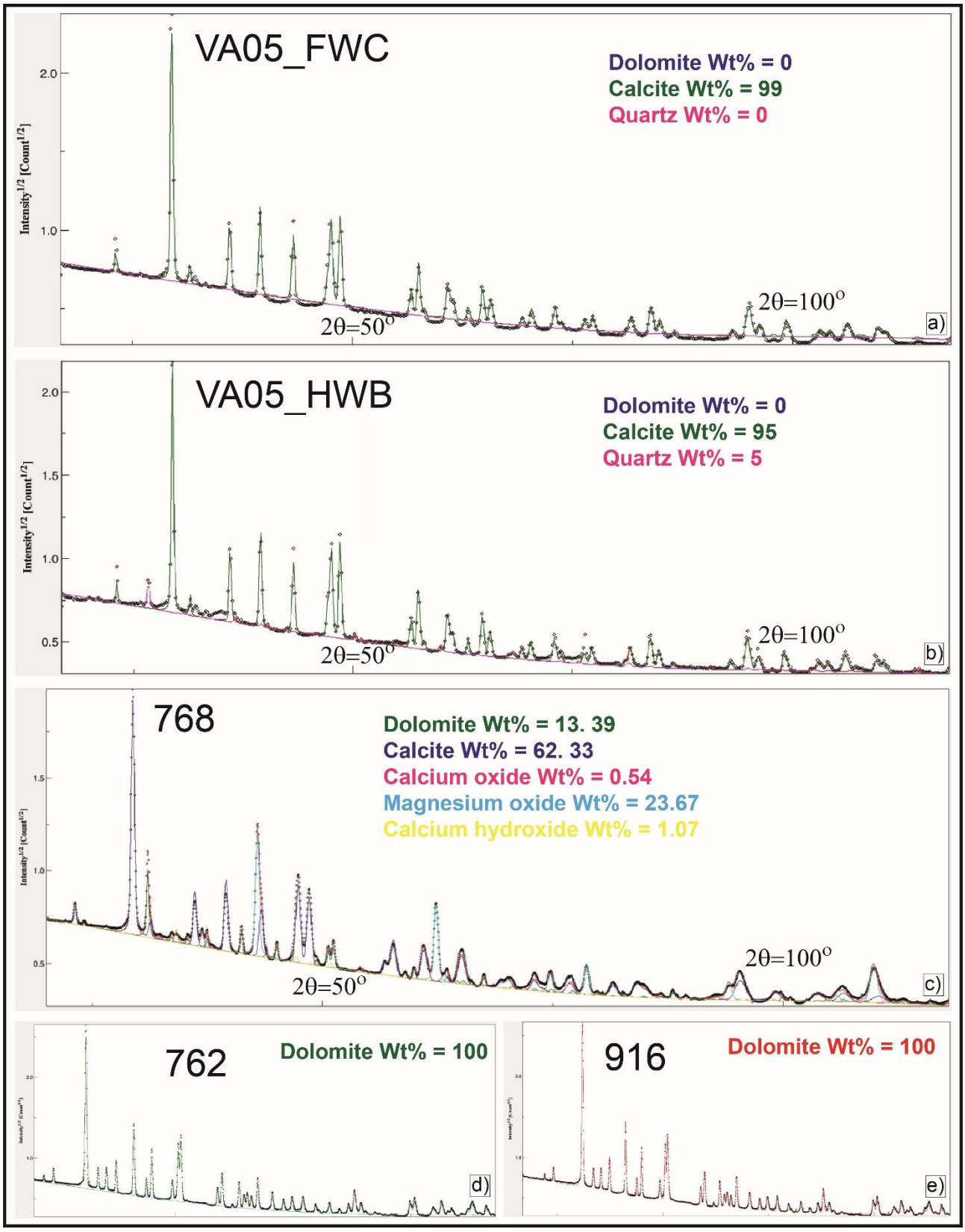


Figure 5.3: X-ray diffraction patterns of natural samples VA05 hangingwall (HWB) and footwall (FWC) and experimental samples 768, 762 and 916. a) The footwall carbonates in the footwall of Valle Force fault are composed for > 99% of calcite, whereas the hangingwall breccias include ~ 5% of quartz among calcite-rich matrix (b). c) The first few tens of microns beneath the slip surface of sample 768 are composed for ~ 13% of initial dolomite and for ~ 24% and ~ 62% of secondary periclase and calcite produced during slip. d-e) At the

limit of detection of the XRD analysis, samples 762 and 916 underwent no mineral phase changes during the experiment.

### 5.3.2 Reconstructed Pole Figures

The pole figures obtained by the computed ODF indicate the volume density of a family of equally spaced crystal planes {hkl} within the polycrystalline aggregate (i.e., texture component) oriented with a specific direction with respect the sample orientation (i.e., x, y, z). The re-constructed pole figures relative to the wall rocks of Valle Force fault indicate no development of clear preferred orientation (i.e., negligible, almost random texture) of calcite grains during slip (note the small range in the scale bar values in Fig. 5.4a). On the contrary, in the PSZ associated with sample 768, the {100} planes of secondary periclase are preferentially oriented orthogonally with the z axes of the probed sample (i.e., cube texture component; Artioli, 2007) and parallel with the sliding direction (Fig. 5.4b, e). Instead, both secondary calcite and dolomite grains do not develop a clear preferred orientation, as well as dolomite in samples 762 and 916 (Fig. 5.4c, d).

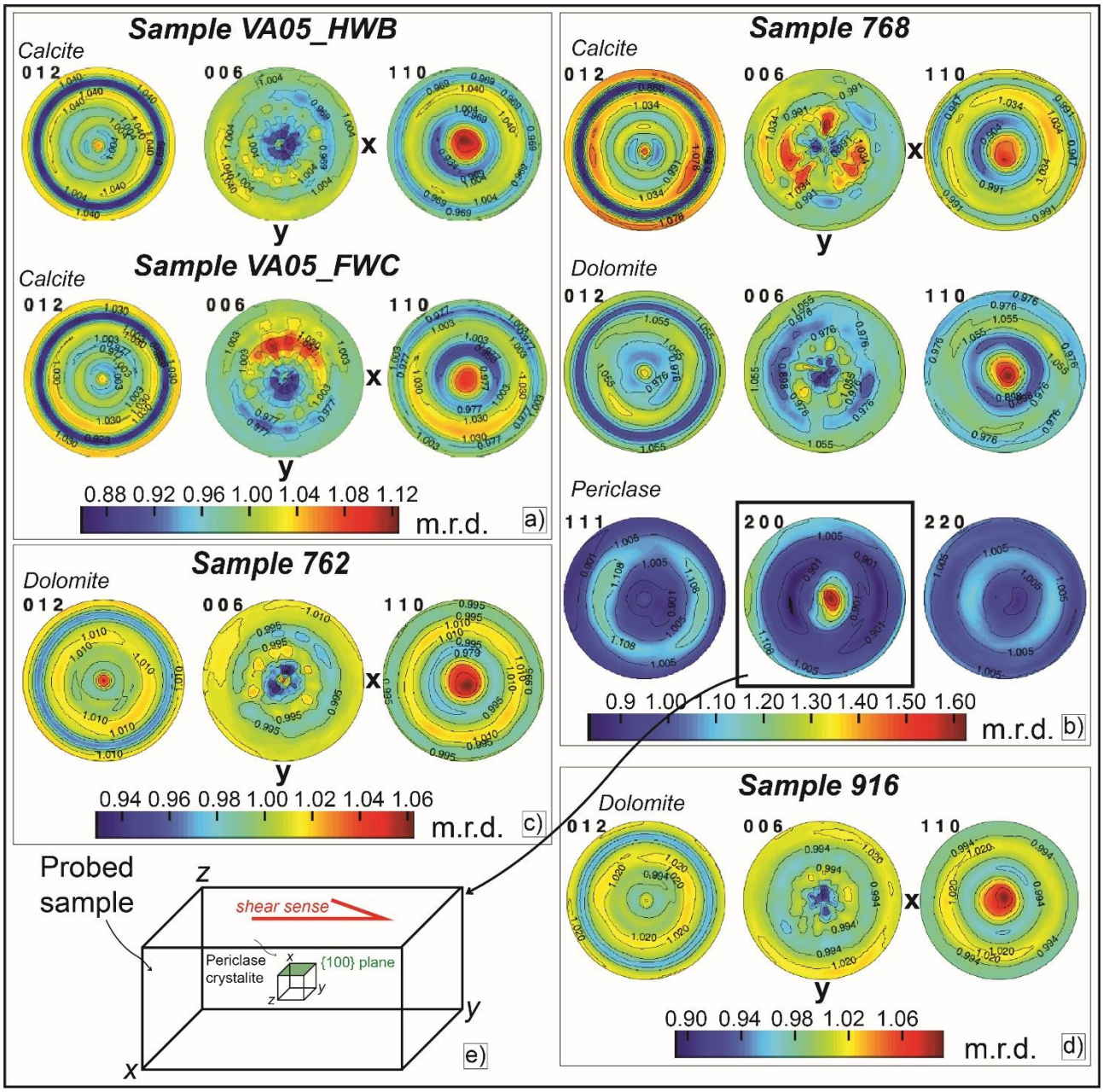


Figure 5.4: Reconstructed Pole Figures of analyzed samples; values of maximum random distribution (m.r.d.) are reported in a probability scale-sample dependent. a) Calcite grains of both hangingwall and footwall rocks of sample VA05 have an almost random distribution. b) Calcite and dolomite micro- to nano-grains of PSZ of sample 768 have a very weak CPO, whereas periclase micro-grains preferentially crystalizes with {100} planes orthogonal with the z axes of probed polycrystalline aggregate, as explained in Fig. e. c-d) Dolomite grains of samples 762 and 916 have no clear CPO (note the small range in the scale bar values).

## 5.4 Discussion

In this work we performed Crystallographic Texture Analyses on calcite-rich carbonates stem from the Valle Force fault scarp and on experimental samples of dolomitic marble sheared at seismic slip velocities (Fig. 5.1).

The Valle Force fault is < 2 km long along-strike and flatten at 2–3 km of depth on a preexisting low angle fault (D'Agostino et al., 1998). The fault juxtaposes Cretaceous limestones with Lower Pleistocene calcareous breccias with few hundreds of meters of displacement. The fault wall rocks have a cataclastic slip zone, with the fine matrix (> 50% of the total volume) mainly composed of packed calcite micro-grains, heterogeneous in size, partially indented, with void spaces locally filled with secondary calcite, clay minerals, oxides and quartz in case of hangingwall rocks (Del Rio et al., 2021; Figs. 5.2a-c, 5.3a-b). These textures are consistent with brittle cataclastic and congruent pressure-solution mechanisms active during and after slip at very low boundary conditions (i.e., $P_{litho}$ < 20 MPa and T < 20$^{o}$C) and slip rates (i.e., from to mm/sec to $\mu$m/sec).

Crystallographic Texture Analyses on natural sample of Valle Force fault wall VA05 indicate a weak preferred orientation of the calcite micro-grains in the PSZ. This result would be consistent with the activation of cataclastic and congruent pressure solution mechanisms in this natural fault. Instead, shear induced CPOs of calcite r-glide systems were observed in < 20 $\mu$m thick shear bands of calcite-rich gouges sheared in the laboratory at v < 100 $\mu$m/s and $\sigma$n = 50 MPa (Verberne et al., 2013a; 2014). CPOs on calcite are also produced on calcite-built rocks through high velocity experiments, during the initial stages of fault weakening. In this case, dislocation creep mechanisms are possibly active up to 600 $^{o}$C (caused by frictional heating) to accommodate the strain in the PSZ (De Paola et al., 2015; Green et al., 2015). The CPO is then reduced in its intensity by the activation of diffusion creep processes that become dominant at T > 900$^{o}$C during the so called steady-state phase (De Paola et al., 2015; Pozzi et al., 2018, 2019; Demurtas et al., 2019; Aretusini et al., 2021).

In the experimental samples 916 (loaded at $\sigma$n = 10 MPa) and 762 (loaded at $\sigma$n = 10 MPa and sheared at v = 10 cm/s), no secondary mineral phases were found, suggesting no bulk decarbonation processes occurred, and the initial dolomite has no clear preferred orientation (Fig. 5.4c, d). Similarly, no CPOs of secondary calcite and dolomite are observed in the PSZ of sample 768, sheared at seismic slip velocities. Instead, {100} planes of the secondary periclase are preferentially oriented perpendicular with the z axes of the probed

sample (Fig. 5.4b, e). Periclase possibly starts to nucleate as an ultra-fine phase at T > 550°C due to the thermal decomposition of dolomite (Hashimoto et al., 1980; De Aza et al., 2002) and crystalizes slowly with the {100} glide planes parallel to the shear direction. Indeed, despite periclase is refractory at the investigated conditions (i.e., the melting temperature is > 2800°C and its crystalline structure changes at P ~ 400 MPa), the temperature increases up to > 1000°C due to frictional heating caused a switch of dominant 1/2<110> {110} to dominant 1/2<110> {100} slip plane with the <110> that align parallel with the shear direction (Stretton et al., 2001; Heidelbach et al., 2003; Amodeo et al., 2018).

The XRD-CTA presented here indicate no CPOs on calcite in the natural samples, supporting the hypothesis that the natural slip zone of the Valle Force fault was produced by fluid-driven and low temperature diffusive processes associated with aseismic slip. Instead, the increases of the MgO content within the PSZ toward the slip surface can represent a possible indicator of seismic slip on faults affecting dolomite-rich carbonates and analyses of CPOs may allow to estimate better the boundary conditions during fault slip.

## 5.5 Conclusions

Most of slip displacement along brittle faults in carbonate rocks is accommodated in the fault core. The latter includes highly localized Principal slip zones (PSZs), few hundreds of micrometers thick, produced by cataclasis and both high temperature viscous deformation mechanisms and low temperature pressure-solution processes.

In this work we investigated a natural sample of a carbonate-hosted normal fault in the central Apennines. The faults is < 2 km long along-strike, < 3 km deep and is supposed to accommodate deformation mainly by aseismic creep. The sample was investigated through XRD, microstructural and, for the first time, Crystallographic Texture Analyses (CTA), to unravel the possible deformation mechanisms operating during slip. For calibrating the technique, we also analyzed experimentally produced polished slip surfaces from dolomitic marbles deformed at seismic slip velocities.

The PSZ of the Valle Force fault wall (sample VA05) have a cataclastic fabric, with the fine matrix essentially composed of 1-5 μm in size calcite micro-grains, locally indented, with void spaces filled with secondary calcite, clay minerals, oxides and quartz in case of hangingwall rocks (~ 5% of the total volume). These textures are consistent with brittle cataclastic and congruent pressure-solution mechanisms active during and after slip at very shallow crustal depths (i.e., $P_{litho}$ < 20 MPa and T < 20°C) and slip rates (i.e., from to mm/sec to μm/sec). The activation of such processes is also in agreement with CTA results, that

indicate a weak preferred orientation of the calcite micro-grains in the PSZ. In fact, intense CPO is produced by dislocation creep processes. In experiments simulating seismic slip, dislocation creep is supposed to be active at T ≤ 600 ºC during the initial stages of fault weakening (i.e., first cm of slip, see De Paola et al., 2015).

In the experimental samples 916 (loaded at σn = 10 MPa) and 762 (loaded at σn = 10 MPa and sheared at v = 10 cm/s), no secondary mineral phases were produced during experiments and the initial dolomite has no evidence preferred orientation. Instead, sample 768 (loaded at σn = 10 MPa and sheared at v ~ 1 m/s) has a polished slip surface with a PSZ beneath composed of sintered nano-grains of calcite (~ 62%), secondary periclase (~ 24%) and dolomite (~ 13%), probably produced by decarbonation processes, with straight boundaries and few pores and cavities among grains. As for samples 916 and 762, calcite and dolomite grains have weak CPOs. Instead, {100} planes of the secondary periclase are preferentially oriented perpendicular with the z axes of the probed sample and parallel to the slip direction. The CPOs found in periclase are consistent with its nucleation as an ultra-fine phase at T > 550ºC due to the thermal decomposition of dolomite and crystallization with the {100} glide planes oriented parallel to the shear sense (Fig. 5.4e). The development of periclase close to the slip surface can represent a possible seismic slip indicator on faults affecting dolomite-rich carbonates. In conclusion, also because less time-consuming than EBSD techniques, Crystallographic Texture Analysis has proven to be a powerful tool to investigate fault slip zones as it allows to investigate hundreds of micrometers thick rock volumes with great accuracy.

## Acknowledgments

This research was funded by the European Research Council Consolidator Grant Project NOFEAR No 614705 (Luca Del Rio, Michele Fondriest, and Giulio Di Toro); by two INGV projects: “Caratterizzazione microstrutturaledi piani di faglia attivi ed esumati e di piani di scivolamento di deformazioni gravitative profonde di versante (DGPV)” and “Investigation of bedrock shear planes microstructures”. The authors thank Leonardo Tauro for thin section preparation; Elena Spagnuolo for conducting laboratory experiments; Andrea Cavallo for SEM analyses of both experimental and natural samples.

# 6. Conclusions of the thesis and future works

In the Italian central Apennines, numerous relief slopes are affected by Deep-Seated Gravitational Slope Deformations (DGSDs) whose movements are strongly controlled by normal faults activity, that commonly triggers post-seismic gravitational collapses of the associated and most unstable slopes (Moro et al., 2012; Albano et al., 2015). However, the formation of DGSDs in central Apennines and their relation with the associated normal faults are still poorly understood.

In chapter III, I conducted macro- to micro-structural analyses of the damage and slip zones in the footwall of four DGSDs located in the footwall of large seismogenic normal faults, and of the Valle Force, a < 2 km long normal fault bordering a karst depression. These analyses allowed me to interpret the loading conditions of the investigated structures at the time of formation and the main deformation mechanisms associated with slip.

In the footwall of Alto di Cacchia DGSD scarp, numerous sub-vertical fissures and joints crosscut sub-horizontal conglomerates, consistent with their formation in tensional regime or at very low confining pressures (i.e., < 500 m). In contrast, in the case of Sant'Erasmo, Mt. Serrone, and Colle Cerese DGSDs, the sub-horizontal Cretaceous limestones in the footwall are cut by regularly spaced sets of joints and conjugate shear fractures with a large scatter of both strike and dip angles. This spatial arrangement is similar with the one of Valle Force fault (< 3 km deep) and indicate a deeper formation depth (i.e., > 1 km of depth) followed by a recent gravitational activity, as suggested by few sub-vertical open fractures (1-15 cm of aperture) locally affecting the carbonate strata. Based on field structural data, most DGSDs in the central Apennines should result from gravity-induced reactivation at surficial conditions (i.e., T < 15°C and $P_{litho}$ < 15 MP) of pre-existing minor faults or shear fractures located in the footwall of large normal seismogenic faults, properly oriented with the actual stress field. Since maximum height values of DGSD scarps are comparable to those of the main seismogenic normal faults in the central Apennines, well-exposed sharp slip surfaces can be produced either by gravitational processes or by tectonic faulting, or by a combination of the two. However, structural, geomorphological and geophysical/seismological features and information, such as the along-strike length and lateral continuity of the scarp, the presence of peculiar morphologies like double-crested ridge, up-hill facing scarps or gravitational trenches and the distribution of earthquakes may allow to relate the scarps to gravitational rather than to tectonic processes.

The major slip surfaces of the two large seismogenic normal faults associated with the studied DGSDs (i.e., the San Benedetto-Gioia dei Marsi and Roccapreturo faults) have a

10-30 cm-thick cataclastic slip zone that includes a ~ 0.5 cm thick ultra-cataclastic layer. In contrast, the slip zones in the footwall of the major scarps accommodating the Sant'Erasmo, Mt. Serrone, and Colle Cerese DGSDs have a proto-cataclastic fabric, whereas those of Valle Force fault and of Alto di Cacchia DGSD are a well-developed cataclasites, but they lack of an ultra-cataclastic layer right beneath the slip surface. The well-developed and thicker slip zones associated with the large normal faults can be explained by the larger amount of slip displacement accommodated by the latter compared with the DGSDs. However, other than these differences in the microstructural organization of the slip zone, there are no microstructural indicators that allow me to distinguish between DGSDs and normal faults. Moreover, since the DGSDs scarps were interpreted to exploit preexisting minor tectonic faults/fractures, the microstructures observed in the DGSD slip zones could have been mainly produced by tectonic sliding, rather than gravitational sliding. Lastly, most of the outcropping scarps in central Apennines are strongly affected by karst processes, that partially reduce the thickness of the PSZ close to the slip surface, possibly obliterating the main microstructures produced during slip.

The matrix of the slip zones of Valle Force fault and of the four DGSDs is composed of calcite micro- to nanograins, with straight to stylolitic-like grain boundaries locally forming triple junctions and isolated pores with widespread clast indentation. The matrix of the ultra-cataclastic layers of San Benedetto-Gioia dei Marsi and Roccapreturo seismogenic faults is similar, but the grain boundaries are straighter, with more widespread triple junctions and smaller pore spaces. These textures are compatible with the activation of pressure-solution processes occurring at very low temperatures and confining pressures (i.e., $T < 15°$, $P_{litho} <$ 15 MPa), with large normal faults that underwent more pressure-solution because of the smaller average grain size that favors the process of pressure-solution (Rutter, 1983; Tada and Siever, 1989; Renard et al., 2000). These observations would suggest that slip zones in carbonate rocks are likely produced by fluid-driven and low temperature diffusive processes active during either seismic or aseismic slip.

In chapter IV, I compared the fault zone architecture and the microstructures of the slip zones in the footwall of the Campo Felice and Cama normal faults. The latter displace carbonate rocks with similar attitude, but with different slip rates and geomorphological landscapes associated.

The maximum estimated geological throw of Campo Felice fault is ~ 1050 m, with a possible overestimate of ~ 425 m. The fault scarp (3-15 m high) is continuous along-strike

and composed of numerous segments arranged in én-echelon step-over zones. Fault core (40 cm to 15 m thick) and the damage zone (> 400 m thick) includes domains of highly fractured rocks (50-150 m thick and < 3 cm of fractures spacing) cut by several high-angle secondary faults and veins. On the contrary, the Cama fault scarp (~ 2 m high) discontinuously outcrops only in the middle and southern sectors. Fault core is almost absent and fractures in the damage zone (< 40 m thick) are usually spaced > 10 cm apart, consistent with the ~ 100 m of maximum geological throw and the estimated low Quaternary throw rates (Salvi et al., 2003). Furthermore, the numerous high-angle fissures and gravitational trenches affecting the footwall host-rocks suggest a lateral spreading of the Mt. D'Ocre ridge accommodated by the major fault scarp. The large differences observed in the fault zones would suggest that, in spite of their proximity (i.e., ~ 2 km of along-strike spacing), the two faults do not link at depth and that the seismogenic source associated with the Ovindoli-L'Aquila Fault System is ~ 9 km shorter, thus reducing the maximum expected earthquake magnitude of the fault system from ~ 6.8 to ~ 6.5 (Wells and Coppersmith, 1994).

The slip zone of Campo Felice fault is a cataclasite composed of angular to sub-rounded grains (1-5 mm thick) surrounded by a fine matrix whose amount increases toward the slip surface. The latter appears quite rough due to karst-related process but it is very smooth where preserved by surficial alteration. On the contrary, the slip zone of Cama fault is a mosaic breccia with 1-10 mm thick angular clasts cut by numerous fractures filled with sparite and oriented at high angles with the very rough slip surface.

The fine matrix of Campo Felice and Cama fault slip zones show similar textures with the ones associated with the previously studied DGSDs. Indeed, it is composed of calcite micro-grains with irregular to stylolitic-like boundaries and pores locally filled with oxides and clay minerals, with incipient triple junctions and indentation structures, consistent with the activation of cataclasis and pressure-solution processes. Also in this case, the Campo Felice fault has a more developed slip zone because of the higher average long-term slip rates and cumulated geological throws and underwent more pressure-solution processes mainly due to the larger amount of clay minerals. The reported observations indicate that normal active faults displacing the same host rocks may have variable damage and slip zones associated, produced by similar deformation mechanisms.

In order to verify if brittle cataclastic and pressure-solution creep processes can be active at both high and very low slip rates (i.e., from m-cm/sec to mm/yr) and shallow crustal levels, as suggested by microstructural observations, I performed Crystallographic Texture

Analyses (CTA) on a sample from the Valle Force fault wall (chapter V). For comparison and calibrating the technique, I also analyzed experimentally produced polished slip surfaces from dolomitic marbles deformed at seismic slip velocities.

Results from CTA indicate a weak preferred orientation of the calcite micro-grains in the PSZ associated with the Valle Force fault, in agreement with the activation of brittle cataclastic and low temperature fluid-assisted processes during slip. Indeed, Crystallographic preferred orientations (CPOs) are commonly produced at both seismic (during the initial stages of fault weakening) and aseismic slip velocities by dislocation creep processes active at T > 600 $^{o}$C (Verberne et al., 2014; De Paola et al..2015; Pozzi et al., 2019; Demurtas et al., 2019).

Regarding experimental dolomitic samples, only the one sheared at seismic velocities (v ~ 1 m/s) experienced decarbonation during slip, with nucleation of periclase at T > 550$^{o}$C due to the thermal decomposition of dolomite and crystallization with the {100} glide planes oriented parallel to the shear direction. The nucleation of periclase close to the slip surface due to decarbonation processes may represent a possible seismic slip indicator on faults affecting dolomite-rich carbonates. In conclusion, also because less time-consuming than EBSD techniques, Crystallographic Texture Analysis has proven to be a powerful tool to investigate fault slip zones as it allows to investigate hundreds of micrometers thick rock volumes with great accuracy.

Our results indicate that no microstructural indicators can allow to uniquely distinguish between DGSDs and normal faults. However, structural analyses of damage and slip zones can (1) integrate geomorphological and geophysical analyses in the characterization of DGSDs and (2) provide further parameters to improve the characterization of seismogenic sources associated with neighbouring faults affecting similar host-rocks with different slip rates. Further studies need to be carried out to obtain better constraints on the exhumation depth of DGSDs, as for example, clumped isotopes analyses of the matrix and cements within and close to the slip zones. Moreover, although microstructural analyses conducted in this work allowed me to interpret the deformation mechanisms associated with DGSDs during slip, the future studies on slip zones in carbonate rocks should be carried out on well-preserved and recently exposed slip surfaces, that have not undergone much karst/erosional processes. Lastly, numerical modeling analyses may significative contribute to study the evolution of DGSDs in central Apennines. Unfortunately, the position of the basal slip surface accommodating the rock-mass sliding is a key parameter to perform such analyses. The latter is much less defined in the basal sector of most DGSDs in central Apennines (and

worldwide) and also buried by the displaced rock-mass that cumulates at the base of the DGSD (Cruden and Varnes, 1996).

I would also spend few words about the important impact of COVID-19 pandemia in my research. Indeed, I had to renounce to several international conferences and to spend part of my research abroad, where I planned to conduct experiments on carbonate rocks at low sliding velocities and boundary conditions. Then I had less time available for field survays and SEM analyses in laboratory (e.g., Certema, Grosseto) although the 6 months extention still allowed me to collect a significant number of meso- and micro-structural data.

## *References*


Albano, M., Barba, S., Saroli, M., Moro, M., Malvarosa, F., Costantini, M., Bignami, C., Stramondo, S., 2015. Gravity-driven postseismic deformation following the Mw 6.3 2009 L'Aquila (Italy) earthquake. Sci. Rep. 5, 16558.

Allmendinger, R. W., Cardozo, N., Fisher, D., 2012. Structural geology algorithms: Vectors and tensors. Cambridge University Press.

Agliardi, F., Crosta, G., Zanchi, A., 2001. Structural constraints on deep-seated slope deformation kinematics. Engineering Geology, 59, 83-102.

Agliardi, F., Zanchi, A., Crosta, G. B., 2009a. Tectonic vs. gravitational morphostructures in the central Eastern Alps (Italy): constraints on the recent evolution of the mountain range. Tectonophysics 474, 250–270.

Agliardi, F., Crosta, G.B., Zanchi, A., Ravazzi, C., 2009b. Onset and timing of deep-seated gravitational slope deformations in the eastern Alps, Italy. Geomorphology 103, 113–129.

Agliardi, F., Crosta, G., Frattini, P., 2012. Slow rock-slope deformation. In: Clague, J.J., Stead, D. (Eds.), Landslides Types, Mechanisms and Modeling (pp. 207-221). Cambridge: Cambridge University Press.

Agliardi F., Riva F., Barbarano M., Zanchetta S., Scotti R., Zanchi A., 2019. Effects of tectonic structures and long-term seismicity on paraglacial giant slope deformations: piz dora (switzerland). engineering geology, 263: 105353. https://doi.org/10.1016/j.enggeo.2019.105353

Agosta, F., Kirschner, D., 2003. Fluid conduits in carbonate-hosted seismogenic normal faults of central Italy. J. Geophys. Res., 108(B4), 2221. 10.1029/2002JB002013.

Agosta, F., Aydin, A., 2006. Architecture and deformation mechanism of a basin bounding normal fault in Mesozoic platform carbonates, central Italy. J. Struct. Geol. 28(8), 1445-1467.

Agosta, F., Ruano, P., Rustichelli, A., Tondi, E., Galindo-Zaldivar, J., De Galdeano, C. S., 2012. Inner structure and deformation mechanisms of normal faults in conglomerates and carbonate grainstones (Granada Basin, Betic Cordillera, Spain): inferences on fault permeability. J. Struct. Geol., 45, 4-20.

Aharonov, E., R. Katsman, 2009. Interaction between pressure solution and clays in stylolite development: Insights from modeling, American Journal of Science, 309 (7), 607-632.

Amato, G., Devoti, R., Fubelli, G., Aringoli, D., Bignami, C., Galvani, A., Moro, M., Polcari, M., Saroli M., Sepe, V., Stramondo, S., 2018. Step-like displacements of a deep-seated gravitational slope deformation observed during the 2016–2017 seismic events in central italy. engineering geology, 246, 337-348. https://doi.org/10.1016/j.enggeo.2018.10.014

Ambrosi, C., Crosta, G. B., 2006. Large sackung along major tectonic features in the Central Italian Alps. Engineering Geology 83, 183-200.

Ambrosi, C., Crosta, G. B., 2011. Valley shape influence on deformation mechanisms of rock slopes. In: Jaboyedoff, M. (Ed.), Slope Tectonics. Geological Society, London, Special Publications 351(1), 215-233.

Amodeo, J., Merkel, S., Tromas, C., Carrez, P., Korte-Kerzel, S., Cordier, P., Chevalier, J., 2018. Dislocations and Plastic Deformation in Mgo Crystals: A Review. Crystals 8, 240.

Aretusini, S., Núñez-Cascajero, A., Spagnuolo, E., Tapetado, A., Vázquez, C., Di Toro, G., 2021. Fast and localized temperature measurements during simulated earthquakes in carbonate rocks. Geophysical Research Letters, 48, e2020GL091856. https://doi.org/10.1029/2020GL091856.

Aringoli, D., Gentili, B., Materazzi, M., Pambianchi, G., 2010. Deep-seated gravitational slope deformations in active tectonics areas of the Umbria-Marche Apennine (central Italy). Geogr. Fis. Dinam. Quat., 33, 127-140.

Artioli, G., 2007. Crystallographic texture analysis of archaeological metals: interpretation of manufacturing techniques. Appl. Physics A. 8: 899–908.

Audemard, F. A., Beck, C., Carrillo, E., 2010. Deep-seated gravitational slope deformations along the active Boconó Fault in the central portion of the Mérida Andes, western Venezuela. Geomorphology 124 (3-4), 164-177.

Barchi, M., Galadini, F., Lavecchia, G., Messina, P., Michetti, A. M., Peruzza, L., Pizzi, A., Tondi, E., Vittori, E., 2000. Sintesi delle conoscenze sulle faglie attive in Italia Centrale: parametrizzazione ai fini della caratterizzazione della pericolosità sismica. CNR Gruppo Nazionale per la Difesa dai Terremoti, Roma, 62.

Bathurst, R. G. C., 1971. Carbonate Sediments and Their Diagenesis. Amsterdam-Oxford-New York: Elsevier.

Bazalgette, L., Petit, J.P., Amrhar, M., Ouanaïmi, H., 2010. Aspects and origins of fractured dip-domain boundaries in folded carbonate rocks. J. Struct. Geol. 32 (4), 523–536.

Benedetti, L., Manighetti, I., Gaudemer, Y., Finkel, R., Malavieille, J., Pou, K., Keddadouche, K., 2013. Earthquake synchrony and clustering on Fucino faults (Central Italy) as revealed from in situ 36Cl exposure dating. Journal of Geophysical Research: Solid Earth, 118(9), 4948-4974.

Benko B., Stead D., 1998. The frank slide: a reexamination of the failure mechanism. Canadian. Geotech. J. 35, 299-311.

Bianchi Fasani G., Di luzio E., Esposito C., Martino S., Scarascia Mugnozza G., 2011. Numerical modelling of plio-quaternary slope evolution based on geological constraints: a case study from the caramanico valley (central apennines, italy). geological society, london, special publications, 351, 201-214. https://doi.org/10.1144/sp351.11

Bianchi Fasani, G., Di Luzio, E., Esposito, C., Evans, S. G., Scarascia Mugnozza, G., 2014. Quaternary, catastrophic rock avalanches in the Central Apennines (Italy): Relationships with inherited tectonic features, gravity-driven deformations and the geodynamic frame. Geomorphology, 211, 22-42.

Boncio, P., Lavecchia, G., Pace, B., 2004. Defining a model of 3D seismogenic sources for seismic hazard assessment applications: the case of central Apennines (Italy). Journal of Seismology, 8(3), 407-425.

Bosi C., Messina P., 1991. Ipotesi di correlazione fra successioni morfo-litostratigrafiche plio-pleistoceniche nell'Appennino Laziale-Abruzzese. Studi Geol. Cam., Special Vol. 1991/2, 257-263.

Bosi, C., Galadini, F., Messina, P., 1993. Neotectonic significance of bedrock fault scarps: case studies from the Lazio-Abruzzi Apennines (central Italy). Z. Geomorphol., Suppl.bd. 94, 187-206.

Bosi, C., Galadini, F., Giaccio, B., Messina, P., Sposato, A., 2003. Plio-Quaternary continental deposits in the Latium-Abruzzi Apennines: the correlation of geological events across different intermontane basins. Il Quaternario, 16, 55-76.

Bovis, M. J., 1982. Uphill-facing (antislope) scarps in the coast mountains, southwest british columbia. geological society of america bulletin, 93(8), 804-812. https://doi.org/10.1130/0016-7606(1982)93%3c804:uasitc%3e2.0.co;2

Bovis, M. J., 1990. Rock-slope deformation at Affliction Creek, southern Coast Mountains, British Columbia. Canadian Journal of Earth Sciences 27, 243-254.

Bozzano, F., Bretschneider, A., Esposito, C., Martino, S., Prestininzi, A., Scarascia Mugnozza G., 2013. Lateral spreading processes in mountain ranges: insights from an analogue modelling experiment. tectonophysics, 605, 88-95. https://doi.org/10.1016/j.tecto.2013.05.006

Bullock, R. J., De Paola, N., Holdsworth, R. E., Trabucho-Alexandre, J., 2014. Lithological controls on the deformation mechanisms operating within carbonate-hosted faults during the seismic cycle, J. Struct. Geol., 58, 22–42, doi:10.1016/j.jsg.2013.10.008.

Bunge, H.J., 2000. in: *Defect and Microstructure Analysis by Diffraction* (University Press, Oxford), pp. 408–531.

Caine, J. S., Evans, J. P., Forster, C. B., 1996. Fault zone architecture and permeability structure. Geology, 24(11), 1025–1028. https://doi.org/10.1130/00917613(1996)

Caine, J. S., Forster, C. B., 1999. Fault Zone Architecture and Fluid Flow: Insights from Field Data and Numerical Modeling. American Geophysical Union Geophysical Monograph, 113, 101-127.

Calamita, F., Pizzi, A., Scisciani, V., De Girolamo, C., Coltorti, M., Pieruccini, P., Turco, E., 2000. Caratterizzazione delle faglie quaternarie nella dorsale appenninica umbro-marchigiano-abruzzese. In: F. Galadini, C. Meletti, and A. Rebez (Eds.), Le Ricerche del GNDT Nel Campo Della Pericolosità Sismica (1996–1999) (pp. 157-169), CNR-Gruppo Nazionale per la Difesa dai Terremoti, Roma.

Carminati, E., Doglioni, C., 2012. Alps vs. Apennines: the paradigm of a tectonically asymmetric Earth. Earth Sci. Rev., 112(1–2), 67-96.

Carminati, E., Lustrino, M., Doglioni, C., 2012. Geodynamic evolution of the central and western Mediterranean: Tectonics vs. igneous petrology constraints. Tectonophysics, 579, 173-192.

Carrio-Schaffhauser, E., Raynaud, S., Latiere, H. J., Mazerolles, F., 1990. Propagation and localization of stylolites in limestones. In: Knipe, R.J., Rutter, E. H. (Eds.), Deformation Mechanisms, Rheology and Tectonics. Geological Society, London, Special Publications, 54, 193-199.

Castellarin, A., Colacicchi, R., & Praturlon, A., 1978. Fasi distensive, trascorrenze e sovrascorrimenti lungo la “linea Ancona-Anzio”, dal Lias medio al Pliocene. Geologica Romana, 17, 161-189.

Cavinato, G. P., Carusi, C., Dall’Asta, M., Miccadei, E., Piacentini, T., 2002. Sedimentary and tectonic evolution of Plio-Pleistocene alluvial and lacustrine deposits of the Fucino Basin (central Italy). Sedimentary Geology, 148, 29-59.

Chateigner, D., Germi, P., Pernet, M., Fréchard, P. Andrieu, S., 1995. Fluorescence corrections in thin-film texture analysis. J. Appl. Cryst. 28, 369–374.

Chateigner, D., Hedegaard, C. Wenk, H. R., 2000. Mollusc shell microstructures and crystallographic textures. J. Struct. Geol. 22, 1723-1735.

Chateigner, D., Lutterotti, L., Morales, M., 2019. Quantitative texture analysis and combined analysis. *International tables for crystallography volume H* (st ed., pp. 555-580). International Union of Crystallography. https://doi.org/10.1107/97809553602060000968

Chester, F. M. Logan, J. M., 1986. Implications for mechanical properties of brittle faults from observations of the Punchbowl fault zone, California. Pure Appl. Geophys. 124, 79–106.

Chester, F. M., Biegel, R. L., Evans, J. P., 1993. Internal structure and weakening mechanisms of the San-Andreas fault. J. Geophys. Res: Solid Earth, 98, 771-786.

Chester, F. M., Chester, J. S., 1998. Ultracataclasite structure and friction processes of the Punchbowl fault, San Andreas system, California. Tectonophysics, 295, 199-221.

Chiaraluce, L., R. Di Stefano, E. Tinti, L. Scognamiglio, M. Michele, E. Casarotti, M. Cattaneo, P. De Gori, C. Chiarabba, G. Monachesi, A. M. Lombardi, L. Valoroso, D. Latorre, and S. Marzorati, 2017. The 2016 Central Italy seismic sequence: a first look at the mainshocks, aftershocks and source models, Seism. Res. Lett., 88(3), doi:10.1785/0220160221.

Chiaraluce, L., Ellsworth, W. L., Chiarabba, C., Cocco M., 2003. Imaging the complexity of an active normal fault system: The 1997 Colfiorito (central Italy) case study, J. Geophys. Res, 108(B6), 2294, doi:10.1029/2002JB002166.

Chigira, M.,1992. Long-term gravitational deformation of rock by mass rock creep. Engng. Geol, 32(3), 157-184.

Chigira, M., Wu, X., Inokuchi, T., Wang, G., 2010. Landslides induced by the 2008 Wenchuan earthquake, Sichuan, China. Geomorphology, 118, 225-238.

Cipollari, P., Cosentino, D., Esu, D., Girotti, O., Gliozzi, E., Praturlon, A., 1999a. Thrust-top lacustrine-lagoonal basin development in accretionary wedges: late Messinian (Lago-Mare) episode in the central Apennines (Italy). Palaeogeogr. Palaeoclimatol. Palaeoecol., 151, 146-166.

Civitelli, G., Corda, L., Mariotti, G., 1988. Il Bacino Sabino: 2) sedimentologia e stratigrafia della serie calcarea e marnosa-spongolitica (Paleogene-Miocene). Mem. Soc. Geol. It. 47-3533.

Cosentino, D., Cipollari, P., Marsili, P., Scrocca, D., 2010. Geology of the central Apennines: a regional review, In: M. Beltrando, A. Peccerillo, M. Mattei, S. Conticelli and C. Doglioni (Eds.), The Geology of Italy, J. Virt. Explor., 36, paper 11.

Cossart, E., Braucher, V., Fort, M., Bourlès, D.L., Carcaillet, J., 2008. Slope instability in relation to glacial debuttressing in alpine areas (Upper Durance catchment, southeastern France): evidence from field data and 10Be cosmic ray exposure ages. Geomorphology 95(1-2), 3-26.

Crippa C., Franzosi F., Zonca M., Manconi A., Crosta G. B., Dei Cas l., Agliardi F., 2020. Unraveling spatial and temporal heterogeneities of very slow rock-slope deformations with targeted dinsar analyses. remote sensing, 12(8), 1329. https://doi.org/10.3390/rs12081329

Crippa, C., Valbuzzi E., Frattini P., Crosta G. B., Spreafico M. C., Agliardi F., 2021. Semi-automated regional classification of the style of activity of slow rock-slope deformations using PS InSAR and SqueeSAR velocity data. Landslides 18, 2445-2463.

Croizé, D., Renard, F., Bjørlykke, K., Dysthe, D. K., 2010. Experimental calcite dissolution under stress: Evolution of grain contact microstructure during pressure solution creep. J. Geophys. Res., 115, B09207, doi:10.1029/2010JB000869.

Croizé, D., Renard, F., Gratier, J. P., 2013. Compaction and porosity reduction in carbonates: a review of observations, theory, and experiments. Adv. Geophys., 54, 181-238.

Crosta G. B., Zanchi A., 2000. Deep-seated slope deformations: huge, extraordinary, enigmatic phenomena. in: bromhead e., dixon n. & isben m.l. (eds.), landslides in research, theory and practice; proceedings of the 8th international symposium on landslides, cardiff, 351-358.

Crosta, G. B., Frattini, P., Agliardi, F., 2013. Deep seated gravitational slope deformations in the European Alps. Tectonophysics, 605, 13-33.

Cruden, D. M., Varnes, D. J., 1996. Landslide types and processes. In: Turner AK, Schuster RL (Eds.) Landslides investigation and mitigation (pp. 36-75). Washington DC: US Geological survey fact sheet.

D'Agostino, N., Chamot-Rooke, N., Funiciello, R., Jolivet, L., Speranza, F., 1998. The role of pre-existing thrust faults and topography on the styles of extension in the Gran Sasso range (central Italy), Tectonophysics, 292, 229-254.

D'Agostino, N., Giuliani, R., Mattone, M., Bonci, L., 2001. Active crustal extension in the central Apennines (Italy) inferred from GPS measurements in the interval 1994-1999. Geophysical Research Letters, 28, 2121-2124.

D'Agostino, N., Mantenuto, S., D'Anastasio, E., Giuliani, R., Mattone, M., Calcaterra, S., Gambino, P., Bonci, L., 2011. Evidence for localized active extension in the central Apennines (Italy) from global positioning system observations. Geology, 39, 291-294, 10.1130/G31796.1

Damiani, A. V., Chiocchini, M., Colacicchi, R., Mariotti, G., Parotto, M., Passeri, L., Praturlon, A., 1992. Elementi litostratigrafici per una sintesi delle facies carbonatiche meso-cenozoiche dell'Appennino centrale. Studi Geologici Camerti, vol. spec., 1991/2, 187-213.

De Aza, H., Rodriguez, M. A. Rodriguez, J.L., De Aza, S., Pena, P., Convert, P., Hansen, T., Turrillas, X., 2002. J. Am. Ceram. Soc., 85 p. 881

De Bresser, J.H.P., Spiers, C. J., 1997. Strength characteristics of the r, f, and c slip systems in calcite. Tectonophysics272 (1), 1–23. https://doi .org /10 .1016 /S0040 -1951(96 )00273 -9.

De Paola, N., Collettini, C., Faulkner, D.R., Trippetta, F., 2008. Fault zone architecture and deformation processes within evaporitic rocks in the upper crust. Tecton-ics27. http://dx.doi.org/10.1029/2007TC002230.

Delchiaro M., Della Seta M., Martino S., Dehbozorgi M., Nozaem R., 2019. Reconstruction of river valley evolution before and after the emplacement of the giant seymareh rock avalanche (Zagros mts., iran). earth surface dynamics, 7, 929-947. https://doi.org/10.5194/esurf-2018-91

Della Seta, M., Esposito, C., Marmoni, G. M., Martino, S., Scarascia Mugnozza, G., Troiani, F., 2017. Morpho-structural evolution of the valley-slope systems and related implications on slope-scale gravitational processes: New results from the Mt. Genzana case history (Central Apennines, Italy). Geomorphology, 289, 60-77.

Delle Piane, C., Clennell, M. Ben, Keller, J.V.A., Giwelli, A., Luzin, V., 2017. Carbonate hosted fault rocks: a review of structural and microstructural characteristic with implications for seismicity in the upper crust. J. Struct. Geol. 103, 17–36. https://doi. org/10.1016/j.jsg.2017.09.003.

Demangeot, J., 1965. Ge`omorphologie des Abruzzes Adriatiques. Centre Recherche et Documentation Cartographiques Memoires et Documents, Numero hors serie, 403.

Demurtas, M., Fondriest, M., Balsamo, F., Clemenzi, L., Storti, F., Bistacchi, A., Di Toro, G., 2016. Structure of a normal seismogenic fault zone in carbonates: the Vado di Corno fault, Campo Imperatore, central Apennines (Italy). J. Struct. Geol., 90, 185-206.

Demurtas M., Smith S., Prior D., Brenker F., Di Toro G., 2019. Grain size sensitive creep during simulated seismic slip in nanogranular fault gouges: constraints from Transmission Kikuchi Diffraction (TKD). J. of Geoph. Res. 127, 10197-10209, 10.1029/2019JB018071.

De Paola, N., Holdsworth, R. E., Viti, C., Collettini, C., Bullock, R., 2015. Can grain size sensitive flow lubricate faults during the initial stages of earthquake propagation? Earth Planet. Sci. Lett., 431, 48-58. https://doi.org/10.1016/j.epsl.2015.09.002.

Di Luzio E., Saroli M., Esposito C., Bianchi Fasani G., Cavinato G. P., Scarascia Mugnozza G., 2004b. Influence of structural framework on mountain slope deformation in the Maiella anticline (central Apennines, italy). geomorphology, 60(3-4), 417-432. https://doi.org/10.1016/j.geomorph.2003.10.004

Di Luzio, E., Discenza, M. E., Di Martire, D., Putignano, M. L., Minnillo, M., Esposito, C., Scarascia Mugnozza, G., 2021. Investigation of the Luco Dei Marsi DSGSD revealing the first evidence of a basal shear zone in the central apennine belt (Italy).

Di Maggio C., Madonia G., Vattano M., 2014. Deep-seated gravitational slope deformations in western Sicily: controlling factors, triggering mechanisms, and morphoevolutionary models. geomorphology, 208, 173-189. https://doi.org/10.1016/j.geomorph.2013.11.023

Di Toro, G., Niemeijer, A., Tripoli, A., Nielsen, S., Di Felice, F., Scarlato, P., et al., 2010. From field geology to earthquake simulation: A new state-of-the-art tool to investigate rock friction during the seismic cycle (SHIVA). Rendiconti Lincei, 21, 95–114. https://doi.org/10.1007/ s12210-010-0097-x

Di Toro, G., Han, R., Hirose, T., De Paola, N., Nielsen, S., Mizoguchi, K., Ferri, F., Cocco, M., Shimamoto, T., 2011. Fault lubrication during earthquakes. Nature 471 (7339), 494–498. https://doi .org /10 .1038 /nature09838.

Discenza, M. E., Esposito, C., 2021. State-of-art and remarks on some open questions about DSGSDs: Hints from a review of the scientific literature on related topics. Italian Journal of Engineering Geology and Environment, 21 (1), 31-59.

Discenza, M. E., Esposito C., Martino S., Petitta M., Prestininzi A., Scarascia Mugnozza G., 2011. The gravitational slope deformation of Mt. Rocchetta ridge (central Apennines, Italy): geological-evolutionary model and numerical analysis. Bulletin of Eng Geol Environ 70:559–575.

Discenza, M.E.; Esposito, C.; Komatsu, G.; Miccadei, E., 2021. Large-Scale and Deep-Seated Gravitational Slope Deformations on Mars: A Review. Geosciences 11, 174. https://doi.org/10.3390/geosciences11040174

Doglioni, C., 1995. Geological remarks on the relationships between extension and convergent geodynamic settings. Tectonophysics, 252, 253-267.

Dramis, F., 1992. Il ruolo dei sollevamenti tettonici a lungo raggio nella genesi del rilievo appenninico. Studi Geologici Camerti, vol. spec., 1992/1, 9-15.

Dramis, F., Sorriso-Valvo, M., 1994. Deep-seated gravitational slope deformations, related landslides and tectonics. Engineering Geology, 38, 231-243.

Ehrenberg, S. N., 2006. Porosity destruction in carbonates platforms, Journal of Petroleum Geology, 29 (1), 41{52, doi:10.1111/j.1747{5457.2006.00041.x.

Elter, P., Giglia, G., Tongiorgi, M., Trevisan, L., 1975. Tensional and compressional areas in the recent (Tortonian to present) evolution of the Northern Apennines. Bollettino di Geofisica Teorica ed Applicata, 17, 3-18.

EMERGEO Working Group, 2010. Evidence for surface rupture associated with the MW 6.3 L'Aquila earthquake sequence of April 2009 (central Italy). Terra Nova, 22(1), 43–51. https://doi.org/10.1111/j.1365-3121.2009.00915.x

Engelder, T., 1987. Joints and shear fractures in rock. In: Atkinson, B. K. (Ed.), Fracture Mechanics of Rock. Academic Press, Orlando, pp. 27-69.

Esposito, C., Martino, S., Scarascia Mugnozza, G., 2007. Mountain slope deformations along thrust fronts in jointed limestone: An equivalent continuum modelling approach. Geomorphology, 90, 55-72.

Esposito C., Di Luzio E., Scarascia Mugnozza G., Bianchi Fasani G., 2014. Mutual interactions between slope-scale gravitational processes and morpho-structural evolution of central Apennines (Italy): review of some selected case histories. rendiconti lincei, 25(2): 151-165. https://doi.org/10.1007/s12210-014-0348-3

Esposito C., Di Luzio E., Baleani M., Troiani F., Della Seta M., Bozzano F. and Mazzanti P., 2021. Fold architecture predisposing deep-seated gravitational slope deformations within a flysch sequence in the northern Apennines (Italy). geomorphology, 380, 107629. https://doi.org/10.1016/j.geomorph.2021.107629

Evans, S. G., Clague, J. J., 1994. Recent climatic change and catastrophic geomorphic processes in mountain environments. Geomorphology, 10, 107-128.

Evans S. G., Scarascia Mugnozza G., Strom A. L., Hermanns R. l., Ischuk A., Vinnichenko S., 2006. Landslides from massive rock slope failure and associated phenomena. in: evans s.g.,

scarascia mugnozza g., strom a. & hermanns r.l. (eds.), landslides from massive rock slope failure. springer, dordrecht, p.p. 3-52. https://doi.org/10.1007/978-1-4020-4037-5_1

Falcucci, E., Gori, S., Moro, M., Pisani, A. R., Melini, D., Galadini, F., Fredi, P., 2011. The 2009 L'Aquila earthquake (Italy): what next in the region? Hints from stress diffusion analysis and normal fault activity. Earth and Planetary Science Letters, 305, 350-358.

Falcucci, E., Gori, S., Moro, M., Fubelli, G., Saroli, M., Chiarabba, C., Galadini, F., 2015. Deep reaching versus vertically restricted Quaternary normal faults: Implications on seismic potential assessment in tectonically active regions. Lessons from the middle Aterno valley fault system, central Italy. Tectonophysics, 305, 350-358. https://doi.org/10.1016/j.tecto.2015.03.021

Falcucci, E., Gori, S., Galadini, F., Fubelli, G., Moro, M., Saroli, M., 2016. Active faults in the epicentral and mesoseismal Ml 6.0 24, 2016 Amatrice earthquake region, central Italy. Methodological and seismotectonic issues. Annals of Geophysics, 59, track 5, doi:10.4401/ ag-7266.

Faulkner, D. R., Lewis, A. C. Rutter, E. H., 2003. On the internal structure and mechanics of large strike-slip faults: field observations from the Carboneras fault, southeastern Spain. Tectonophysics 367, 235–251.

Faulkner, D. R., Mitchell, T. M., Jensen, E., Cembrano, J., 2011. Scaling of fault damage zones with displacement and the implications for fault growth processes. J. Geophys. Res. 116. https://doi.org/10.1029/2010JB007788.

Ferraro, F., Grieco, D. S., Agosta, F., Prosser, G., 2018. Space-time evolution of cataclasis in carbonate fault zones. J. Struct. Geol., 110, 45–64.

Ferraro F., Agosta, F., Ukar, E., Grieco D. S., Cavalcante F., Belviso C., Prosser, G., 2019. Structural diagenesis of carbonate fault rocks exhumed from shallow crustal depths: An example from the central-southern Apennines, Italy. Journal of Structural Geology, 122, 58-80.

Fondriest, M., Smith, S. A. F., Di Toro, G., Zampieri, D., Mittempergher, S., 2012. Fault zone structure and seismic slip localization in dolostones, an example from the Southern Alps, Italy. Journal of Structural Geology, 45, 52–67. https://doi.org/10.1016/j. jsg.2012.06.014.

Fondriest, M., Smith S. A., Candela T., Nielsen S. B., Mair K., Di Toro G., 2013. Mirror-like faults and power dissipation during earthquakes, Geology, 41(11), 1175-1178.

Fondriest, M., Aretusini, S., Di Toro, G., Smith, S. A. F., 2015. Fracturing and rock pulverization along an exhumed seismogenic fault zone in dolostones: The Foiana Fault Zone (Southern Alps, Italy). Tectonophysics, 654, 56-74.

Fondriest, M., Doan M. L., Aben, F., Fusseis, F., Mitchell, T. M., Voorn, M., Secco, M., Smith, S. A. F., 2017. Static versus dynamic fracturing in shallow carbonate fault zones. Earth and Planetary Science Letters, 461, 8-19.

Fondriest, M, Balsamo, F., Bistacchi, A., Clemenzi, L., Demurtas, M., Storti, F., Di Toro, G., 2020. Structural complexity and mechanics of a shallow crustal seismogenic source (Vado di Corno Fault Zone, Italy). Journal of Geophysical Research – Solid Earth, doi:10.1029/2019JB018926.

Forno, M.G., Gattiglio, M., Gianotti, F., Guerreschi, A., Raiteri, L., 2013. Deep-seated gravitational slope deformations as possible suitable locations for prehistoric human settlements: an example from the Italian Western Alps. Quat. Int. 303, 180–190. https://doi.org/10.1016/j.quaint.2013.03.033.

Fossen, H., 2010. Structural Geology, Cambridge University Press pp. 463.

Frattini, P., Crosta G. B., Rossini M., Allievi J., 2018. Activity and kinematic behaviour of deepseated landslides from PS-InSAR displacement rate measurements. Landslides 15: L1–L18. https://doi.org/10.1007/s10346-017-0940-6

Galadini, F., 1999. Pleistocene changes in the central Apennine fault kinematics: A key to decipher active tectonics in central Italy. Tectonics, 18(5), 877-894.

Galadini, F., Galli, P., 1999. The Holocene paleoearthquakes on the 1915 Avezzano earthquake faults (central Italy): implications for active tectonics in central Apennines, Tectonophysics, 308, 143–170.

Galadini, F., Galli, P., 2003. Paleoseismology of silent faults in the central Apennines (Italy): the Mt. Vettore and Laga Mts. Faults. Ann. Geophis. 46, 815-836.

Galadini, F., Galli, P., 2000. Active tectonics in the central Apennines (Italy) — input data for seismic hazard assessment. Natural Hazards, 22, 225-270.

Galadini F., Meletti, G., Vittori, E., 2000. Stato delle conoscenze sulle faglie attive in Italia: elementi geologici di superficie. In: F. Galadini, C. Meletti, and A. Rebez (Eds.), Le Ricerche del GNDT Nel Campo Della Pericolosità Sismica (1996–1999) (pp. 107-136), CNR-Gruppo Nazionale per la Difesa dai Terremoti, Roma.

Galadini, F., Messina, P., Giaccio, B., Sposato, A., 2003. Early uplift history of the Abruzzi Apennines (central Italy): available geomorphological constraints. Quaternary International, 101-102, 125-135.

Galadini, F., Messina, P., 2004. Early-middle Pleistocene eastward migration of the Abruzzi Apennine (central Italy) extensional domain. Journal of Geodynamics, 37, 57-81.

Galadini, F., 2006. Quaternary tectonics and large-scale gravitational deformations with evidence of rock-slide displacements in the Central Apennines (central Italy). Geomorphology, 82, 201-228.

Galadini, F., Falcucci, E., Galli, P., Giaccio, B., Gori, S., Messina, P., Moro, M., Saroli, M., Scardia, G., and Sposato, A., 2012. Time intervals to assess active and capable faults for engineering practices in Italy, Engineering Geology 139–140, 50–65.

Galli, P., 2020. Recurrence times of central-southern Apennine faults (Italy): Hints from palaeoseismology. Terra Nova, 32, 399-407.

Galli, P., Galadini, F., Pantosti D., 2008. Twenty years of paleoseismology in Italy. Earth Sci. Rev., 88, 89-117.

Giaccio, B., Galadini, F., Sposato, A., Messina, P., Moro, M., Zreda, M., Cittadini, A., Salvi, S., todero, A., 2003. image processing and roughness analysis of exposed bedrock fault planes as a tool for paleoseismological analysis: results from the campo felice fault (central Apennines, italy). geomorphology, 49, 281-301.

Giraudi, C., 1995. Considerations on the significance of some postglacial fault scarps in the Abruzzo Apennines (Central Italy). Quat. Int. 25, 33-45.

Giraudi, C., 2001. I sedimenti di riempimento di piccole conche sulle morene dell'Appennino Centrale: un contributo alla comprensione delle variazioni ambientali postglaciali. Italian Journal of Quaternary Sciences, 14(2), 131-136.

Giraudi, C., Bodrato, G., Lucchi, M. R., Cipriani, N., Villa, I. M., Giaccio, B., Zuppi, G. M., 2011. Middle and late Pleistocene glaciations in the Campo Felice Basin (central Apennines, Italy). Quaternary Research, 75(1), 219-230. https://doi.org/10.1016/j.yqres.2010.06.006

Giraudi, C., Giaccio, B., 2017. Middle Pleistocene glaciations in the Apennines, Italy: new chronological data and preservation of the glacial record. Geological Society of London Special Publication 433, 161-178.

Gori, S., Falcucci, E., Dramis, F., Galadini, F., Galli, P., Giaccio, B. et al., 2014. Deep-seated gravitational slope deformation, large-scale rock failure, and active normal faulting along Mt. Morrone (Sulmona basin, Central Italy): Geomorphological and paleoseismological analyses. Geomorphology, 208, 88-101.

Goudie, A.S. (Ed.), 2004. Encyclopedia of Geomorphology. Routledge, London.

Gratier, J.-P., Richard, J., Renard, F. S., Mittempergher, S., Doan, M. L., Di Toro, G., et al., 2011. Aseismic sliding of active faults by pressure solution creep: Evidence from the San Andreas fault observatory at depth. Geology, 39, 1131–1134.

Gratier, J. P., Dysthe, D., Renard, F., 2013. The role of pressure solution creep in the ductility of the Earth's upper crust. Adv. Geophys., 54, 47-179.

Gratier, J. P., Noiriel, C., Renard, F., 2015. Experimental evidence for rock layering development by pressure solution. Geology, 43, 871-874.

Green II, H.W., Shi, F., Bozhilov, K., Xia, G., Reches, Z., 2015. Phase transformation and nanometric flow cause extreme weakening during fault slip. Nat. Geosci.8 (6), 484-489. https://doi.org /10 .1038 /ngeo2436.

Gundersen, E., Renard, F., Dysthe, D. K., Bjorlykke, K., Jamtveit, B., 2002. Coupling between pressure solution creep and diffusive mass transport in porous rocks. Journal of Geophysical Research-Solid Earth, 107. doi:10.1029/2001JB000287.

Gutiérrez-Santolalla, F., Acosta, E., Ríos, S., Guerrero, J., Lucha, P., 2005. Geomorphology and geochronology of sackung features (uphill-facing scarps) in the Central Spanish Pyrenees. Geomorphology 69 (1-4), 298-314.

Han, R., Shimamoto, T., Hirose, T., Ree, J.-H., Ando, J., 2007. Ultralow friction of carbonate faults caused by thermal decomposition. Science (80-.) 316, 878–881. https://doi.org/10.1126/science.1139763.

Han, R., Shimamoto, T., Hirose, T., Ree, J.-H., and Ando, J., 2007b. Ultralow friction of carbonate faults caused by thermal decomposition: Science, 316, 878–881, doi:10.1126/science.1139763.

Hashimoto, H., Komaki, E., Hayashi, F., Uematsu U., 1980. Partial decomposition of dolomite in $CO_2$ J. Solid State Chem., 33, 181-188.

Heidelbach, F.; Stretton, I., Langenhorst, F., Mackwell, S., 2003. Fabric evolution during high shear strain deformation of magnesiowüstite (Mg0.8Fe0.2O). J. Geophys. Res. 108, 2154.

Heilbronner, R., Tullis, J., 2002. The effect of static annealing on microstructures and crystallographic preferred orientations of quartzites experimentally deformed in axial compression and shear. In: De Meer S, Drury MD, de Bresser JHP Pennock GM (eds) Deformation mechanisms, rheology and tectonics: current status and future perspectives. Special Publication 200, GSL, pp 191–218.

Hermann, S. W., Madritsch, G., Rauth, H., Becker, L. P., 2000. Modes and Structural Conditions of Large-Scale Mass Movements (Sackungen) on Crystalline Basement Units of the Eastern Alps (Niedere Tauern, Austria). Mitt, naturwiss. Ver. Steiermark, 130, 31-42.

Hermanns R. L., Longva O., 2012. Rapid rock-slope failures. in: Clague J.J. & Stead D. (eds.), landslides: types, mechanisms and modeling. cambridge university press, cambridge, p.p. 59-70.

Hippolyte J. C., Brocard G., Tardy M., Nicoud G., Bourles D., Braucher R., Ménard G., Souffaché B., 2006. The recent fault scarps of the Western Alps (France): tectonic surface ruptures or gravitational sackung scarps? a combined mapping, geomorphic, levelling, and 10be dating approach. tectonophysics, 418(3-4): 255-276. https://doi.org/10.1016/j.tecto.2006.02.009

Huijser-Gerits, E. M. C., Rieck, G. D., 1974. Defocusing effects in the reflexion technique for the determination of preferred orientation. J. Appl. Cryst. 7, 286–290.

Hungr O., Evans S. G., 2004. Entrainment of debris in rock avalanches: an analysis of a long run-out mechanism. geological society of america bulletin, 116(9-10): 1240-1252. https://doi.org/10.1130/b25362.1

Hungr O., Leroueil, S., Picarelli, L., 2014. The Varnes classification of landslide types, an update. Landslides, 11, 167-194.

Hunstad. I., Selvaggi, G., D'Agostino, N., England Clarke P., Pierozzi M., 2003. Geodetic strains in peninsular Italy between 1875 and 2001 Geophys. Res. Lett., 30-1828.

Hürlimann M., Ledesma A., Corominas J., Prat P.C., 2006. The deep-seated slope deformation at Encampadana, Andorra: representation of morphologic features by numerical modelling. engineering geology, 83(4): 343-357. https://doi.org/10.1016/j.enggeo.2005.11.008

Hutchinson, J.N., 1988. General report: morphological and geotechnical parameters of landslides in relation to geology and hydrogeology. Proceedings of the 5th International Symposium on Landslides, Lausanne, CH, vol. 1. Balkema, Rotterdam, pp. 3±35.

Iezzi, F., Roberts, G., Walker, J. F., Papanikolaou, I., 2019. Occurrence of partial and total coseismic ruptures of segmented normal fault systems: Insights from the Central Apennines, Italy. Journal of Structural Geology, 126, 83-99. https://doi.org/10.1016/j.jsg.2019.05.003.

Jaboyedoff, M., Penna, I., Pedrazzini, A., Baroň I., Crosta G.B., 2013. An introductory review on gravitational-deformation induced structures, fabrics and modeling. tectonophysics, 605, 1-12. https://doi.org/10.1016/j.tecto.2013.06.027

Jahn, A., 1964. Slow morphological features resulting from gravitation. Zeitschr. Geomorph., 5, 59-72.

Jarman D., Harrison S., 2019. Rock slope failure in the british mountains. geomorphology, 340: 202-233. https://doi.org/10.1016/j.geomorph.2019.03.002

Jibson, R. W., Harp, E. L., Schulz, W., Keefer, D. K., 2004. Landslides triggered by the 2002 Denali fault, Alaska earthquake and the inferred nature of the strong shaking. Earthquake Spectra, 20, 669-691.

Kastelic, V., Burrato, P., Carafa, M. Basili, R., 2017. Repeated surveys reveal nontectonic exposure of supposedly active normal faults in the central Apennines, Italy. J. Geophys. Res. Earth surf., 122, 114-129. doi:10.1002/2016JF003953.

Kim S., Ree J., Han R., Kim N., Jung H., 2018. Tectonophysics Fabric transition with dislocation creep of a carbonate fault zone in the brittle regime, Tectonophysics, 723, 107-116.
Law, R.D., Casey, M., Knipe R.J., 1986. Kinematic and tectonic significance of microstructures and crystallographic fabrics within quartz mylonites from the Assynt and Eriboll regions of the Moine thrust zone, NW Scottland. Trans R Soc Edinb Earth Sci 77:99–125.

Lehner, F. K., 1995. A model for intergranular pressure solution in open systems. Tectonophysics, 245, 153-170.

Leonard, M., 2010. Earthquake fault scaling: Self-consistent relating of rupture length, width, average displacement, and moment release. Bulletin of the Seismological Society of America, 100(5A), 1971-1988.

Li, T., Chen, J., Thompson Jobe, J. A., Burbank, D. W., Cheng, X., Xu, J., et al., 2018. Active bending-moment faulting: Geomorphic expression, controlling conditions, Accommodation of Fold Deformation. Tectonics, 37,2278–2306. https://doi.org/10.1029/ 2018TC004982.

Lucca, A., Storti, F., Balsamo, F., Clemenzi, L., Fondriest, M., Burgess, R., Di Toro., G., 2019. From submarine to subaerial out-of-sequence thrusting and gravity-driven extensional faulting: gran sasso massif, central Apennines, Italy Tectonics, 38, 4155-4184.

Lutterotti, L. Matthies, S., Wenk. H.-R., 1999. MAUD: a friendly Java program for material analysis using diffraction. IUCr: Newsletter of the CPD, 21:14-15.

Lutterotti, L., Chateigner, D., Ferrari, S. Ricote, J., 2004. Texture, residual stress and structural analysis of thin films using a combined X-ray analysis. Thin Solid Films, 450, 34–41.

Madritsch H., millen B. M. J., 2007. Hydrogeologic evidence for a continuous basal shear zone within a deep-seated gravitational slope deformation (eastern alps, Tyrol, Austria). landslides, 4(2), 149-162. https://doi.org/10.1007/s10346-006-0072-x.

Mahr T., Nemčok A., 1977. Deep-seated creep deformations in the crystalline cores of the tatry mts. bulletin of the international association of engineering geology, 16(1), 104-106. https://doi.org/10.1007/bf02591461

Mahr T., 1977. Deep-reaching gravitational deformations of high mountain slopes. bulletin of the international association of engineering geology, 16(1): 121-127. https://doi.org/10.1007/bf02591467

Mainprice. D., Nicolas. A., 1989. Development of shape and lattice preferred orientations: application to the seismic anisotropy of the lower crust. J Struct Geol 11:175-190.

Malinverno, A., Ryan, W. B. F., 1986. Extension in the Tyrrhenian Sea and shortening in the Apennines as result of arc migration driven by sinking of the lithosphere. Tectonics, 5, 227-245.

Mancinelli, A., Chiocchini, M., Coccia, B., 2003. Orbitolinidae and Alveolinidae (Foraminiferida) from the uppermost Albian-lower Cenomanian of Monti d'Ocre (Abruzzi, Italy). Cretaceous Res 24, 729–741.

Mancinelli, P., Porreca, M., Pauselli, C., Minelli, G., Barchi, M. R., Speranza, F., 2019. Gravity and magnetic modeling of Central Italy: Insights into the depth extent of the seismogenic layer. Geochemistry, Geophysics, Geosystems, 20, 2157-2172.

Mancinelli, P., Scisciani, V., Patruno, S., Minelli, G., 2021. Gravity modeling reveals a Messinian foredeep depocenter beneath the intermontane Fucino basin (central Apennines) Tectonophysics, 821, 229144, 10.1016/j.tecto.2021.229144

Mariani G. S., Zerboni, A., 2020. Surface Geomorphological Features of Deep-Seated Gravitational Slope Deformations: A Look to the Role of Lithostructure (N Apennines, Italy). Geosciences, 10, 334. doi:10.3390/geosciences10090334.

Mariotto F. P., Tibaldi A., 2015. Inversion kinematics at deep-seated gravity slope deformations: a paleoseismological perspective. Nat. Hazards Earth Syst. Sci. Discuss., 3, 4585-4617. doi:10.5194/nhessd-3-4585-2015

Mariucci M. T., Muller B., 2003. The tectonic regime in Italy inferred from borehole breakout data. Tectonophysics, 361, 21-35.

Marshak, S., Haq, S. S., Sen, P., 2019. Ramp initiation in fold-thrust belts: Insight from PIV analysis of sandbox models, J. Struct. Geol., 118, 308-323, https://doi.org/10.1016/j.jsg.2018.11.006.

Martel, S. J., 2006. Effect of topographic curvature on near-surface stresses and application to sheeting joints. Geophysical Research Letters, 33. doi:10.1029/2005GL024710.

Martino S., Prestininzi A., Scarascia Mugnozza G., 2004. Geological-evolutionary model of a gravity-induced slope deformation in the carbonate central apennines (italy). quarterly journal of engineering geology and hydrogeology, 37(1): 31-47. https://doi.org/10.1144/1470-9236/03-030

Martino S., Della Seta M. and Esposito C., 2017. Back-analysis of rock landslides to infer rheological parameters. in: feng x.t. (ed.), rock mechanics and engineering, analysis, modeling and design. taylor and francis, london, vol. 3, p.p. 237-268.

Masoch, S., Gomila, R., Fondriest, M., Jensen, E., Mitchell, T., Pennacchioni, G., Cembrano, J., Di Tori, G., 2021. Structural evolution of a crustal-scale seismogenic fault in a magmatic arc: The Bolfin Fault Zone (Atacama Fault System). Tectonics, 40, e2021TC006818. https://doi.org/10.1029/2021TC006818.

Matthies, S., Wenk, H.R., Vinel, G.W., 1988. J. Appl. Cryst. 21, 285

Matthies, S., Lutterotti, L., Wenk, H.R., 1997. J. Appl. Cryst. 30, 31

McCalpin, J. P., 1999. Criteria for determining the seismic significance of sackungen and other scarp-like landforms inmountainous regions. Techniques for Identifying Faults and Determining their Origins. Washington, DC: U.S. Nuclear Regulatory Commission.

Meyers, W. J., Hill, B. E., 1983. Quantitative studies of compaction in Mississippian skeletal limestones, New Mexico. J. Sediment. Petrol., 53, 231-242.

Mercuri, M., Scuderi, M., Tesei, T., Carminati, E., Collettini, C., 2018. Strength evolution of simulated carbonate bearing faults: The role of normal stress and slip velocity. J. Struct. Geol., 109, 1-9.

Molnar, P., 2004. Interactions among topographically induced elastic stress, static fatigue, and valley incision. Journal of Geophysical Research, 109.

Morales, M., Chateigner, D., Lutterotti, L. Ricote, J., 2002. X-ray combined QTA using a CPS applied to a ferroelectric ultrastructure. Mater. Sci. Forum, 408-412, 113–118.

Morales, M., Chateigner, D. Fruchart, D., 2003. Texture and magnetocrystalline anisotropy analysis of an oriented ErMn4Fe8C powder sample. J. Magn. Magn. Mater. 257, 258-269.

Morewood N. G., Roberts G. P., 2000. The geometry, kinematics and rates of deformation within an en échelon normal fault segment boundary, central Italy. Journal of Structural Geology, 22, 1027-1047.

Moro, M., Saroli, M., Salvi, S., Stramondo, S., Doumaz, F., 2007. The relationship between seismic deformation and deep-seated gravitational movements during the 1997 Umbria–Marche (Central Italy) earthquakes. Geomorphology, 89, 297-307.

Moro, M., Saroli, M., Tolomei C., & Salvi, S., 2009. Insights on the kinematics of deep-seated gravitational slope deformations along the 1915 Avezzano earthquake fault (Central Italy), from time-series DInSAR. Geomorphology, 112, 261-276.

Moro, M., Saroli, M., Gori, S., Falcucci, E., Galadini, F., & Messina, P., 2012. The interaction between active normal faulting and large scale gravitational mass movements revealed by paleoseismological techniques: A case study from central Italy. Geomorphology, 151-152, 164-174.

Moro, M., Gori, S., Falcucci, E., Saroli, M., Galadini, F., Salvi, S., 2013. Historical earthquakes and variable kinematic behaviour of the 2009 L'Aquila seismic event (central Italy) causative fault, revealed by paleoseismological investigations. Tectonophysics, 583, 131-144.

Nemčok A., 1972. Gravitational slope deformation in high mountains. in: proceedings of the 24th international geological congress, montreal, sect. 13, 132-141.

Nemčok A., 1982. Zosuvy v slovenských karpatoch (in Slovak with english summary). Veda, Bratislava.

Niemeijer, A., Di Toro, G., Nielsen, S., Di Felice, F., 2011. Frictional melting of gabbro under extreme experimental conditions of normal stress, acceleration, and sliding velocity. J. Geophys. Res. 116, B07404. https://doi.org/10.1029/2010JB008181.

Ohl, M., Plümper, O., Chatzaras, V., Wallis, D., Vollmer C., Drury M., 2020. Mechanisms of fault mirror 772 formation and fault healing in carbonate rocks, Earth and Planetary Science Letters, 530, 115886.

Pánek, T., Tábořík, P., Klimeš, J., Komárková, V., Hradecký, J., Šťastný, M., 2011a. Deepseated gravitational slope deformations in the highest parts of the Czech Flysch Carpathians: evolutionary model based on kinematic analysis, electrical imaging and trenching. Geomorphology 129, 92-112.

Panek, T., Klimeš, J., 2016. Temporal behavior of deep-seated gravitational slope deformations: A review. Earth-Science Reviews, 156, 14-38.

Pantosti, D., D'Addezio, G. Cinti, F. R., 1996. Paleoseismicity of the Ovindoli-Pezza fault, central Apennines, Italy: A history including a large, previously unrecorded earthquake in the Middle Ages (860–1300 A.D.), J. Geophys. Res. 101, 5937-5959.

Pašek J., 1974. Gravitational block-type slope movements. in: proceedings of the 2nd international congress of the international association of engineering geology, sao paulo, vol. 2, 1-9.

Passchier, C., Trouw, R., 2005. Microtectonics. Springer-Verlag, Berlin Heidelberg, pp. 366.

Patacca, E., Scandone, P., 1989. Post-Tortonian mountain building in the Apennines. The role of the passive sinking of a relic lithospheric slab. In: The Lithosphere in Italy, Eds. Boriani A., Bonafede M., Piccardo G.B. and Vai G.B. Atti dei Convegni Lincei 80, 157-176.

Patacca, E., Sartori, R., Scandone P., 1992a. Tyrrhenian basin and Apenninic arcs: kinematic relations since late Tortonian times. Mem. Soc. Geol. It. 45, 425-451.

Pizzi, A., C., Coltorti, M., Pieruccini, P., 2002. Quaternary normal faults, intramontane basins and seismicity in the Umbria-Marche-Abruzzi Apennine ridge (Italy): Contribution of neotectonic analysis to seismic hazard assessment. Boll. Soc. Geol. It., 1, 923-929.

Poirier, J.-P., 1985, Creep of Crystals: Cambridge, UK, Cambridge University Press, 260 p., https:// doi.org /10 .1017 /CBO9780511564451.

Pollard, D. Aydin, A., 1988. Progress in understanding jointing over the past century: Geological Society of America Bulletin, 100, 1181-1204.

Pozzi, G., De Paola, N., Nielsen, S. B., Holdsworth, R. E., Bowen, L., 2018. A new interpretation for the nature and significance of mirror-like surfaces in experimental carbonate-hosted seismic faults. Geology., 46, 583-586.

Pozzi, G., De Paola, N., Holdsworth, R. E., Bowen, L., Nielsen, S. B., Dempsey, E. D., 2019. Coseismic ultramylonites: an investigation of nanoscale viscous flow and fault weakening during seismic slip. Earth Planet. Sci. Lett., 516, 164-175.

Pozzi G., De Paola N., Nielsen S.B., Holdsworth R.E., Tesei T., Thieme M., Demouchy S., 2021. Coseismic fault lubrication by viscous deformation, Nat. Geosci., 14, 437–442.

Power, W. L., Tullis, T. E., 1989. The relationship between slickenside surfaces in fine grained quartz and the seismic cycle. J. Struct. Geol., 11(7), 879-893. doi:10.1016/0191-8141(89) 90105-3.

Prior, D. J., Mariani, E., Wheeler, J., 2009. EBSD in the Earth sciences: Applications, common practice, and challenges. Electron Backscatter Diffraction in Materials Science (pp. 345–360). Boston, MA: Springer. https://doi.org/10.1007/978-0-387-88136-2.

Prior, D.J., Boyle, A.P., Brenker, F., Cheadle, M.C., Day, A., Lopez, G., Peruzzo, L., Potts, G.J., Reddy, S., Spiess, R., Timms, N.E., Trimby, P.W., Wheeler, J., Zetterström, L., 1999. The application of electron backscatter diffraction and orientation constrast imaging in th SEM to textural problems in rocks. Am. Mineral. 84, 1741–1759. https://doi.org/10.2138/am-1999-11-1204.

Radbruch-Hall, D., Varnes, D.J., Colton, R.B., 1977. Gravitational spreading of steep-sided ridges (“Sackung”). Colorado J. Res. U.S. Geol. Surv. 5(3), 359±363.

Rempe, M., Di Toro, G., Mitchell T. M., Smith, S. A. F., Hirose, T., Renner, J., 2020. Influence of effective stress and pore-fluid pressure on fault strength and slip localization in carbonate slip zones. Journal of Geophysical Research: Solid Earth, 10.1029/2020JB019805, JGRB54497 in press.

Renard, F., Ortoleva, P. J.,1997. Water films at grain-grain contacts: Debye-Huckel osmotic model of stress, salinity, and mineralogy dependence. Geochem. Cosmochim., Acta 61, 1963-1970.

Renard, F., Gratier, J. P., Jamtveit, B., 2000. Kinetics of crack-sealing, intergranular pressure solution, and compaction around active faults J. of Struct. Geol., 22(10), 1395-1407.

Renard, F., Dysthe D., Feder, J., Bjørlykke, K., Jamtveit. B., 2001. Enhanced pressure solution creep rates induced by clay particles: Experimental evidence in salt aggregates. Geophys. Res. Lett., 28, 1295-1298.

Rice, J.R., 2006. Heating and weakening of faults during earthquake slip. J. Geophys. Res., Solid Earth111 (B5), B05311. https://doi .org /10 .1029 /2005JB004006.

Roberts, G. P., Michetti, A. M., 2004. Spatial and temporal variations in growth rates along active normal fault systems: an example from the Lazio–Abruzzo Apennines, central Italy. Journal of Structural Geology, 26, 339-376.

Rovida, A., Locati, M., Camassi, R., Lolli, B., Gasperini, P., 2020. The Italian earthquake catalogue CPTI15. Bulletin of Earthquake Engineering, 18, 2953-2984.

Rowe, C. D., Griffith, W. A., 2015. Do faults preserve a record of seismic slip: a second opinion. J. Struct. Geol. 78, 1e26.

Rutter, E. H., 1983. Pressure solution in nature, theory and experiment. J. Geol. Soc. Lond., 140, 725-740.

Rutter, E.H., Casey, U.K.M., Burlini, L., 1994. Preferred crystallographic orientation development during the plastic and superplastic flow of calcite rocks. J. Struct. Geol.16 (10), 1431-1446.

Savage, W. Z., Varnes, D. J., 1987. Mechanics of gravitational spreading of steep-sides ridges (sackung). IAEG Bull., 35, 31-36.

Schirripa Spagnolo, G., Mercuri, M., Billi, A., Carminati, E., Galli. P., 2021. The segmented Campo Felice normal faults: seismic potential appraisal by application of empirical relationships between rupture length and earthquake magnitude in the central Apennines, Italy Tectonics, 40 (7) e2020TC006465

Scholle, P. A., Halley, R. B., 1985. Burial diagenesis: out of sight, out of mind. In: Carbonate Cements, 36, Society of Economic Paleontologists and Mineralogists, 309-334.

Serpelloni, E., Anzidei, M., Baldi, P., Casula, G., Galvani, A., 2005. Crustal velocity and strain-rate fields in Italy and surrounding regions: new results from the analysis of permanent and non-permanent GPS networks. Geophys J. Int., 161(3), 861-880.

Salvi, S., Nardi, A., 1995. The Ovindoli Fault: a segment of a longer, active fault zone in central Abruzzi, Italy, in *Perspectives in Paleoseismology,* Vol. 6, pp. 101–113, eds Serva, L. & Slemmons, D.B., Bull. Assoc. Eng. Geol.

Salvi, S., Cinti, F. R., Colini, L., D'addezio, G., Doumaz, F., Pettinelli, E., 2003. Investigation of the active Celano-L'Aquila fault system, Abruzzi (central Apennines, Italy) with combined ground-penetrating radar and paleoseismic trenching. Geophysical Journal International, 155(3), 805-818. https://doi.org/10.1111/j.1365-246X.2003.02078.x.

Sibson R. H., 1975. Generation of pseudotachylyte by ancient seismic faulting. Geophys J R Astr Soc 43:775–794.

Sibson, R. H., 1977. Fault rocks and fault mechanisms: Geological Society of London Journal, v. 133, 191-231.

Sibson, R. H., 2003. Thickness of the seismic slip zone, Bull. Seismol. Soc. Am., 93, 1169-1178.

Siman-Tov, S., Aharonov, E., Sagy, A., Emmanuel S., 2013. Nanograins form carbonate fault mirrors. Geology, 41, 703-706.

Siman-Tov, S., Aharonov, E., Boneh, Y., Reches, Z.E., 2015. Fault mirrors along carbonate faults: formation and destruction during shear experiments. Earth Planet. Sci. Lett. 430, 367e376.

Smeraglia, L., Billi, A., Carminati, E., Cavallo, A., Doglioni, C., 2017a. Field-to nano-scale evidence for weakening mechanisms along the fault of the 2016 Amatrice and Norcia earthquakes, Italy. Tectonophysics, 712-713, 156-169.

Smeraglia, L., Bettucci, A., Billi, A., Carminati, E., Cavallo, A., Di Toro, G., Natali, M., Passeri, D., Rossi, M., Spagnuolo, E., 2017b. Field-to nano-scale evidence for weakening mechanisms along the fault of the 2016 Amatrice and Norcia earthquakes, Italy. Tectonophysics, 712-713, 156-169.

Smith, S. A. F., Billi, A., Di Toro, G., Spiess, R., 2011. Principal slip zones in limestone: Microstructural characterization and implications for the seismic cycle (Tre Monti fault, Central Apennines, Italy). Pure and Applied Geophysics, 168(12), 2365–2393. https://doi.org/10.1007/s00024-011-0267-5.

Smith, S. A. F., Di Toro, G., Kim, S., Ree, J. H., Nielsen, S., Billi, A., Spiess, R., 2013. Coseismic recrystallization during shallow earthquake slip. Geology, 41, 63-66.

Spagnuolo, E., Plümper, O., Violay, M. E. S., Cavallo, A., Di Toro, G., 2015. Fast-moving dislocations trigger flash weakening in carbonate-bearing faults during earthquakes. Scientific Reports, 5. https://doi.org/10.1038/srep16112

Stramondo, S., Saroli, M., Moro, M., Atzori, S., Tolomei, C., Salvi, S., 2005. Monitoring long term ground movements and Deep-Seated Gravitational Slope Deformations by InSAR time series: cases studies in Italy. Extended Abstract in Proceedings ESA Esrin, 28 November - 2 December 2005, Frascati, Italy.

Stretton, I., Heidelbach, F., Mackwell, S., Langenhorst, F., 2001. Dislocation creep of magnesiowüstite (Mg0.8Fe0.2). Earth Planet. Sci. Lett. 194, 229-240.

Tada, R., Siever, R., 1989. Pressure solution during diagenesis. Annu. Rev. Earth Planet Sci., 17, 89-118.

Tarquini, S. Isola, I. Favalli, M., Mazzarini, F., Bisson, M., Pareschi, M.T., Boschi E., 2007. TINITALY/01: a new triangular irregular network of Italy Annals of Geophysics, 50, 407-425.

Tavani, S., Storti, F., Lacombe, O., Corradeti, A., Muñoz, J. A., Mazzoli, S., 2015. A review of deformation pattern templates in foreland basin systems and fold and thrust belts: Implications for the state of stress in the frontal regions of thrust wedges. Earth-ScienceReviews, 141, 82-104. https://doi.org/10.1016/j.earscirev.2014.11.013.

Tesei, T., Carpenter, B. M., Giorgetti, C., Scuderi, M., Sagy, A., Scarlato, P., Collettini, C., 2017. Friction and scale-dependent deformation processes of large experimental carbonate faults. J. Struct. Geol., 100, 12-23. 05.008.

Tinti, E., L. Scognamiglio, A. Michelini, M. Cocco., 2016. Slip heterogeneity and directivity of the ML 6.0, 2016, Amatrice earthquake estimated with rapid finite-fault inversion, Geophys. Res. Lett. 43, 10,745–10,752, doi: 10.1002/2016GL071263.

Tolomei, C., Taramelli, A., Moro, M., Saroli, M., Aringoli, D., Salvi, S., 2013. Analysis of the deep-seated gravitational slope deformations over Mt. Frascare (Central Italy) with geomorphological assessment and DInSAR approaches. Geomorphology 201, 281–292.

Tozer, R. S. J., Butler R. W. H., & Corrado S., 2002. Comparing Thin- and Thick-Skinned thrust tectonic models of the central Apennines, Italy, Stephan Mueller Spec. Publ. Ser., 1, 181-194.

Valensise, G., Pantosti, D., 2001. Database of potential sources for earthquakes larger than M 5.5 in Italy. Annali di Geofisica, 44, 287-306.

Valoroso, L., Chiaraluce, L., Collettini, C., 2014. Earthquakes and fault zone structure. Geology, 42, 343-346. doi:10.1130/G35071.1

Varnes, D. J., 1978. Slope movements types and processes. In: Schuster, R.L., Krizek, R.J. (Eds.), Landslides: Analysis and Control (11-35).

Varnes, D.J., Radbruch-Hall, D., Savage, W.Z., 1989. Topographic and structural conditions in areas of gravitational spreading of ridges in the Western United States. United States Geological Survey Professional Paper 1496 (28 pp.).

Varnes, D.J., Radbruch-Hall, D., Varnes, K. L., Smith, W. K., Savage, W. Z., 1990. Measurement of ridge-spreading movements (sackungen) at Bald Eagle Mountain, Lake County, Colorado, 1975–1989. U.S. Geological Survey Open-File Report, 90-543 (13 pp.).

Verberne, B. A., Spiers, C. J., Niemeijer, A. R., De Bresser, J. H. P., De Winter, D. A. M., Plümper, O., 2013. Frictional properties and microstructure of Calcite-rich fault gouges sheared at sub-seismic sliding velocities. Pure Appl. Geophys., 171, 2617-2640. http://dx.doi.org/10.1007/s00024-013-0760-0.

Verberne, B. A., de Bresser, J. H. P., Niemeijer, A. R., Spiers, C. J., de Winter, D. A. M., Plümper, O., 2013a. Nanocrystalline slip zones in calcite fault gouge show intense crystallographic preferred orientation: Crystal plasticity at subseismic slip rates at 18–150 °C. Geology, 41, 863–866. https://doi.org/10.1130/G34279.1.

Verberne, B. A., Plümper, O., de Winter, M. D. A., Spiers, C. J., 2014. Superplastic nanofibrous slip zones control seismogenic fault friction. Science, 346, 1342–1344. https://doi.org/10.1126/science.1259003

Vezzani, L., Ghisetti, F.,1998. Carta Geologica dell'Abruzzo, scala 1:100.000. Regione Abruzzo, settore urbanistica-beni ambientali e cultura. S.EL.CA., Firenze.

Vezzani, L., Festa, A., Ghisetti, F. C., 2010. Geology and tectonic evolution of the Central-Southern Apennines, Italy. Geological Society of America, Special Paper, 469, 1-58.

Villani, F., Pucci, S., Civico, R., De Martini, P. M., Cinti, F. R., Pantosti, D., 2018. Surface faulting of the 30 October 2016 Mw 6.5 central Italy earthquake: Detailed analysis of a complex coseismic rupture. Tectonics, 37. https://doi.org/10.1029/ 2018TC005175.

Viola, G., Scheiber, T., Fredin, O., Zwingmann, H., Margreth, A., Knies, J., 2016. Deconvoluting complex structural histories archived in brittle fault zones. *Nature Communications*, **7**, 13448. https://doi.org/10.1038/ncomms13448.

Wenk, H.-R., 1985. Preferred Orientation in Deformed Metals and Rocks: An Introduction to Modern Texture Analysis. New York: Academic Press.

Wenk, H.R., 2002. Rev. Mineral. Geochem. 51, 291

Wenk, H.-R., Chateigner, D., Pernet, M., Bingert, J., Hellstrom, E. Ouladdiaf, B., 1996. Texture analysis of Bi-2212 and 2223 tapes and wires by neutron diffraction. Physica C, 272, 1–12.

Wells, D. L., Coppersmith, K. J., 1994. New empirical relationships among magnitude, rupture length, rupture width, rupture area, and surface displacement. Bulletin of the seismological Society of America, 84(4), 974-1002.

Wesnousky, S. G., 2008. Displacement and geometrical characteristics of earthquake surface ruptures: Issues and implications for seismic-hazard analysis and the process of earthquake rupture. Bulletin of the Seismological Society of America, 98(4), 1609-1632.

Wibberley, C. A. J., Shimamoto T., 2003. Internal structure and permeability of major strike-slip fault zones: The Median Tectonic Line in Mid Prefecture, southwest Japan, J. Struct. Geol., 25, 59-78.

Wibberley, C.A.J., Yielding, G., Di Toro, G., 2008. Recent advances in the understanding of fault zone internal structure: a review. Geol. Soc. Lond. Spec. Publ. 299, 5–33. https://doi.org/10.1144/SP299.2.

Wilkinson, M., Roberts, G. P., McCaffrey, K., Cowie, P. A., Walker, J. P. F., Papanikolaou, I., Wedmore, L., 2015. Slip distributions on active normal faults measured from LiDAR and field mapping of geomorphic offsets: an example from L'Aquila, Italy, and implications for modelling seismic moment release. Geomorphology, 237, 130-141.

Woodcock, N. H., Mort, K., 2008. Quantifying fault breccia geometry: Dent fault, NW England. Journal of Structural Geology, 30(6), 701–709. https://doi.org/10.1016/j.jsg.2008.02.005

Yasuhara, H., Marone, C., Elsworth, D., 2005. Fault zone restrengthening and frictional healing: the role of pressure solution, Journal of Geophysical Research-Solid Earth, 110, B06310.

Zangerl, C., Eberhardt, E., Perzlmaier, S., 2010. Kinematic behavior and velocity characteristics of a complex deep-seated crystalline rockslide system in relation to its interaction with a dam reservoir. Engineering Geology 112 (1-4), 53–67.

Záruba Q., Mencl V., 1982. Landslides and their control, 2nd completely revised edition. academia, prague.

Zhang, S., Karato, S., 1995. Lattice preferred orientation of olivine aggregates deformed in simple shear. Nature 375, 774–777.

Zischinsky, U., 1966. On the deformation of high slopes. Ist. Conf. Int. Soc. Rock Mech., 2, 179-185.

Zischinsky, U., 1969. Uber Sackungen. Rock Mechanics, 1, 30-52.

# Appendix 1

| LOCATION | GPS (WGS 84) LAT (N) | GPS (WGS 84) LONG (E) | OUTCROPPING ROCKS | Structural Element | DIP AZIMUT | DIP | PITCH | SAMPLE | NOTE | OM | SEM | CTA |
|---|---|---|---|---|---|---|---|---|---|---|---|---|
| Alto Di Cacchia DGSD | 42069202 | 13563760 | SILT/CLAYS | Silty layer | | | | AC00_2019 | | | | |
| Alto Di Cacchia DGSD | 4206947 | 1356540 | Cemented Conglom. | MAJOR SCARP | 190 | 60 | N_Dip_Slip | AC01_2019 | Scarp Wall_Karstified | X | | |
| Alto Di Cacchia DGSD | 4206947 | 1356540 | | | | | | AC02_2019 | | X | X | |
| Alto Di Cacchia DGSD | 4206947 | 1356540 | | | | | | AC03_2019 | | | | |
| Alto Di Cacchia DGSD | 4206951 | 1356522 | Cemented Conglom. | MAJOR SCARP | 178 | 67 | | AC04_2019 | Karstified | | | |
| Alto Di Cacchia DGSD | 4206909 | 1356404 | Cemented Conglom. | Sec. HW Scarp | 200 | 65 | | AC05_2019_H_F | Scarp wall | X | X | |
| Alto Di Cacchia DGSD | 4206909 | 1356404 | | | | | | AC06_2019 | Hangingwall | | | |
| Alto Di Cacchia DGSD | 4206909 | 1356404 | Cemented Conglom. | MAJOR SCARP | 190 | 65 | | AC07_2019 | Karstified | | | |
| Alto Di Cacchia DGSD | 4206909 | 1356404 | | | | | | AC08_2019 | | | | |
| Alto Di Cacchia DGSD | 4206909 | 1356404 | | | | | | AC09_2019 | | X | X | |
| | | | | | | | | | | | | |
| | | | | | | | | | | | | |
| Valle Force normal fault | 42329858 | 13609551 | Platform Carbonates | MAJOR SCARP | 30 | 72 | | VA01_2019 | Karstified; HW Breccia | X | X | |
| Valle Force normal fault | 42329473 | 13610250 | Platform Carbonates | MAJOR SCARP | 35 | 55 | | VA02_2019 | Possible fault wall | X | | |
| Valle Force normal fault | 42332566 | 13605636 | Platform Carbonates | MAJOR SCARP | 40 | 50 | | VA03_2019 | sharp fault wall | X | X | |
| Valle Force normal fault | 42332566 | 13605636 | | | | | | VA04_2019 | | | | |
| Valle Force normal fault | 42332566 | 13605636 | | | | | | VA05_2019_H_F | Very sharp fault wall | X | X | X |
| Valle Force normal fault | | | Platform Carbonates | MAJOR SCARP | 38 | 55 | | VA06_2019 | Sharp slip surface on breccias | | | |
| | | | | | | | | | | | | |
| | | | | | | | | | | | | |
| Sant'Erasmo DGSD | 42207558 | 13694766 | Platform Carbonates | MAJOR SCARP | 10 | 65 | | SAE01_K | Karstified with HW Breccias | X | X | |
| Sant'Erasmo DGSD | 42207819 | 13694406 | Platform Carbonates | MAJOR SCARP | 30 | 75 | | SAE02A_K | Karstified with HW Breccias | X | X | |
| Sant'Erasmo DGSD | 42207891 | 13694300 | Platform Carbonates | MAJOR SCARP | 60 | 65 | | SAE02B_K | Karstified with HW Breccias | | | |
| | | | | | | | | | | | | |
| | | | | | | | | | | | | |
| Colle Cerese DGSD | 41981774 | 13667000 | Platform Carbonates | MAJOR SCARP | 230 | 42 | | CC01_H_F_a_b | Fault Wall | X | X | |
| | | | | | | | | | | | | |
| | | | | | | | | | | | | |
| Mt. Serrone DGSD | 41947815 | 13724335 | Platform Carbonates | MAJOR SCARP | 45 | 58 | | SE01_K | Karstified: FW | | | |
| | 41947815 | 13724335 | | | | | | SE02_K | Karstified: FW | X | X | |
| | | | | | | | | | | | | |
| Campo Felice Fault | 42222379 | 13457858 | Platform Carbonates | MAJOR SCARP | 230 | 50 | | CF_01_2018 | | | | |
| | 42223802 | 13454787 | Platform Carbonates | UltraCataclasites | | | | CF_02 | UC samples | X | | |
| | 42223802 | 13454787 | | | | | | CF_03 | | | | |
| | 42222379 | 13457858 | Platform Carbonates | MAJOR SCARP | 230 | 50 | | CF_04_2021 | Karstified Surface | X | X | |
| Same Stop of CF01 | 42223802 | 13454787 | Platform Carbonates | Minor fault | 90 | 85 | N_Dip_Slip | CF_05 | polished_lineated_step | X | X | X |
| | 42225018 | 13453982 | Platform Carbonates | Minor fault | 50 | 75 | | CF_06 | lineated surface with fibers | X | X | |
| | 42227763 | 13445174 | Platform Carbonates | MAJOR SCARP | 195 | 59 | | CF_07 | Karstified_cleavage_red matrix | X | X | |
| | 42227763 | 13445174 | | | | | | CF_08 | Karstified | X | X | |
| | 42228392 | 13443268 | Platform Carbonates | MAJOR SCARP | 210 | 55 | | CF_09 | Karstified (> 10 m high) | X | | |
| | 42228401 | 13443210 | Platform Carbonates | MAJOR SCARP | 201 | 55 | | CF_10 | Karstified | | | |
| | 42234216 | 13437394 | Platform Carbonates | Secondary Fault | 220 | 50 | | CF_11 | Fault wall (HW with cleavage) | X | X | |
| | 42238080 | 13431350 | Platform Carbonates | Secondary Fault | 212 | 88 | 75 EST | CF_12 | Lineated | | | |
| | 42238520 | 13430920 | Platform Carbonates | Secondary Fault | 210 | 89 | | CF_13 | Sec. faults in Mosaic breccias | | | |
| | 42238520 | 13430920 | Platform Carbonates | MAJOR SCARP | 217 | 56 | | CF_14 | | | | |
| | 42238820 | 13430460 | Platform Carbonates | MAJOR SCARP | 215 | 49 | | CF_15 | | | | |
| | 42238820 | 13430460 | | | | | | CF_16_a_b_c | | | | |
| | 42238820 | 13430460 | | | | | | CF_17 | | | | |
| | 42239200 | 13429650 | Platform Carbonates | MAJOR SCARP | 219 | 55 | | CF_18 | | | | |
| | 42238950 | 13429980 | Platform Carbonates | MAJOR SCARP | 218 | 53 | | CF_19 | FW whitish cataclasite | X | | |
| Same Stop of CF01 | 42223870 | 13454730 | Platform Carbonates | Minor fault | 145 | 85 | N_DIP_SLIP | CF_20 | | | | |
| | 42223770 | 13455450 | Platform Carbonates | Minor fault | 187 | 89 | | CF_21 | 5_10 m from MF (HF/FB) | | | |
| | 42212650 | 13466430 | Platform Carbonates | MAJOR SCARP | 250 | 55 | 81 W | CF_22_P | Polished Surf_Bauxite level | X | X | |
| | 42211930 | 13468280 | Platform Carbonates | Minor fault | 247 | 9 | Dextral | CF_23 | | | | |
| | | | | | | | | | | | | |
| | | | | | | | | | | | | |
| Mt. D'Ocre Fault_DGSD | 42277599 | 13406571 | Platform Carbonates | MAJOR SCARP | 205 | 49 | | MO_01_2018 | Karstified | X | X | |
| | 42275030 | 13411420 | Platform Carbonates | MAJOR SCARP | 228 | 70 | | MO_01_02_2021 | Karstified | X | X | |
| | 42284814 | 13394777 | Platform Carbonates | MAJOR SCARP | 195 | 65 | | MO_03_04 | Karstified | X | X | |
| | 42275030 | 13411420 | Platform Carbonates | MAJOR SCARP | 226 | 65 | | MOF01_2021 | Karstified | X | X | |
| | 42276340 | 13409490 | Platform Carbonates | MAJOR SCARP | 210 | 56 | | MOF02 | Karstified | | | |
| | 42283250 | 13398110 | Platform Carbonates | MAJOR SCARP | 209 | 57 | | MOF03_A_B | Karstified | | | |
| | 42284810 | 13394800 | Platform Carbonates | MAJOR SCARP | 215 | 65 | | MOF4_A_B | Karstified_FW Cataclasite | | | |

# Acknowledgments

First of all, I would like to thank my main supervisors Giulio Di Toro and Marco Moro for all their efforts to support me during the PhD. They have always been ready to all my requests and always adviced and helped me to find the best solution for my future.

I would like also to thank my other co-supervisors, Stefano Gori, Emanuela Falcucci, Michele Saroli and co-authors, Michele Fondriest, Fawzi Doumaz, Andrea Cavallo, Evgeny Borovin because I grew up a lot working with them. In particular, I would like to thank Simone Masoch, a special friend to me other than a great workmate.

I would also thank Leonardo Tauro and Silvia Cattò to have prepared my thin sections, Elena Spagnuolo for conducting laboratory experiments and my two thesis revisors Federico Agliardi and Nicola De Paola, for their very important and relevant comments.

Finally, I would like to thank all my PhD and work mates, for making my stay in padua truly unforgettable: La Cinzia, La Sofi, Leonardo, La Ally, La Rosalia, Francesco, La Vero, La Miriana, Telemaco, Wei.

Last of all, I want to thank my family for all their efforts and support.